Quantification of T-cell dynamics in health and disease:
Mathematical modeling of experimental data

Kwantificering van T-cel-dynamiek in gezondheid en ziekte:
Wiskundige modellering van experimentele data

(met een samenvatting in het Nederlands)

Proefschrift

ter verkrijging van de graad van doctor aan de Universiteit Utrecht op gezag van de rector magnificus, prof.dr. J.C. Stoof, ingevolge het besluit van het college voor promoties in het openbaar te verdedigen op dinsdag 16 maart 2010 des middags te 4.15 uur

door

Tendai Mugwagwa

geboren op 2 november 1979 te Gokwe, Zimbabwe

Promotor:	Prof. dr. R. J. De Boer
Co-promotor:	Dr. J. A. M. Borghans

The studies in this thesis were financially supported by the Netherlands Organization for Scientific Research (NWO, grant 016.048.603).

Reading committee:

Prof. dr. F. Miedema
Prof. dr. D. C. Macallan
Prof. dr. L. Willems
Prof. dr. R. Callard
Prof. dr. J. Carneiro

Paranimfen:

D. Tavarwisa
H. Malleko

ISBN: 9789039353097

The printing of this thesis was financially supported by Utrecht University.

Contents

Contents **iv**

1 General introduction. **1**
1.1 The adaptive immune system: T cells 1
1.2 When things go wrong. 2
1.3 Thesis outline. 3

2 Naive and memory T cell turnover in mice. **5**
2.1 Introduction 6
2.2 Results 7
2.3 Discussion 11
2.4 Materials and methods 14
2.5 Supplementary information. 18

3 Lack of peripheral division in naive T cell maintenance: a mouse-man divide. **19**
3.1 Introduction 20
3.2 Results 21
3.3 Discussion 26
3.4 Methods 28
3.5 Supplementary information. 32

4 No evidence for separate dynamics of recent thymic emigrants: thymus grafting experiments revisited. **39**
4.1 Introduction 40
4.2 Results 41
4.3 Discussion 46
4.4 Methods 48
4.5 Supplementary information. 50

5 T cell exhaustion and depletion in mice with chronic immune activation via CD27/CD70 costimulation. **53**
5.1 Introduction 54
5.2 Results 55

5.3 Discussion 61
5.4 Materials and Methods 62
5.5 Supplementary information. 65

6 Qualitative changes in T cell turnover during HIV-1 infection. 71
6.1 Introduction 72
6.2 Results 73
6.3 Discussion 78
6.4 Material and Methods 81
6.5 Supplementary information. 84

7 Biphasic TREC dynamics during HIV-1 infection. 87
7.1 Introduction 88
7.2 Results 90
7.3 Discussion 95
7.4 Materials and Methods 98

8 Can TRECs and telomeres be affected differently by naive T cell dynamics? 101
8.1 Introduction 102
8.2 Mathematical model 103
8.3 Results 105
8.4 Discussion 111
A Appendix: The age structured model. 119
B Appendix: The cascade model. 122

9 General Discussion. 123
9.1 T cell dynamics in healthy mice and humans. 123
9.2 RTEs: a separate sub-population? 125
9.3 T cell dynamics during HIV infection. 126

Bibliography 129

Summary 145

Samenvatting 147

Curriculum Vitæ 149

Publications 151

Acknowledgments 155

1

General introduction.

1.1 The adaptive immune system: T cells

The adaptive immune system plays an important role in defending the host against pathogens. An essential branch of the adaptive immune system is formed by T cells which mature in the thymus. Thymocytes undergo a maturation process that is also referred to as thymic education. T cells that might be beneficial to the immune system are spared by a process called positive selection, while those T cells that might evoke a detrimental autoimmune response are eliminated by a process called negative selection (Reviewed in [84]). Each T cell that passes through this education process has a T cell receptor (TCR) that can bind peptides presented by major histocompatibility complex (MHC) molecules on the surface of antigen presenting cells (APCs). Thymic selection determines the composition of the TCR repertoire. These T cells (recent thymic emigrants, RTEs) then emigrate to peripheral organs such as the spleen and lymph nodes and remain as naive T cells until they encounter antigen.

There is a broad range of potential pathogens that can infect a host, and some pathogens even evolve to evade detection by the host's immune system. Given that TCRs are very specific, their repertoire has to be very diverse [12, 23]. Indeed, T cells are highly diverse, in the sense that almost every T cell generated in the thymus expresses a different TCR. To ensure protection of the host from infection by diverse and evolving pathogens, the host has to maintain a diverse pool of naive T cells throughout life.

On encountering a pathogen, naive T cells become activated, proliferate and provide help to humoral and cellular immune responses (in the case of $CD4^+$ T cells), or become activated to kill specific infected target cells (in the case

of $CD8^+$ T cells). Activated T cells that are directly involved in combating pathogens are referred to as effector T cells. Some activated T cells mature into memory T cells. Memory T cells ensure extended protection of the host against re-encounters with similar pathogens, i.e. they provide immunological memory. T cell populations that have previously encountered specific pathogens can persist for decades. On encountering the same pathogen, they are activated, proliferate rapidly and resume effector function to combat that pathogen. The concept of immunization is based on immunological memory, and was first used as far back as the 1790s when Edward Jenner developed the smallpox vaccine. Exposure to antigens early in life should reduce the risk of the same antigen causing illness later in life.

1.2 When things go wrong.

With the features of the adaptive immune response described above, T cells should be able to provide effective protection for the host. However, T cells at times fail to protect the host against pathogens or in some cases even harm the host. The immune system may attack the host, as is the case in autoimmune disorders such as rheumatoid arthritis, myasthenia gravis and diabetes mellitus type 1. Several studies have shown that the diversity of the naive T cell repertoire shrinks with the age of the host (reviewed in [40]). The reason for this decline in repertoire diversity is unclear, but one suggestion is that it is due to a lack of new naive T cells from the thymus as the thymus involutes with age [40, 92, 142]. In other cases the absence of T cells be detrimental to the host as is the case in immunodeficiency diseases such as in severe combined immunodeficiency disease (SCID), or acquired immunodeficiency syndrome (AIDS).

To address why things go wrong, one needs to understand how things work normally and also how to rectify problematic situations by therapeutic strategies. A full understanding of T cell dynamics requires both a qualitative and quantitative understanding of the processes involved. For example, the mere knowledge that T cells can develop immunological memory to a specific pathogen is not enough to make a successful vaccine. We need to know how many effector cells are required, how fast they accumulate at the site of infection and how many infected targets they can kill [21].

Great strides have been made in immunological research over the years, and scientists have developed techniques and animal models to study different processes in immunology. However, the complex nature of the immune system and its interaction with pathogens, can make the interpretation of immunological data a formidable task. Furthermore recent advances in the development of new technologies for obtaining and storing immunological data, has made critical the need to develop tools to assimilate and interpret the data. Mathematical models are one such tool that can be used to help interpret immunological data, provide substantial insights into components of otherwise complex processes, and make predictions of what may follow as time evolves or as the

characteristics of the system are modified. Most of the immunological research is skewed towards a qualitative understanding, and in this thesis we seek to strike a balance between the qualitative and quantitative understanding of T cell dynamics. Our focus is on broadening the insights into mechanisms behind normal dynamics of T cells, and the causes of T cell decline during HIV infection. This thesis is in itself an illustration of how mathematical modeling and immunological experiments complement each other in gaining a better understanding.

1.3 Thesis outline.

Part I: T cell dynamics in health.
This section focuses on understanding and quantifying the dynamics of different T cell subsets in healthy mice.

• **Chapter 2:** A number of methods have been developed to study T cell dynamics in vivo. One such method makes use of labeling DNA of proliferating cells with the non-radioactive stable isotope deuterium (^{2}H). A meta-analysis of ^{2}H labeling studies suggested that the estimated average turnover rate depends on the length of the labeling period. In this chapter we show that this dependence on the length of the labeling period is a consequence of the mathematical model that was used to interpret the data. We develop a new mathematical model which explicitly accounts for possible kinetic heterogeneity in the different T cell subsets, and we show that average turnover rates of different T cell subsets can be evaluated independently of the length of the labeling period. We use this model to estimate the expected lifespans of naive and memory T cells in mice.

• **Chapter 3:** Although we are able to estimate the production rate and lifespan of naive T cells using ^{2}H labeling, this method cannot distinguish between thymic production and peripheral proliferation. To assess the contribution of the thymus, we thymectomized 7 week old mice and measured the sizes of the different T cell subsets in the spleen and peripheral lymph nodes for 65 weeks after thymectomy. Using mathematical models to describe this data, we found that throughout life, naive T cell production in mice almost exclusively occurs in the thymus. This is in contrast to findings from human studies, which have shown a significant contribution from peripheral naive T cell proliferation, particularly in adult life.

• **Chapter 4:** Contrary to previous studies that have suggested that recent thymic emigrants (RTEs) form a separate sub-population with different dynamics from resident naive T cells, we did not find any evidence for such a distinction (Chapters 2-3). We were able to describe both the naive T cell ^{2}H labeling data, and the naive T cell dynamics in control and thymectomized mice, without explicitly separating the RTEs from resident naive T cells. In this chapter we revisit the thymus implantation experiments that were the basis of the current consensus that RTEs in mice have a faster rate of turnover than resident naive T cells. We show that the data from thymus transplan-

tation studies are fully compatible with a mathematical model in which there is no kinetic distinction between RTE and resident naive T cells. Collectively, these analysis takes away the evidence that RTE form a kinetically distinct sub-population within the naive T cell pool.

Part II: T cell dynamics during HIV infection.
The mechanism behind the CD4 T cell decline during HIV infection remains unclear. Several studies have suggested that chronic immune activation is responsible for the loss of T cells while other studies have pointed at reduced thymic output. The goal of this section is to investigate the role of immune activation and thymic output in CD4 T cell decline during HIV infection.

• **Chapter 5:** Mice over-expressing CD70 are a model for chronic immune activation. By comparing T cell dynamics in CD70 Tg mice to wild-type mice, we investigated the effect of chronic immune activation and thymic output on naive T cell depletion. by fitting a mathematical model to experimental data, we show that chronic immune activation on its own is sufficient to cause naive T cell depletion, while reduced thymic output accelerates this.

• **Chapter 6:** Using in vivo ^{2}H labeling of T cells from HIV$^+$ and HIV$^-$ individuals, we show that in HIV$^+$ patients there is a shift in the kinetics of both naive and memory CD4 and CD8 T cells to faster turnover rates compared to healthy controls. The kinetics of the naive T cell pool changes most dramatically upon HIV infection: while naive T cells typically form a kinetically homogeneous population of cells, upon HIV infection naive T cells become heterogeneous and a sub-population of naive T cells acquires faster turnover rates.

• **Chapter 7:** Changes in T cell dynamics in HIV infection have been studied using TRECs and telomeres. The decline in CD4 T cells during HIV infection has been shown to be accompanied by a dilution of TRECs. In a longitudinal study, we show that this decrease in TRECs is biphasic. Using a mathematical model, we show that this data can be explained by massive recruitment of a large fraction of naive T cells into the effector/memory pool, where they are quickly lost.

• **Chapter 8:** Although TREC content data was initially proposed as a marker for thymic output, it was shown in previous studies that the interpretation of TREC data is complicated by dilution by T cell proliferation. Reversely, telomere length dynamics, which were initially proposed as a measure of the proliferative history of T cells, were shown to be influenced by thymic output. In this chapter we review the use of these two markers in understanding T cell dynamics in general, and apply our analysis to HIV infection. We find that typically both markers are affected by thymic output and proliferation. In one exceptional a case (where thymic output is small), TREC dilution was observed without a significant change in average telomere length. Our model explains the observations on TREC and telomere dynamics in HIV$^+$ patients when we allow for increased proliferation, in combination with either increased death rates and/or decreased thymic output.

2

Naive and memory T cell turnover in mice.

Tendai Mugwagwa[1,*], Ineke den Braber[2,*], Lydia Kwast[2], Elise H.R. Schrijver[2], Gerrit Spierenburg[2], Koos Gaiser[2], An F.C. Ruiter[3], Mariette T. Ackermans[3], Rob J. de Boer[1,#], Kiki Tesselaar[2,#], and José A.M. Borghans[1,2,#]

[1] Department of Theoretical Biology, Utrecht University, Utrecht, The Netherlands

[2] Department of Immunology, University Medical Center Utrecht, Utrecht, The Netherlands

[3] Department of Clinical Chemistry, Academic Medical Center, University of Amsterdam, Amsterdam, The Netherlands

[*,#] These authors contributed equally to this work.

Abstract

Our limited knowledge of the expected life spans of naive and memory T cells during health and disease hampers our understanding of the functioning of the immune system. Life spans have been estimated in mice and men with various labeling approaches, with disturbingly different outcomes. Even results based on stable-isotope labeling, which provides the most reliable tool to measure lymphocyte life spans that is currently available, differ significantly between laboratories. Here we investigate whether this difference in estimated turnover rates could be due to differences in the length of the labeling period. When applied to kinetically heterogeneous cell populations, such as the effector/memory T cell pool in mice, current models may lead to underestimation of the average life span when labeling periods are long, because sub-populations with the highest rates of turnover may approach maximum label intake during the labeling period. Such problems do not arise in kinetically homogeneous cell populations, such as the naive T cell pool in mice and men. We introduce a new model that can estimate labeling-time-independent average life spans of heterogeneous cell populations. We estimate that in mice, naive $CD4^+$ and $CD8^+$ T cells have average life spans of 48 and 91 days, respectively, while memory $CD4^+$ and $CD8^+$ T cells live on average 12 and 17 days, respectively.

2.1 Introduction

Knowledge on the average life spans of different leukocyte populations has important consequences for our insights in diverse immunological processes. The long life span of naive T cells in humans, for example, suggests that priming of specific naive T cells is a rare event, and that reconstitution of these cells after depletion, for example due to HIV infection, may take considerable time. Leukocyte life spans are generally estimated by *in vivo* labeling experiments of traceable components built into the DNA of proliferating cells. Recently, the non-radioactive stable isotopes $^2H_2$-glucose and ^2H_2O have been introduced for *in vivo* DNA labeling and quantification of leukocyte production and death in humans [58, 93]. The average life spans of naive, memory and total $CD4^+$ and $CD8^+$ T cells that have been estimated using these two compounds, however, differ considerably between laboratories [10]. The origin of these differences has so far not been explained.

It has been shown before that, if cell populations are kinetically heterogeneous, the rate at which labeled cells are lost after label cessation tends to decrease when the length of the labeling period increases. As labeled cells are by definition cells that have recently divided, loss of label may be biased towards cells with relatively rapid turnover. For longer labeling periods, the rate at which label is lost more closely resembles the average turnover rate of the cell population [5]. Importantly, the *average* turnover rate - which is used to estimate the average life span - of a cell population should *not* depend on the

length of the labeling period.

Although part of the discrepancies between laboratories might result from the use of different stable isotopes, we observed a consistent positive correlation between estimated average life spans and the duration of label administration, even when the same stable isotope was used [10]. In line with this, studies based on deuterated glucose - which tends to be administered for shorter periods than deuterated water - consistently reported shorter average T cell life spans than deuterated water studies [10]. We therefore investigated how the length of the labeling period could influence estimated average life spans. Current models used to fit stable isotope labeling data typically assume that the labeling phase can be described by a single exponential [5, 88]. We studied the hypothesis that if there are sub-populations of cells with such high rates of turnover that their label incorporation starts saturating during the labeling period while that of other cells does not, such models may underestimate the average turnover rate of the cell population as a whole, especially when labeling periods are long.

Here we experimentally tested our hypothesis that longer labeling periods may lead to underestimation of the average rate of cell turnover of kinetically heterogeneous cell populations when fitted to a single-exponential model. We performed ^2H_2O experiments in mice which only differed in the length of the labeling period, and analysed the kinetics of naive and effector/memory T cells. We found that effector/memory T cells in mice form a kinetically heterogeneous population, and when fitted to a single exponential model [5] longer labeling periods resulted in longer estimated average life spans. In contrast, naive T cells in mice were found to be kinetically homogeneous, and their estimated average turnover rate was not influenced by the length of the labeling period. We introduce an alternative modeling strategy, based on a multi-compartment model [38], which fits average life spans independent of the length of the labelingg period even for populations that are kinetically heterogeneous. Fitting this new model to all the labeling data that we collected in mice yielded reliable estimates of the average T cell life spans in mice, which varied from 48 and 91 days for naive $CD4^+$ and $CD8^+$ T cells, to 12 and 17 days for memory $CD4^+$ and $CD8^+$ T cells, respectively.

2.2 Results

Estimated average turnover rates can be dependent on the length of the labeling period

To investigate whether the length of label administration may influence the estimated average life span of T cells, we gave 12-week old C57Bl/6 mice a bolus of ^2H_2O and subsequently 4% ^2H_2O in the drinking water for one, four, or eight weeks. Total thymocytes and naive and effector/memory $CD4^+$ and $CD8^+$ T cells were isolated from the spleen during the up- and down-labeling phases and deuterium enrichment in the DNA was measured. The enrichment curves of naive and effector/memory T cells for the three different labeling periods (Fig.

2.1), were fitted with a single exponential model proposed by Asquith et al. [5]. In this model cells have an average turnover (or production) rate p and labeled cells disappear at rate d^*. Production of labeled naive T cells is a combination of thymic output and proliferation, whereas labeled effector/memory T cells emanate from self-renewal and differentiation of naive T cells. Labeled naive and effector/memory T cells disappear by differentiation, migration and/or cell death [56]. The model was extended to correct for the ^2H_2O concentration in the plasma (see Materials and Methods). After withdrawal of deuterium from the drinking water the concentration of the label in the plasma dropped with a half-life of 2.7 days.

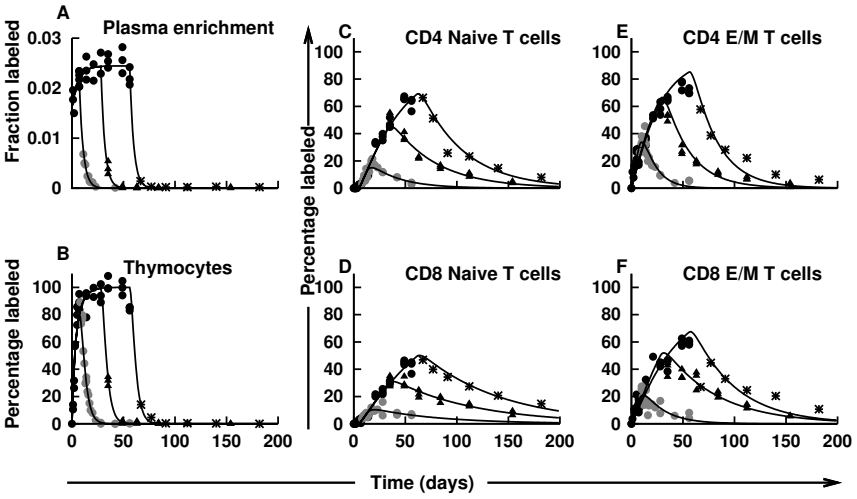

Fig. 2.1: Best fits of the single exponential model to the naive and effector/memory T cell data. Label enrichment was corrected for ^2H_2O enrichment in plasma (A) and scaled between 0 and 100% by normalizing for the percentage label obtained in thymocytes (B). At different time points before, during and after labeling, the percentages of labeled naive $CD4^+$ (C), naive $CD8^+$ (D), effector/memory $CD4^+$ (E) and effector/memory $CD8^+$ T cells (F) in the spleen were determined. The black dots are all data measured during labeling, the grey dots, black triangles and black asterix are the 1, 4 and 8 week down-labeling data, respectively. Data were fitted separately for each labeling period, using the single exponential model to estimate the average turnover rate p of the total population and the disappearance rate d^* of the labeled cell population. (see Table S.2.2 for parameter values.)

Each of the data sets was fitted separately with the single exponential model (Materials and Methods and Fig. 2.1). The disappearance rate d^* of labeled naive T cells did not depend on the length of the labeling period, while that of

effector/memory T cells decreased significantly when the length of the labeling period increased (Fig. 2.2B). This suggests that effector/memory T cells in mice form a kinetically heterogeneous population [5], while naive T cells are kinetically homogeneous (Den Braber et al. unpublished). Fitting the different effector/memory data sets with the single exponential model confirmed the unexpected observation in the literature [10] that even the estimated average turnover rates p can depend on the length of the labeling period (Fig. 2.2A). The resulting estimated average life spans of $CD4^+$ and $CD8^+$ effector/memory T cells based on the one-week labeling experiment were $1/p = 15$ (12-16 days) and 28 days (22-32 days), respectively, while the estimates based on the longer labeling experiments were $1/p$ =25 (22-27 days) and 45 days (38-49 days), respectively. For naive $CD4^+$ and $CD8^+$ T cells, we estimated average life spans of $1/p = 48$ (33-48 days) and 83 (51-83 days) days, respectively, independent of the length of the labeling period.

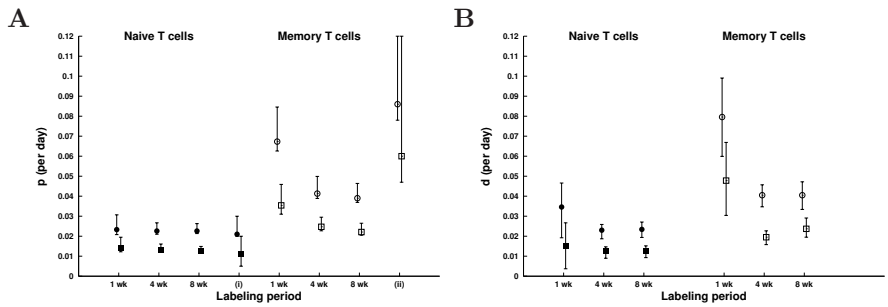

Fig. 2.2: Effect of the length of the labeling period on the average turnover rates and the disappearance rates of labeled cells. The estimated average turnover rates, p, of the total populations (A) and the disappearance rates, d^*, of the labeled cell populations (B) based on the single exponential model, for the different labeling periods. The estimates were based on the best fits through the 1, 4 or 8 week labeling data of naive $CD4^+$ (solid squares), naive $CD8^+$ (solid circles), effector/memory $CD4^+$ (open squares) and effector/memory $CD8^+$ (open circles) T cells (Fig. 2.1). The points indicated by (i) and (ii) are the average turnover rates from simultaneously fitting all data sets to the two-compartment model.Bars with whiskers represent the 95% confidence intervals on the average turnover rates.(see Table S.2.2)

Dependence on the labeling period due to the modeling approach. We investigated whether the dependence of the estimated average turnover rate on the length of the labeling period could be due to the mathematical model used. Although the model introduced by Asquith et al. [5] captures kinetic heterogeneity in the sense that the rate at which labeled DNA accumulates during label administration may differ from the rate at which it is lost after label cessation, both the accrual and loss of label are described by a single

exponential. Such a model may not correctly describe the average turnover rate of a cell population that contains cells which proliferate so rapidly that their label incorporation starts saturating during the labeling phase and cells that proliferate more slowly. Instead the model will seek a compromise between the true average turnover rate which is reflected in the initial rapid label increase, and the subsequent labeling of the cells with slower rates of turnover. Such compromises may cause underestimation of the true average turnover rate especially for longer labeling periods.

Our own experiments described above are illustrative of this problem. Theoretically, the up-slopes of the three labeling experiments should follow exactly the same curve and approach the same asymptote. In fact, the separate fits of the 1, 4, and 8-week labeling data of effector/memory cells show different slopes during the labeling phase (Figure 1). According to the model by [5], at the asymptote a fraction p/d^* of the DNA is labeled. Because short labeling periods lead to high values of the disappearance rate of labeled cells, d^*, the asymptotes could paradoxically only be the same if the estimated average turnover rate, p, would be higher for short labeling periods. Hence, differences in average turnover rates may even be imposed by the different down-slopes.

Estimating T cell turnover with a multi-compartment model. To overcome these problems we introduce a new modeling approach, which explicitly takes into account kinetic heterogeneity between sub-populations of cells [38]. The new model splits the cell population of interest into an arbitrary number of kinetically different compartments, each with a different turnover rate. Kinetic heterogeneity between sub- populations has indeed been reported. For instance, memory T cells in both mice and men can be phenotypically separated into effector-memory (T_{EM}) and central-memory (T_{CM}) cells [114], with kinetic differences, e.g., the estimated turnover rate of human $CD4^+$ T_{EM} cells is three times faster than that of $CD4^+$ T_{CM} cells [81]. The generalized mathematical model considers n different sub-populations, each forming a fraction α_i of the total population, with average turnover rate p_i (where $i = 1, 2, ..n$). We have demonstrated that as the number of compartments in the model increases, the estimated average turnover rate increases until it saturates at the true average turnover rate (Bartha et al. unpublished). By systematically fitting the general model to the individual data-sets and each time testing whether adding an extra kinetic sub-population changed the estimated average turnover rate, we found that the effector/memory labeling data could be described by two kinetic sub- populations. In contrast to the single exponential model, the two compartment model correctly described the 1, 4, and 8-week labeling data with almost overlapping up-labeling curves (Fig. 2.3). As a result, the estimated average turnover rates became independent of the length of the labeling period (Fig. 2.4). Thus, estimates for cellular life spans are no longer dependent on the length of the labeling period when mathematical models are used that correctly capture the multi-phasic nature of labeling curves. As expected, the estimated average turnover rates of naive T cells remained independent of the

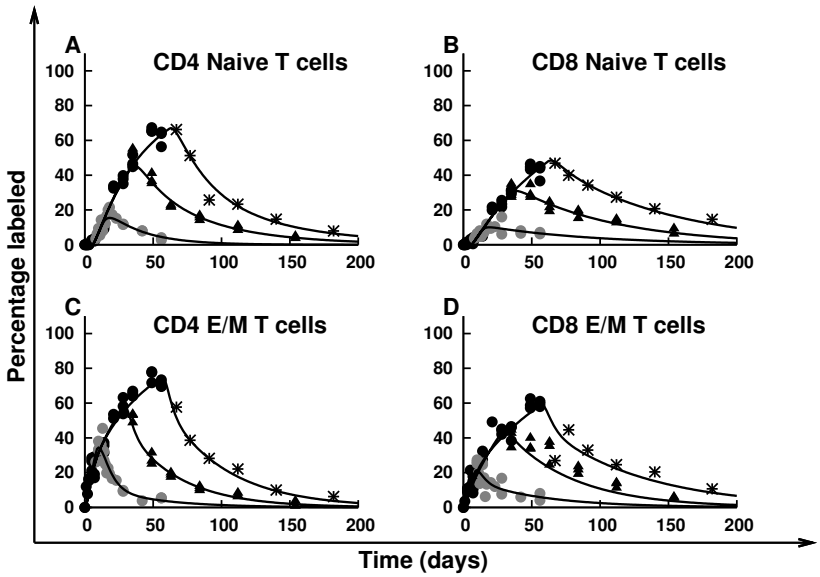

Fig. 2.3: Best fits of the two-compartment model to the naive and effector/memory T cell data. At different time points before, during and after labeling, the fraction of labeled naive $CD4^+$ (A), naive $CD8^+$ (B), effector/memory $CD4^+$ (C) and effector/memory $CD8^+$ T cells (D) in the spleen were determined. The black dots are all data measured during labeling, the grey dots, black triangles and black asterix are the 1, 4 and 8 week down-labeling data, respectively. Data were individually fitted to a two-compartment model to estimate the average turnover rates of the different T cell populations.

length of the labeling period (Fig. 2.4), further supporting the notion that the naive T cell pool in mice is kinetically homogeneous.

We took advantage of the three different detests per T cell population that we collected, by fitting all labeling experiments simultaneously using our new modeling approach. Based on these extensive data sets, we estimated that $CD4^+$ and $CD8^+$ effector/memory T cells in mice have average turnover rates of 0.086 and 0.060 per day, yielding average life spans of $1/p = 12$ and 17 days, respectively (Table 2.1). Naive $CD4^+$ and $CD8^+$ T cells in mice were estimated to live on average 48 and 91 days, respectively (Table 2.1).

2.3 Discussion

Estimated average T cell life spans based on stable-isotope labeling have previously been shown to differ between laboratories [10]. Our study shows that differences in estimated average life spans may in part be caused by dif-

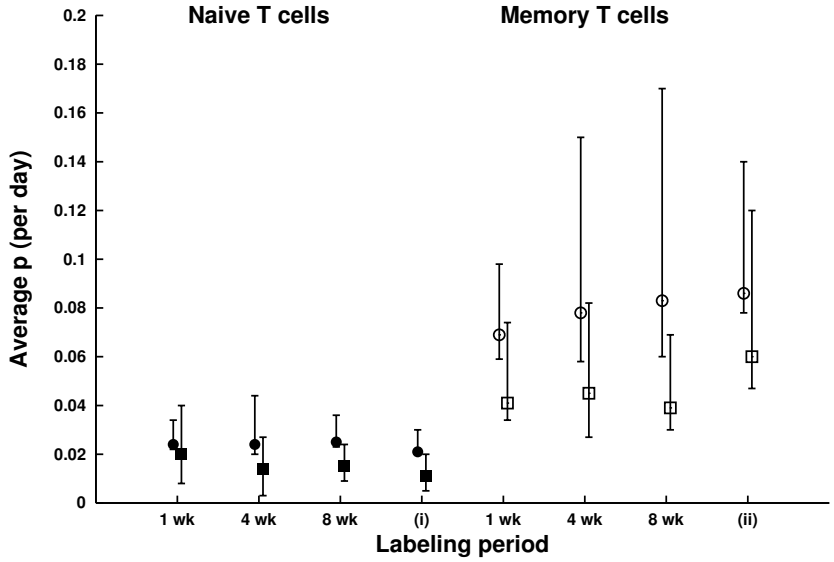

Fig. 2.4: The two compartment model estimates the same average turnover rate regardless of the length of the labeling period. The estimated average turnover rates, p, of the different T cell populations based on the two compartment model. The estimates were based on the individual best fits through the 1-, 4- and 8-week labeling data of naive $CD4^+$ (solid squares), naive $CD8^+$ (solid circles), effector/memory $CD4^+$ (open squares) and effector/memory $CD8^+$ (open circles) T cells (Fig. 2.3). The points indicated by (i) and (ii) give the average turnover rates resulting from simultaneous fits to the 1, 4 and 8 week labeling data of naive $CD4^+$, naive $CD8^+$, effector/memory $CD4^+$ and effector/memory $CD8^+$ T cells (see Fig. 2.5). Bars with whiskers represent the 95% confidence intervals on the average turnover rates.

ferences in the labeling periods, with longer labeling periods giving rise to longer estimated average life spans. By varying the labeling period from one to eight weeks in one experimental setting, and by fitting effector/memory T cell labeling data with a single exponential model [5], we found that the estimated average turnover rate decreased as the labeling period became longer (Fig. 2.2). This dependence of the estimated average turnover rate on the labeling period was probably caused by a sub-population of cells that had such a high rate of turnover that its level of label incorporation started to saturate during the labeling phase while that of other cells did not. Because the single exponential model could not correctly capture the biphasic nature of the up- and down-labeling curves, the model yielded a compromise and thereby underestimated the average turnover rate of the effector/memory population, especially when the labeling period was long. We demonstrate that the use of a multi-compartment model [38] solves these problems and gives rise to average

Table. 2.1: Estimated turnover rates of naive and effector/memory T cells based on simultaneously fitting the one, four and eight week labeling data using the two-compartment model. 95% confidence intervals are given in parentheses.

	Parameter	Naive	Effector/memory
$CD4^+$	$p_1(\text{day}^{-1})$	0.024 (0.020 - 0.201)	0.257 (0.196 - 0.461)
	$p_2(\text{day}^{-1})$	0.010 (0.000 - 0.199)	0.024 (0.011 - 0.053)
	α	0.793 (0.031 - 0.995)	0.272 (0.212 - 0.343)
	average $p(\text{day}^{-1})$	0.021 (0.020 - 0.029)	0.086 (0.078 - 0.139)
$CD8^+$	$p_1(\text{day}^{-1})$	0.092 (0.042 - 0.471)	0.446 (0.247 - 1.000)
	$p_2(\text{day}^{-1})$	0.012 (0.001 - 0.142)	0.018 (0.005 - 0.075)
	α	0.000 (0.000 - 0.047)	0.101 (0.079 - 0.148)
	average $p(\text{day}^{-1})$	0.011 (0.005 - 0.019)	0.060 (0.048 - 0.120)
Shared	Δ	4.105 (3.717 - 4.417)	0.000 (0.000 - 0.488)

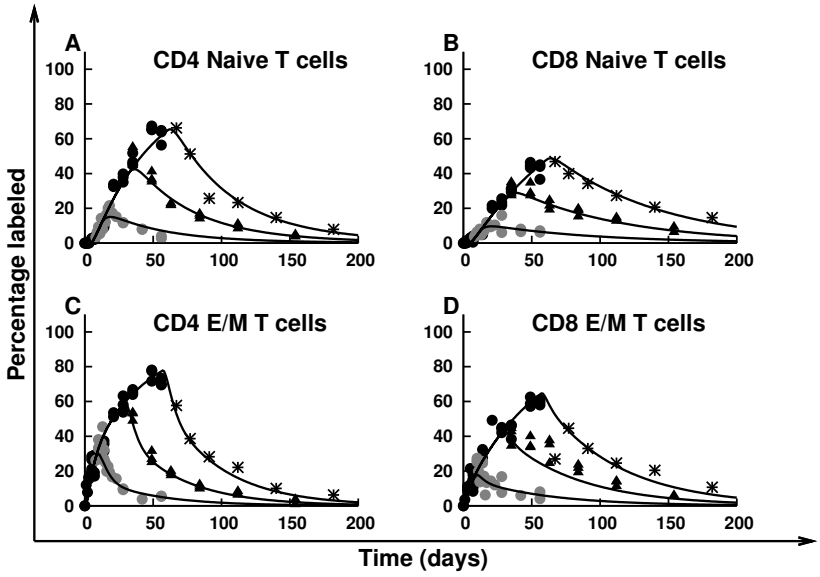

Fig. 2.5: Best fits of the two compartment model, when all naive and effector/memory Tcell data were fitted simultaneously. At different time points before, during and after labeling, the fraction of labeled naive $CD4^+$ (A), naive $CD8^+$ (B), effector/memory $CD4^+$ (C) and effector/memory $CD8^+$ T cells (D) in the spleen were determined. The dots are all data measured during labeling, the grey dots, black triangles and black asterix are the 1-, 4- and 8-week down-labeling data, respectively. Data were simultaneously fitted with a two-compartment model to estimate the average turnover rate of each T cell population.

turnover rates that are independent of the labeling period.

Our new modeling approach improves upon previous models, especially when fitting experiments with long labeling periods. Long-term labeling has considerable advantages over short-term labeling, because long labeling periods i) allows even cells with relatively slow turnover to become labeled, ii) allows for more data sampling during the labeling phase, which is essential to estimate the average turnover rate, and iii) allows for detailed analysis of the kinetic composition of the cell population under investigation. In order to obtain reliable estimates in future labeling studies, we therefore suggest to perform long-term labeling experiments with relatively dense sampling during the start of the labeling phase (because that is when the slope of the labeling curve most closely resembles the true average turnover rate), and to apply our new modeling strategy to help the interpretation of the experiments.

It is widely believed that naive T cells in mice exist in two separate populations with different kinetics: recent thymic emigrants with a turnover of approximately three weeks [7, 8] and resident naive T cells, with an estimated life span of several months [25, 99, 130]. Our labeling data provided no evidence whatsoever for such kinetic heterogeneity in the naive T cell population: 1) when the one exponential model [5] was fitted to the naive $CD4^+$ and $CD8^+$ labeling data, the average turnover rate p was similar to the loss rate of labeled cells d^*, and the loss rate of labeled cells d^* did not depend on the length of the labeling period, and 2) when the new model was fitted to the naive $CD4^+$ and $CD8^+$ T cell labeling data, the introduction of a second kinetic compartment neither improved the quality of the fits, nor changed the parameter estimates. Both observations suggest that the naive T cell population in mice is in fact kinetically homogeneous. The observation that effector/memory T cells are kinetically heterogeneous is not surprising, because phenotypically separate sub-populations of effector-memory (T_{EM}), central-memory (T_{CM}), and quiescent bone marrow memory cells with kinetic differences have been described before [81, 114, 129].

Based on our labeling experiments, which to the best of our knowledge form the most extensive labeling data set collected in mice to date, we estimate that naive $CD4^+$ and $CD8^+$ T cells in mice have an expected lifespan of 48 and 91 days, respectively. Effector/memory $CD4^+$ and $CD8^+$ T cells, which are kinetically heterogeneous, have expected life spans of 12 and 17 days respectively.

2.4 Materials and methods

Mice

C57Bl/6 mice were maintained by in-house breeding at the Central Animal Facility at Utrecht University under specific pathogen-free conditions in accordance with institutional and national guidelines. ^2H_2O labeling was achieved

by giving 12-week old mice one boost injection (i.p.) of 16.5 ml/kg of 90% ^2H_2O in PBS (Cambridge Isotopes, Cambridge, MA), followed by subsequent feeding with 4% ^2H_2O in drinking water for 1, 4 or 8 weeks.

Antibodies
FITC-labeled CD8 (clone 53-6.7), PE-conjugated CD62L (clone MEL-14), PerCP-labeled CD4 (clone RM4-5) and APC-labeled CD44 (clone IM7) were purchased from BD Biosciences PharMingen (San Diego, CA).

Cell preparation and flow cytometry
Spleen and thymus were isolated from C57Bl/6 mice at different time points before, during and after ^2H_2O labelingg. After mechanical disruption, the cells were prepared and stained as previously described [136]. Cells were analyzed on a LSR II flow cytometer and BD FACSDiva software. Naive ($CD62L^+$, $CD44^-$) and effector/memory ($CD44^+$) T cells were sorted using a FACSAria cell sorter and FACSDiva software (BD). Purity of the sorted cells was comparable between the different labeling experiments. The average purity was: 98.3 ± 1.6 % (naive $CD4^+$,91.1 - 99.9 %), 97.9 ± 1.4 % (effector/memory $CD4^+$, 92.8 - 99.7 %), 98.4 ± 1.2 (naive $CD8^+$, 92.9 - 100 %) and 96.7 ± 1.7 % (effector/memory $CD8^+$, 89.6 - 99.6 %). Thymocytes and sorted T cells were frozen until further processed.

Measurement of ^2H_2O enrichment in plasma and DNA
Deuterium enrichment in serum was measured as reported by Previs et al. [106]. The isotopic enrichment of DNA was determined as previously described [136].

Mathematical modeling of ^2H_2O data.
Following Vrisekoop et al. [136], the availability of heavy water at any moment in time was calculated by fitting the ^2H enrichment in the plasma during up- and down-labeling to the following equations:

$$S(t) = f(1 - e^{-\delta t}) + S_0 e^{-\delta t} \text{during label intake}(t \leq \tau), \text{and} \quad (2.1)$$

$$S(t) = \left[f(1 - e^{-\delta \tau}) + S_0 e^{-\delta \tau}\right] e^{-\delta(t-\tau)} \text{after label intake}(t > \tau). \quad (2.2)$$

In these equations, $S(t)$ represents the fraction of ^2H_2O in plasma at time t (in days), f is the fraction of ^2H_2O in the drinking water, labeling was stopped at $t = \tau$ days, δ represents the turnover rate of body water per day, and S_0 is the plasma enrichment attained after the i.p. boost of label at day 0. The best fits for the plasma data are shown in Fig. 2.1A and the parameter estimates are given in Supplementary Table S.2.1.

To model the label enrichment of adenosine in the DNA of cells we previously extended the single exponential model proposed by Asquith et al. [5] to include the dependence on the actual enrichment of the body water (as estimated by $S(t)$) [136]. To determine the maximal level of label incorporation that could possibly be attained, we fitted this model [136] to labeling data from mouse thymocytes (see Fig. 2.1B and Supplementary Table S.2.1), which are known to have a high rate of turnover [59, 93]. Parameters based on the single

exponential model for the different T cell subsets were subsequently determined as described before [136].

Alternatively, labeling data from the different T cell subsets were fitted to a multiple compartment model [38] in which each kinetic sub-population i contains a fraction α_i of cells with turnover rate p_i. Assuming a steady state for each kinetic sub-population, label enrichment of adenosine in the DNA of each sub-population i was modeled by the following differential equation:

$$l_i' = p_i c S(t) \alpha_i A - p_i l_i \tag{2.3}$$

where l_i is the total amount of labeled adenosine in the DNA of sub-population i, A the total amount of adenosine, c is an amplification factor that needs to be introduced because the adenosine deoxyribose (dR) moiety contains seven hydrogen atoms that can be replaced by deuterium, and p_i is the average turnover rate of the sub-population. Basically one writes that each adenosine residue in sub-population i replicates at rate p_i and will incorporate a deuterium atom with probability $cS(t)$. For naive T cells this replication may occur both in the periphery and the thymus. Scaling this equation by the total amount of adenosine in the DNA of sub-population i, i.e., defining $L_i = l_i/(\alpha_i A_i)$, yields:

$$L_i' = p_i c S(t) - p_i L_i \tag{2.4}$$

throughout the up- and down-labeling period, where L_i represents the fraction of labeled deoxyribose residues of adenosine in the DNA of sub-population i. The corresponding analytical solutions are
During label intake:

$$L_i(t) = \frac{c}{\delta - p_i}\left[p_i(S_0 e^{-p_i t} - S(t)) + \delta f(1 - e^{-p_i t})\right] \text{ if } (t \le \tau), \tag{2.5}$$

After label intake:

$$L_i(t) = \frac{p_i c}{\delta - p_i}\left[S(\tau)e^{-p_i(t-\tau)} - S(t)\right] + L(\tau)e^{-p_i(t-\tau)} \text{ if } (t > \tau), \tag{2.6}$$

Because we observed a lag in appearance of labeled naive T cells in the spleen after start of labeling, suggesting that cells divided in the thymus and then migrated to the spleen, we modified Equations 2.5 and 2.6 by introducing a time delay, Δ, when fitting to naive T cell data. The corresponding equations are:
If $t \le \Delta$:

$$L_i(t) = 0$$

If $\Delta < t \le \tau + \Delta$:

$$L_i(t) = \frac{c}{\delta p_i}\left[p_i(S_0 e^{-p_i(t-\Delta)} - S(t-\Delta)) + \delta f(1 - e^{-p_i(t-\Delta)})\right]$$

If $t > \tau + \Delta$:

$$L_i(t) = \frac{p_i c}{\delta p_i}\left[S(\tau)e^{-p_i(t-\Delta-\tau)} - S(t-\Delta)\right] + L(\tau)e^{-p_i(t-\Delta-\tau)}$$

The fraction of labeled DNA in the total T cell population under investigation was subsequently derived from

$$L(t) = \sum \alpha_i L_i(t)$$

and the average turnover rate p was calculated from

$$p = \sum \alpha_i p_i$$

Best fits were determined by minimizing the sum of squared residuals after arcsin(square-root) transformation, because all enrichment data were expressed as fractions. The 95% confidence intervals (CIs) for the inferred parameters were determined using a bootstrap method [33], where the residuals to the optimal fit were resampled 500 times.

Statistical analysis.
All statistical analyses were performed using the software program SPSS 15.0 (SPSS Inc, Chicago, Illinois). Differences with $p < 0.05$ were considered significant.

*A*cknowledgments
The authors acknowledge Becca Asquith for very inspiring and helpful discussions, and Joyce Visser and Sabine Versteeg for technical assistance and excellent animal care. This research has been funded by the Landsteiner Foundation for Blood Transfusion Research (LSBR grant 0210), the Netherlands Organization for Scientific Research (NWO, VICI grant 92750029, VIDI grant 917.96.350 and visitor's grant 040.11.128), and by the Research Council for Earth and Life Sciences (ALW) with financial aid from the Netherlands Organisation for Scientific Research (NWO, grant 836.07.002).

2.5 Supplementary information.

Table. S.2.1: Parameters values of deuterium enrichment in the plasma and in thymocytes[a]. We take the deuterium enrichment in the plasma to reflect the enrichment in the body water. S_0 represents the baseline plasma enrichment attained after the boost at the end of day 0. δ is the turnover rate of body water and f the fraction of ^2H_2O in the drinking water. Labeling in thymocytes was measured to normalize the data (see Materials and Methods).

	Paremeter	Value (95% confidence interval)
Plasma	S_0	0.015 (0.012-0.018)
	$\delta(day^{-1})$	0.261 (0.230-0.272)
	$f(day^{-1})$	0.006 (0.006-0.007)
Thymocytes	$p(day^{-1})$	0.416 (0.377-0.468)
	c	3.093 (2.974 -3.161)

[a]Values are estimates of the best fit depicted in (Fig. 2.1A) and (Fig. 2.1B) .

Table. S.2.2: Parameter values[a] from the best fits of the single exponential model to the naive and effector/memory T cell data. Data were fitted separately for each labeling period (see Fig. 2.1), using the single exponential model to estimate the average turnover rate p of the total population and the disappearance rate d^* of the labeled cell population for each labeling period.

τ^b		7 days	28 days	56 days
Naive				
$CD4^+$	p	0.023 (0.021-0.031)	0.023 (0.021-0.027)	0.023 (0.021-0.026)
	d	0.035 (0.019-0.047)	0.023 (0.019-0.026)	0.023 (0.019-0.027)
$CD8^+$	p	0.014 (0.012-0.020)	0.013 (0.012-0.016)	0.013 (0.012-0.015
	d	0.015 (0.004 -0.027)	0.012 (0.009-0.015)	0.013 (0.009-0.015)
Memory				
$CD4^+$	p	0.067 (0.063-0.085)	0.041 (0.039-0.050)	0.039 (0.037-0.046)
	d	0.080(0.060 -0.099)	0.041 (0.035-0.046)	0.041 (0.033-0.047)
$CD8^+$	p	0.035 (0.031-0.046)	0.025 (0.023-0.030)	0.022 (0.020-0.026)
	d	0.048 (0.030 -0.067)	0.019 (0.016-0.023)	0.024 (0.019-0.029)

[b]Value (95% confidence interval)
[a]Length of labeling period.

3

Lack of peripheral division in naive T cell maintenance: a mouse-man divide.

Ineke den Braber[1,*], Tendai Mugwagwa[2,*], Liset Westera[1], Elise H.R. Schrijver[1], Gerrit Spierenburg[1], Koos Gaiser[1], An F.C. Ruiter[3], Mariette T. Ackermans[3], Frank Miedema[1], José A.M. Borghans[1,2,#], Rob J. de Boer[2,#], and Kiki Tesselaar[1,#].

[1] Department of Immunology, University Medical Center Utrecht, Utrecht, The Netherlands

[2] Theoretical Biology, Utrecht University, Utrecht, The Netherlands

[3] Department of Clinical Chemistry, Academic Medical Center, University of Amsterdam, Amsterdam, The Netherlands

[*,#] These authors contributed equally to this work.

Abstract

The contribution of thymus output to the maintenance of the naive T cell pool is still controversial. Using a combination of deuterium labeling and thymectomy experiments, we show that, throughout life, naive T cell maintenance in mice depends almost completely on thymus output. In contrast to the situation in men, peripheral naive T cell division hardly contributes to the naive T cell pool in mice, which was confirmed by the absence of T cell receptor excision circle (TRECs) dilution of mouse naive T cells with age. Naive $CD4^+$ and $CD8^+$ T cells in young adult mice have a life expectancy of about 7 and 11 weeks, respectively. The differences in naive T cell dynamics between mice and men point to a serious limitation regarding extrapolation from mouse to man and vice versa.

3.1 Introduction

Naive T cells are generated via two different pathways: de novo production in the thymus, giving rise to naive T cells with new T cell receptor (TCR) specificities [67, 127], and peripheral cell division which does not add novel T cell specificities. Both in mice and men, daily output of T cells from the thymus declines with age [45, 124]. Thymus involution is probably responsible for the gradual decline in naive $CD4^+$ and $CD8^+$ T cell numbers with age, although naive T cell numbers in both mice and men decline less dramatically than thymocyte numbers [34, 117]. In line with this, at old age the peripheral T cell pool becomes dominated by memory T cells [34, 78], coinciding with severe perturbations of the naive T cell repertoire and impaired immunity at very old age [1, 92, 142]. Because of the parallels between T cell kinetics in mice and men, insights into the role of thymus output in the maintenance of the T cell pool, and in particular into the role of recent thymic emigrants, are widely extrapolated from mice to men, and vice versa. In fact it is unknown, how the average life spans of $CD4^+$ and $CD8^+$ T cells of mice and men relate to the longevity of the species, and whether the source of cells responsible for naive T cell maintenance is similar in mice and men.

TREC analysis has been used to estimate the role of thymus output and peripheral T cell proliferation. It has been used to show that peripheral proliferation contributes substantially to the establishment and maintenance of the human peripheral naive T cell pool [53]. The recently introduced technique of stable isotope labeling has paved the way for reliable quantification of human lymphocyte turnover. Mathematical interpretation of deuterium labeling data from healthy human adults has revealed that human naive T cells are long-lived, with an average life expectancy of six years for naive $CD4^+$ and nine years for naive $CD8^+$ T cells, and that recently-produced naive T cells live even longer [136].

Using deuterium labeling we found that the life span of murine naive $CD4^+$

and CD8$^+$ T cells is much shorter than that in humans, i.e. in the order of 6-7 weeks throughout life. In contrast to humans, in whom peripheral T cell division is a major source of naive T cells from early life onward [53], in mice naive T cells are predominantly derived from thymus output, even at old age. Our data thus show that maintenance of the naive T cell pool is fundamentally different in mice and men, with obvious limitations for the extrapolation of insights into lymphocyte dynamics obtained from murine models to humans and vice versa.

3.2 Results

Turnover of naive T cells.
To determine the normal turnover rates of naive CD4$^+$ and CD8$^+$ T cells in young adult mice, 12-week old C57Bl/6 mice were administered a bolus of 99.8% deuterated water (^2H_2O) followed by long-term maintenance labeling with 4% deuterated water in the drinking water. Deuterium enrichment in the DNA of thymocytes and naive T cells from the spleen was determined during four weeks of label administration and a subsequent 18 weeks down-labeling period. It took about a week for the first labeled naive T cells to appear in the spleen, where they kept on accumulating up to a week after the end of labeling (Fig. 3.1A), suggesting that these cells were labeled by cell division in another compartment.

The cellular turnover rates were estimated by fitting the labeling data to a mathematical model [5, 136], which distinguishes between an average turnover or production rate, p, and a death rate of labeled cells, d^* (see Methods). The average turnover rates of naive CD4$^+$ and CD8$^+$ T cells in young adult mice were found to be 0.021 and 0.013 per day (Fig. 3.1A), corresponding to average life spans ($1/p$) of 47 and 80 days, respectively (Table 3.1). In contrast to what is commonly observed in deuterium labeling studies in man [5], the death rates of labeled cells, d^*, did not significantly differ from the average turnover rates, p (Fig. 3.1), suggesting that naive T cells form a dynamically homogeneous population in the mouse.

Thymus output.
Although deuterium labeling experiments provide the most reliable tool to estimate cellular turnover rates, they fail to distinguish between production of naive T cells in the thymus and their peripheral renewal [10]. In a separate set of experiments we therefore enumerated single positive (SP) CD4$^+$ and CD8$^+$ thymocytes (Fig. S.3.1A) and naive CD4$^+$ and CD8$^+$ T cells in the spleen and PLNs of normal euthymic or sham-thymectomized mice and mice that had been thymectomized at seven weeks of age (Fig. 3.2). There were no significant differences in thymocyte or naive T cell numbers between normal mice and sham-thymectomized mice at any age (data not shown), allowing us to combine the data from both types of mice in one euthymic control group. In euthymic mice, the numbers of SP CD4$^+$ and CD8$^+$ thymocytes were found to increase

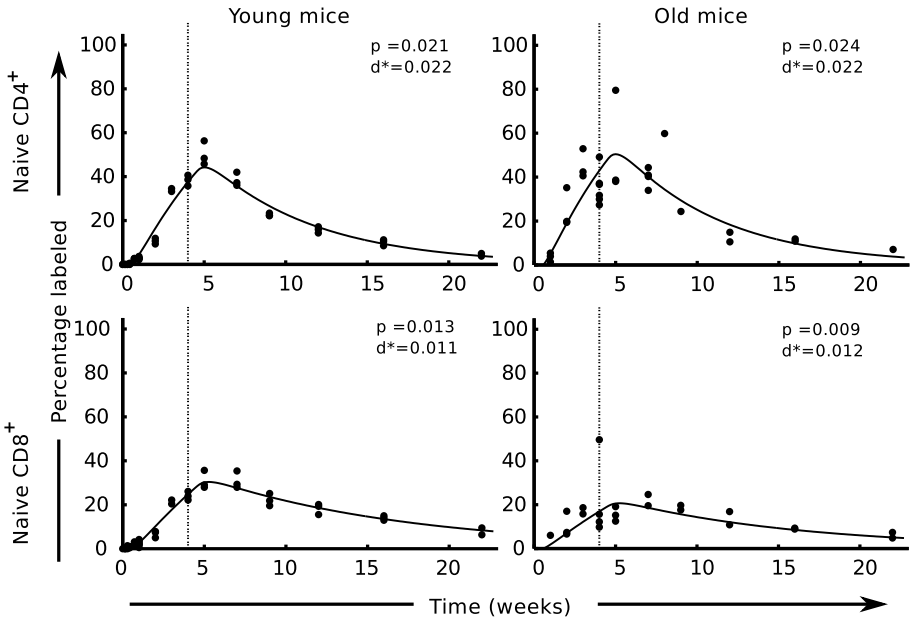

Fig. 3.1: Estimating average naive $CD4^+$ and $CD8^+$ T cell turnover rates from deuterium labeling experiments. (a) 12-week old and (b) 85 week-old mice were given 4% ^2H_2O for four weeks. Each dot in the graphs represents the normalized deuterium enrichment in the DNA of naive $CD4^+$ (upper graphs) or naive $CD8^+$ T cells (lower graphs) in the spleen of one C57Bl/6 mouse. The vertical lines mark the end of ^2H_2O administration at four weeks. The level of label enrichment was normalized to that of thymocytes (see Methods). The data were fitted with a mathematical model described in Methods. The estimated average turnover rates (p) and death rates of the labeled cells (d^*) are given in each graph.

exponentially after birth, after which they peaked at week 6/7, and decreased by almost 40% during week seven. Thereafter, thymocyte numbers declined exponentially at a rate of 50% per year (see Methods and Fig. S.3.1A). Naive T cell numbers in spleen and PLNs peaked at week 7/8, and subsequently declined more slowly than thymocyte numbers. In combination with the long-lasting slow decline of naive T cell numbers after thymectomy, these data suggest that a homeostatic mechanism compensates for loss of thymus output.

Homeostatic compensation through decreased peripheral cell death. A likely homeostatic mechanism by which cell numbers are regulated is a cellular survival rate that depends on the population density [37]. When T cell numbers are low, T lymphocytes will experience less competition for survival signals, such as contact with MHC-peptide ligands or cytokines, and thus have a longer life expectancy. To study the relative contribution of thymus output

Table. 3.1: Estimated average life spans of naive $CD4^+$ and $CD8^+$ T cells in euthymic and thymectomized mice.

Method	Age	Average life spans (days) [a]	
		Naive $CD4^+$	Naive $CD8^+$
^2H_2O	12 weeks	47 (41 - 54)[b]	80 (67 - 92)
	85 weeks	41 (36 - 47)	116 (94 -139)
Cell counts	7 weeks	23 (22 - 25)	70 (63 - 78)
	12 weeks	31 (29 - 33)	72 (65 - 75)
	85 weeks	46 (43 - 49)	101 (94 - 105)
	12 weeks (Tx)	62 (61 - 64)	113 (105 - 117)

[a] The average life spans of young-adult and old mice were based on the estimated turnover rate (life span = $1/p$) from the deuterium labeling experiments (^2H_2O), and on the combination of estimated parameters from the homeostatic cell death model and the T cell counts at the indicated ages (Cell counts; where the average life span is defined as $1/(r + dnN)$, where N is the average number of naive T cells at the indicated age).

[b] 95% confidence limits are given in brackets.

and peripheral T cell proliferation to the maintenance of the naive T cell pool in mice, we developed a simple mathematical model with parameters that were optimally fitted to the naive T cell counts of euthymic and thymectomized mice of different ages that were measured experimentally. The model describes thymus output, peripheral T cell renewal, and naive T cell loss, which represents both cell death and priming of naive T cells into the memory T cell pool (see Material and Methods), and which depends on the number of T cells present (Fig. S.3.1B). The naive $CD4^+$ and $CD8^+$ T cell counts of euthymic and thymectomized mice turned out to be described very well with a simple model that totally lacks peripheral renewal of naive T cells but allows for an increase in the average life span when T cell numbers decline (Fig. 3.2).

According to this homeostatic survival model, the average life spans of naive $CD4^+$ and $CD8^+$ T cells in 12-week old mice are 31 and 72 days, respectively, which is in reasonable agreement with the 47 and 80 day expected life spans estimated from the deuterium labeling experiments (Table 3.1). Because the export of naive T cells from the thymus is proportional to the number of SP thymocytes [7] (depicted in Fig. S.3.1A), we could estimated that every day 3.4% (3.2 - 3.6%) of the SP-thymocyte pool emigrates from the thymus to the spleen (Table S.3.1). In 14-week old mice this corresponds to a daily emigration of 3.6×10^5 newly produced naive $CD4^+$ and 1.4×10^5 naive $CD8^+$ T cells to the spleen. These estimates were solely derived from modeling of thymocyte numbers and naive T cell numbers in euthymic and thymectomized mice. From the ^2H_2O labeling experiments in euthymic mice described above, we independently calculated the total daily production of naive T cells by multiplying the average turnover rates (p) with the actual number of naive

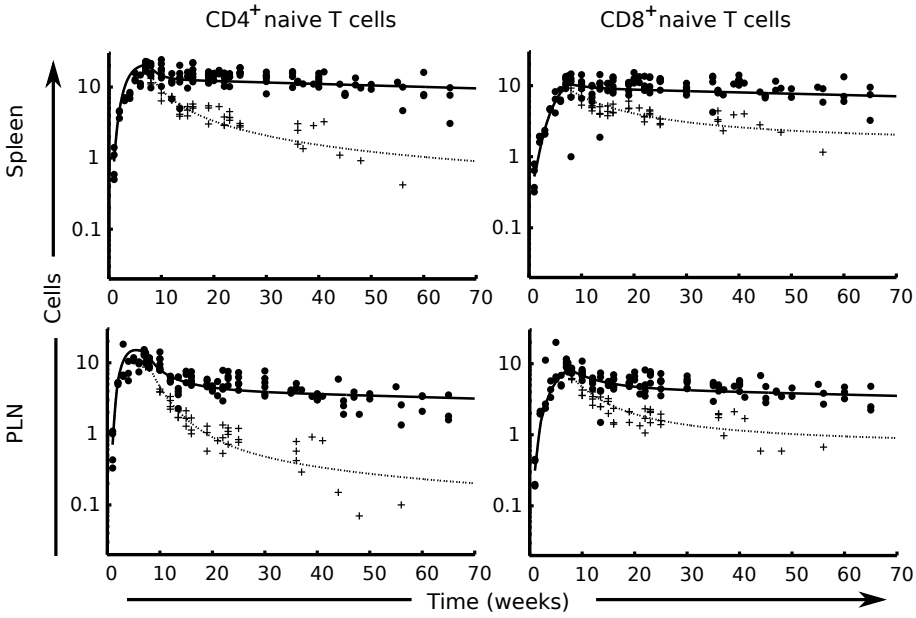

Fig. 3.2: Size of the naive $CD4^+$ and $CD8^+$ T cell populations over age in euthymic and thymectomized mice: the population density model. Numbers ($\times 10^6$) of naive $CD4^+$ (left panels) and naive $CD8^+$ T cells (right panels) were determined in spleen (upper graphs) and PLNs (lower graphs) of euthymic mice (•) and mice that had been thymectomized at week 7 (+). The population densities in control and thymectomized mice were fitted to a mathematical model allowing for a source from the thymus proportional to the number of SP thymocytes, and a cellular death rate that increases linearly with the population density (model (i)) (Fig. S.3.1B and Methods). The best fit of the model to the combined data sets of spleen and lymph nodes of normal and thymectomized mice is depicted by the continuous and dotted lines. Best fitting parameters are given in Table S.3.2, and corresponding average life spans are given in Table 3.1.

T cells in the spleen (N), yielding a total daily production of 2.9×10^5 naive $CD4^+$ and 1.3×10^5 naive $CD8^+$ T cells (supplemental Fig. S.3.2). Since total daily production and daily thymic output are quite similar we conclude that naive $CD4^+$ and $CD8^+$ T cells in young adult C57Bl/6 mice are almost entirely thymus derived and are hardly formed by peripheral T cell proliferation.

Homeostatic compensation through increased peripheral cell division. Since some studies have suggested that T cell proliferation rates may increase when T cell numbers decrease [126], we also analyzed the data with an alternative model, in which the rate of T cell proliferation increases when cell numbers become low (Fig. S.3.1C). The fit of this alternative model to the data of euthymic and thymectomized mice was almost as good as the fit with the model

in which T cell death rates are dependent on T cell densities (Fig. S.3.3). T cell proliferation rates resulting from these analyses were used to calculate average inter-division times: In normal 12-week old mice, the average time between T cell divisions was estimated to be 218 and 655 days for naive $CD8^+$ and $CD4^+$ T cells, respectively. Comparing the estimated average life spans from the deuterium labeling experiments with these average inter-division times shows that naive $CD8^+$ and $CD4^+$ T cells in euthymic mice live on average 3- to 14-fold shorter than their average inter-division times, implying that during their stay in the naive T cell pool most naive T cells never divide.

T cell dynamics in old mice.
Knowing that naive T cell production in young adult mice is almost exclusively due to T cell production by the thymus, we studied naive T cell life spans in old mice which have much lower thymus output. To this end, we performed deuterium labeling experiments in 85-week old mice (Fig. 3.1B). Naive $CD4^+$ T cells in aged mice were found to have an average life span of 41 days, which did not significantly differ from that in 12-week old mice (47 days). The expected life span of naive $CD8^+$ T cells was found to be 116 days, which is nearly 50% longer than that in young adult mice (80 days, Table 3.1). Total daily naive $CD4^+$ T cell production ($p \times N$) in old (60-65 weeks of age) mice was on average 1.9×10^5 cells, of which 1.7×10^5 were produced by the thymus (Fig. S.3.2). Similarly, of the 0.63×10^5 naive $CD8^+$ T cells produced per day in old (60-65 weeks of age) mice, all cells were produced by the thymus (Fig. 3.3B). Thus, even in old mice, in which thymus output has dropped significantly, naive $CD4^+$ and $CD8^+$ T cells are almost entirely produced by the thymus, and hardly by peripheral T cell proliferation.

TREC dynamics in mice.
The result that peripheral T cell proliferation hardly contributes to the maintenance of the naive T cell pool in mice is in sharp contrast with observations on TREC dynamics in humans. TRECs are stable episomal DNA circles that can only be formed in the thymus, and are not replicated during cell division. The fraction of $TREC^+$ naive T cells is therefore proportional to the fraction of naive T cells that were originally produced by the thymus [32, 51] (see also the SI). In humans the fraction of $TREC^+$ naive T cells declines approximately 5% [69, 105] (Vrisekoop, unpublished data) to 10% per year [46, 107], suggesting that in humans the number of naive T cells that originally came from the thymus halves every 7 to 14 years. An experimental prediction that naturally follows from our results is that in contrast to humans the fraction of $TREC^+$ naive $CD4^+$ and $CD8^+$ T cells in healthy mice should not decrease with age. We tested this prediction by comparing the average TREC contents of SP thymocytes and naive T cells from normal euthymic mice of 20-39 and 82-104 weeks of age. We found less than a two-fold difference between the TREC content of SP thymocytes and peripheral naive T cells, and no evidence for TREC dilution in mouse naive T cells with age (Fig. 3.3). This is independent experimental confirmation of our main finding that irrespective of their age

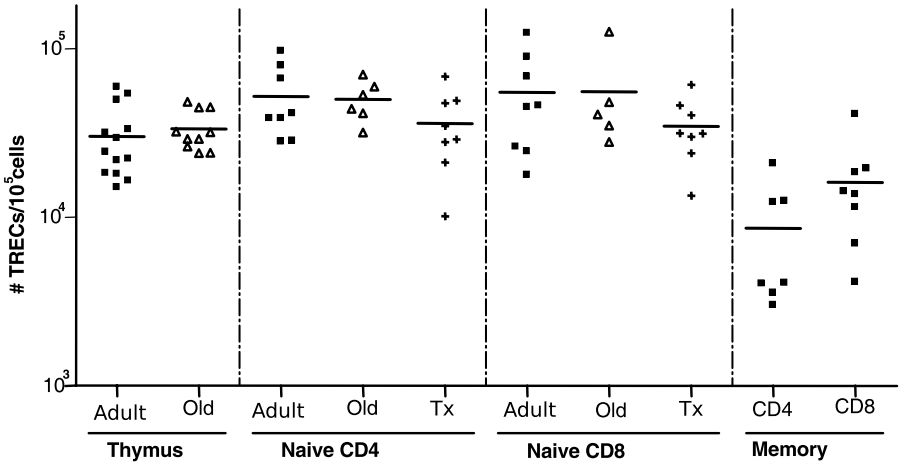

Fig. 3.3: TREC analysis in SP thymocytes and peripheral T cell subsets. The number of SjTRECs per naive T cell were determined by real time quantitative PCR in adult (20-39 week old) mice (control or thymectomized [Tx] at week 7) and in old (82-104 week old) mice. Horizontal bars depict median values. As controls, TREC contents of effector/memory (E/M) T cells and SP thymocytes were included. There were no significant differences between TREC contents in naive T cells from young adult, old or Tx mice. TREC contents in SP thymocytes tended to be slightly higher than in naive T cells ($p = 0.047$ for $CD4^+$ T cells), whereas TREC contents in memory T cells were significantly lower than those in naive T cells ($p = 0.000$ for $CD4^+$ and $p = 0.002$ for $CD8^+$ T cells).

naive $CD4^+$ and $CD8^+$ T cells in euthymic mice are almost exclusively formed by thymus output. Interestingly, even in thymectomized mice the fractions of $TREC^+$ naive T cells were hardly decreased, showing that even under these relatively lymphopenic conditions mouse naive T cells are hardly formed by peripheral T cell division.

3.3 Discussion

We here present several lines of evidence that in contrast to human naive T lymphocytes mouse naive T cells are hardly formed by peripheral T cell proliferation. The limited role for peripheral T cell proliferation in the maintenance of the naive T cell pool in mice that we report here is fully compatible with in vivo BrdU labeling results in classical studies [127, 130, 135], and with our own previous findings of deuterium labeling experiments in thymectomized C57Bl/6 mice [136]. Converting the 10 % of labeled cells in terms of a daily production rate, these data suggest that per day maximally 0.3% of all naive T cells in euthymic mice undergo peripheral proliferation while maintaining the

naive phenotype, which is 5-10 times less than the total daily production rates of naive $CD4^+$ and $CD8^+$ T cells in normal mice that we estimated here. These findings are perfectly in line with our observation that TREC frequencies of naive T cells in thymectomized mice are hardly diluted. In fact, in 12-week old mice thymectomized at 7 weeks of age, the numbers of naive $CD4^+$ and $CD8^+$ T cells in the periphery could fully be explained by an increase of average life spans (of 62 and 113 days, respectively, Table 3.1). Apparently, if present at all, almost all naive peripheral proliferation induces loss of the naive phenotype. This agrees well with the view that most naive T cells triggered to divide by lymphopenia obtain effector or memory (like) T cells characteristics [126].

The conclusion that peripheral T cell proliferation hardly contributes to the maintenance of the naive T cell pool in mice was independently and experimentally confirmed by our demonstration of a lack of TREC dilution in the naive T cell compartment of aging mice. In humans, there is ample evidence that naive T cell TREC contents decline about 100-fold from early adulthood to old age [46, 65, 69]. This gradual TREC dilution has been shown to be evidence for peripheral T cell proliferation within the naive lymphocyte pool of humans [32, 51]. Studies from our own laboratory have pointed out that in healthy children total body TREC numbers are stable when total body naive T cell numbers are still increasing, suggesting that even in young children a substantial proportion of naive T cells is derived from peripheral T cell renewal [53]. Our current finding that naive T cells in the mouse have a relatively short life span, and are almost completely thymus derived, contrasts strongly with the long life span of naive T cells and the predominant role of peripheral T cell proliferation in the maintenance of the naive T cell pool in humans.

It has previously been proposed that the naive T cell pool consists of two different subsets with different kinetics: a pool of recent thymus emigrants (RTE), with an expected life span of about 3 weeks, and a subset of resident naive T cells with slower turnover [8, 25, 99, 130]. Our previously reported deuterium labeling studies in young human adults has provided no evidence for such kinetic differences within the naive T cell pool [136]. On the contrary, recently produced naive T cells in human adults were found to have a longer life expectancy than resident naive T cells, because the loss rate of labeled cells, d^*, was found to be lower than the average production rate, p [136]. In mice, the loss rates of labeled cells, d^*, did not significantly differ from the average production rates, p, suggesting that naive T cells in adult mice form a kinetically homogeneous population, and that there is no kinetically separate RTE population. In addition, we here show that naive T cell numbers in euthymic and thymectomized mice can perfectly be explained by a model that does not incorporate separate RTE dynamics. Different biological markers are used to identify naive T cells in mice, (CD67L and CD44 and in humans (CD27 and CD45RA). This difference in naive T cell definition may be the driving force behind the difference in dynamics and composition of naive T cells between mice and humans. However since extrapolation from mice to

humans is generally done based on these markers, our conclusions therefore still hold.

The present findings have bearing on our understanding of the maintenance of naive T cell numbers and the diversity of the TCR repertoire throughout life and how this fundamentally differs between mouse and man. In mice, the naive T cell repertoire is sustained because of a total thymus dependency of naive T cells. In humans, T cell maintenance is less dependent on the thymus and is sustained by peripheral T cell generation at the expense of the breadth of the TCR repertoire. The major implication of this work is that one cannot freely extrapolate insights obtained from naive T cell kinetic data from young adult (or old) mice to young adult (or old) humans, for the source by which naive T cell numbers are maintained is qualitatively different between mice and men.

3.4 Methods

Mice
C57Bl/6 mice were maintained by in house breeding at the Netherlands Cancer Institute in Amsterdam (thymectomy experiments) or the Central Animal Facility at Utrecht University in Utrecht (^2H_2O labeling) under specific pathogen free conditions in accordance with institutional and national guidelines. Thymectomy was performed as previously described [136]. ^2H_2O labeling was achieved by giving mice one boost injection (i.p.) of 15 ml/kg with 99.8% ^2H_2O (Cambridge Isotopes, Cambridge, MA), followed by subsequent feeding with 4% ^2H_2O in the drinking water for four weeks.

Antibodies
PE-conjugated antibodies recognizing CD62L (clone MEL-14), PerCP-labeled CD4 (clone RM4-5) and CD8 (clone 53-6.7), and APC-labeled CD44 (clone IM7) were purchased from BD Biosciences PharMingen (San Diego, CA).

Cell preparation and flow cytometry
Spleen, (axillary, brachial, inguinal and superficial cervical) peripheral lymph nodes (PLNs) and (if present) thymus were isolated from C57Bl/6 mice of different ages and mechanically disrupted to obtain single cell suspensions. Cell preparation and FACS staining were performed as previously described [136]. Cells were analyzed on an LSR II flow cytometer and BD FACSDiva software. Naive ($CD62L^+$, $CD44^-$) cells were sorted using a FACSAria cell sorter and FACSDiva software (BD). The average purity was: 98.4 ± 1.0% (naive $CD4^+$, 96.3 - 99.7%), 97.2 ± 1.6% (effector/memory $CD4^+$, 92.8 - 99.2%), 98.4 ± 1.1% (naive $CD8^+$, 94.8 - 99.7%) and 96.0 ± 2.1% (effector/memory $CD8^+$, 89.6 - 99.3%). Thymocytes and sorted T cells were frozen until further processed.

Measurement of ^2H_2O enrichment in plasma and DNA
Deuterium enrichment in plasma was measured as reported by Previs et al. [106]. The isotopic enrichment of DNA was determined as previously described [136].

Mathematical modeling of ^2H_2O data
Enrichment data were fitted using a previously developed mathematical model [5] which was extended to allow for a delay with which labeled cells reach the spleen. Best fits were determined by minimizing the sum of squared residuals after arc-sin(square-root) transformation, because all enrichment data were expressed as fractions. The best fits for the enrichment in plasma and rapidly turning over thymocytes are shown in Fig. S.3.4 and the corresponding parameter estimates are given in Table S.3.3. All cellular enrichment data were normalized by the maximal enrichment level observed in thymocytes [136]. The 95% confidence intervals (CIs) for the inferred parameters were determined using a bootstrap method [33], where the residuals to the optimal fit were resampled 500 times.

Mathematical modeling of thymectomy data
We devised a mathematical model to quantify naive T cell dynamics in control and thymectomized mice, and we considered that under normal conditions naive T cells are maintained by thymic output and peripheral T cell proliferation, while they are lost via differentiation into effector/memory T cells, and through cell death. Thymic output was described by a phenomenological function $f_1(t)$, which is proportional to the number of single positive (SP) thymocytes. The fraction of sp thymocytes exported to the spleen daily is given by ϵ . The function is a modification of the thymus involution function described by Steinmann et al. [124] and is explained below.

Both cell death rates (d_nN, Fig. S.3.1B) and proliferation rates ($\frac{r}{1+N/h}$, Fig. S.3.1C) were allowed to be density-dependent, i.e, we allowed cells to live longer and/or proliferate more frequently under lymphopenic conditions, when survival signals are more abundant. The differential equation for the number of naive T cells (N) is consequently given by:

$$N' = \epsilon f_1(t) + \frac{r}{1+N/h}N - d_nN^2$$

To investigate the minimum model required to describe the data we considered two extreme cases of the mathematical model by allowing for:
(i) density-independent proliferation and density-dependent death rates,
i.e: $N' = \epsilon f_1(t) + rN - d_nN^2$, or for:
(ii) density-independent death and density-dependent proliferation rates,
i.e: $N' = \epsilon f_1(t) + \frac{r}{1+N/h}N - d_nN$.
Since naive T cells have an intrinsic (limited) lifespan [25], density-independent death should always be present. As proliferation, differentiation and density-independent cell death rates were all proposed to be constants, a net proliferation rate (r) was used in model (i). Similarly, in model (ii) the net death rate d_n includes differentiation.

Since T cells continuously recirculate through the body, it seems reasonable to let naive T cell dynamics in different organs be similar. We therefore

simultaneously fitted the dynamics in the spleen and PLN, and related the two with a proportionality function, $f_2(t)$ (described below), which was fitted to the cell densities in the two organs, i.e. $N_{PLN} = f_2(t)N_{Spleen}$ where N_{PLN} and N_{Spleen} are the numbers of naive $CD4^+$ and $CD8^+$ T cells in peripheral lymph nodes and spleen, respectively. Parameter estimates of the differential equations were obtained by fitting the prediction of the total cell number, N, to the data (taking the natural logarithm) based on the Levenberg-Marquardt algorithm [83] for solving nonlinear least-squares problems. The 95% confidence intervals (CIs) for the inferred parameters were determined using a bootstrap method [33], where the residuals to the optimal fit were resampled 500 times.

Mathematical modeling of the thymic output function and the proportionality function

We described both the thymic output function and the proportionality function between cell numbers in lymph nodes and spleen by a phenomenological function $f_i(t)$ (where $i = 1$ for the function describing thymic output and $i = 2$ for the proportionality function):

$$f_i(t) = \begin{cases} \sigma(1 - e^{-s_1 t}) & \text{for} \quad t \leq t_{off} \\ f_i(T_{off}) \left[\alpha e^{-s_2(t-T_{off})} + (1+\alpha)e^{-s_3(t-T_{off})}\right] & \text{for} \quad t > T_{off} \end{cases}$$

The function is composed of a sum of exponents with constants s_1, s_2 and s_3. The initial increase of the function until time $t = T_{off}$ has an up-slope given by s_1 and reaches a maximum σ if $T_{off} \to T$. Starting at T_{off}, the biphasic decrease of the function is described by a sum of two exponents with s_2 describing the initial fast slope and s_3 the later slower slope. These two exponents are weighted by a constant $0 \leq \alpha \leq 1$. The parameter values of the best fit of this function $f_i(t)$ to the SP thymocyte data ($f_1(t)$, Fig. S.3.1A) are shown in Table S.3.1, and the parameter estimates of the best fit of the function to the ratios of the lymphocyte counts in lymph nodes and spleen (N_{PLN}/N_{Spleen}) for control and thymectomized mice ($f_2(t)$, Fig. S.3.5) are given in Table S.3.4.

Mathematical modeling of TREC dynamics

Writing a model for naive T cell dynamics and their TRECs [51], demonstrates that at quasi steady state the average TREC content, A, obeys the equation $A/c = \epsilon f_1(t)/(\epsilon f_1(t)+pN)$, where c is the TREC content of an RTE, and $\epsilon f_1(t)$ and pN are the daily production rates of naive T cells by the thymus and by peripheral renewal, respectively. The scaled TREC content, A/c, thus provides a measure for the fraction of naive T cells that were originally produced by the thymus. This result is also intuitive, because one could view a TREC as a marker that is unique for a cell that was originally produced by the thymus, and that is not passed on to new daughter cells upon peripheral division.

Statistical analysis

The Mann-Whitney test was performed to determine differences between mouse groups. All statistical analyses were performed using the software program

SPSS 15.0 (SPSS Inc, Chicago, Illinois). Differences with $p \leq 0.05$ were considered significant. Mathematical models (model (i) and model (ii)) were compared using the sum of squared residuals.

*A*cknowledgments

Our special thanks go to Vitaly Ganusov, Mette Hazenberg, Loes Rijswijk, Henk Starrevelt, Sjaak Greeven, and Linda Nijdam for their technical assistance and theoretical input. We thank Linde Meyaard and Grada van Bleek for stimulating discussions. This research has been funded by the Landsteiner Foundation for Blood Transfusion Research (LSBR grant 0210) and the Netherlands Organization for Scientific Research (NWO, grants 016.048.603 and 836.07.002).

3.5 Supplementary information.

Table. S.3.1: Parameters values of the best fit of the thymic output function $f_1(t)$ to $CD4^+$ and $CD8^+$ single positive thymocyte data[a].

	Parameter	Value (confidence limits)[b]
$CD4^+$ SP[c]	$\sigma(\times 10^7$ cells$)^d$	3.459 (3.224 - 3.772)
	s_1 (day^{-1})^d	0.084 (0.065 - 0.106)
$CD8^+$ SP[c]	$\sigma(\times 10^7$ cells$)^d$	1.679 (1.074 - 9.786)
	s_1 (day^{-1})^c	0.023 (0.003 - 0.056)
$CD4^+$ SP , $CD8^+$ SP[c]	s_2 (day^{-1})^e	0.524 (0.187 - 2.961)
	s_3(day^{-1})^e	0.001 (0.001 - 0.002)
	T_{off} (days)	46.88 (42.00 - 48.58)
	α	0.352 (0.313 - 0.384)

[a] Values are estimates of the best fit depicted in Fig. S.3.1A.

[b] 95% confidence intervals.

[c] While the generation of $CD4^+$ and $CD8^+$ SP thymocytes differs, the mechanism and driving force of thymus involution is the same. Therefore, we allowed $CD4^+$ and $CD8^+$ SP thymocytes to have different dynamics during the establishment of the immune system (σ, s_1) but to have the same thymus involution dynamics $(s_2, s_3, T_{off}$ and $\alpha)$

[d] $\sigma \times s_1$ is the initial rate at which the thymus becomes populated by thymocytes.

[e] s_2 and s_3 describe the involution of the thymus. The initial involution rate (s_2) was so fast that the number of SP thymocytes halved within a week.

Table. S.3.2: Parameters values of two mathematical models describing naive T cell numbers.

	Parameter	Value (confidence limits)[a]
	Model (i): density-dependent death[b]	
$CD4^+$	$d_n(\times 10^{-9}$ day$^{-1})$	2.479 (2.328 - 2.674)
	r_n (day^{-1})	0
$CD8^+$	$d_n(\times 10^{-9}$ day$^{-1})$	1.489 (1.366 - 1.623)
	r_n (day-1)	0
Shared[c]	ϵ (day^{-1})	0.034 (0.032 - 0.036)
	Model (ii): density-dependent renewal[d]	
$CD4^+$	d_n (day^{-1})[e]	0.021
	r_n (day^{-1})[f]	1
	$h(\times 10^4$ cells)	2.415 (1.750 - 2.415)
$CD8^+$	d_n (day^{-1})[e]	0.013
	r_n(day^{-1})[f]	1
	$h(\times 10^4$ cells)	3.015 (2.630 - 3.524)
Shared[c]	ϵ (day^{-1})	0.022 (0.021 - 0.023)

[a] 95% confidence intervals.

[b] Values are estimates of the best fit depicted in Fig. 3.2.

[c] These parameters were forced to be equal when fitting $CD4^+$ and $CD8^+$ data.

[d] Values are estimates of the best fit depicted in Fig. S.3.3.

[e] Parameter fixed to deuterium enrichment estimate.

[f] The best fit of the model gives a maximal renewal rate $r_n = 1$ for both $CD4^+$ and $CD8^+$ naive T cells.

Table. S.3.3: Parameters values of deuterium enrichment in plasma and in thymocytes[a].

	Parameter	Value (confidence limits)[b]
Plasma[c]	S_0^d	0.015 (0.012 - 0.018)
	d_s (day^{-1})[e]	0.261 (0.230 - 0.272)
	α(day^{-1})[f]	0.006 (0.006 - 0.007)
Thymocytes[g]	$p_{\text{young mice}}$(day^{-1})	0.416 (0.377 - 0.468)
	$p_{\text{old mice}}$ (day^{-1})	0.307 (0.254 - 0.470)

[a] Values are estimates of the best fit depicted in Fig. S.3.4.

[b] 95% confidence intervals.

[c] We take the deuterium enrichment in the plasma to reflect the enrichment in the body water.

[d] s_0 represents the baseline plasma enrichment attained after the boost at the end of day 0.

[e] d_s is the turnover rate of body water.

[f] α is the fraction of deuterated water consumed daily.

[g] Thymocytes where used to normalize the data as described in Vrisekoop et al. [136].

Table. S.3.4: Parameters values of the function $f_2(t)$ a describing the ratio of the number of naive T cells in the PLN over those in the spleen.

Parameter	Value (confidence limits)[b]	
	$CD4^+$	$CD8^+$
Control[c]		
σ	1.578 (1.197 - 2.373)	5.401 (1.399 - 18.58)
s_1	0.098 (0.049 - 0.168)	0.017 (0.004 - 0.096)
s_2	0.024 (0.020 - 0.030)	0.022 (0.015 - 0.030)
s_3	0	0
α	0.723 (0.692 - 0.750)	0.576 (0.523 - 0.618)
T_{off}	14.00 (11.56 - 18.16)	14.72 (11.56 - 19.50)
After thymectomy[d]		
s_2	0.025 (0.016 - 0.041)	0.024 (0.011 - 0.054)
s_3	0	0
α	0.679 (0.597 - 0.784)	0.459 (0.363 - 0.589)

[a] Values are estimates of the best fit depicted in Fig. S.3.5.

[b] 95% confidence intervals.

[c] The upper part of the table shows parameter values of the best fit to control mice data.

[d] The lower part shows parameters values of the best fit to data from thymectomized mice (from the time of thymectomy onward, $t > 49$ days).

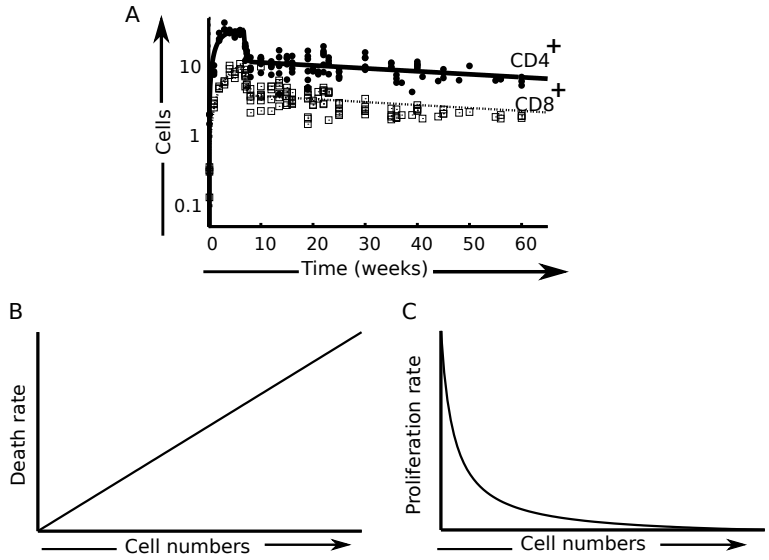

Fig. S.3.1: Visual representation of model parameters. The number ($\times 10^6$) of single positive thymocytes from C57Bl/6 mice of different ages (a). The continuous and dotted lines represent the best fits of the thymic output function $f_1(t)$ to $CD4^+$ ($\bullet$) and $CD8^+$ ($\square$) SP thymocyte data. Model parameters are given in Table S.3.1. Graphical representation of the dependence of the death rate on T cell population densities in the first model (b), and dependence of the proliferation rate on T cell population densities in the second model(c).

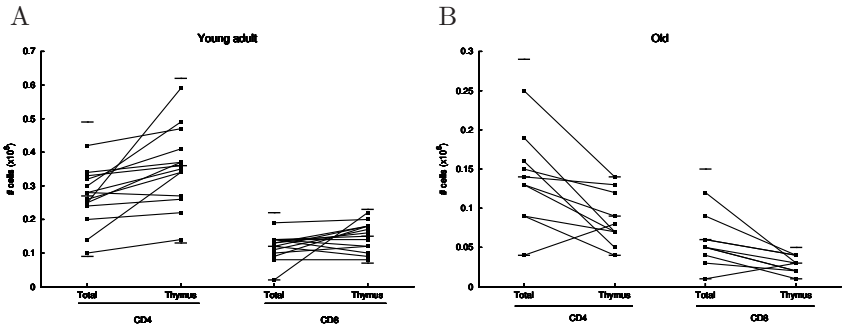

Fig. S.3.2: Comparison of total daily naive T cell production and thymic output over age Total daily naive T cell production in spleens from young adult mice and old mice were estimated by multiplying the average production rates from the ^2H_2O-labeling experiment in young adult (Fig. 3.1A) and old (Fig. 3.1B) mice with the naive T cell numbers in the spleen of each mouse. Thymic output of the same mice was calculated by multiplying the estimated thymic output rate ($\epsilon = 0.034$) with the absolute number of single positive thymocytes of the mice. The medians of the data in each group are indicated by a dashed line.

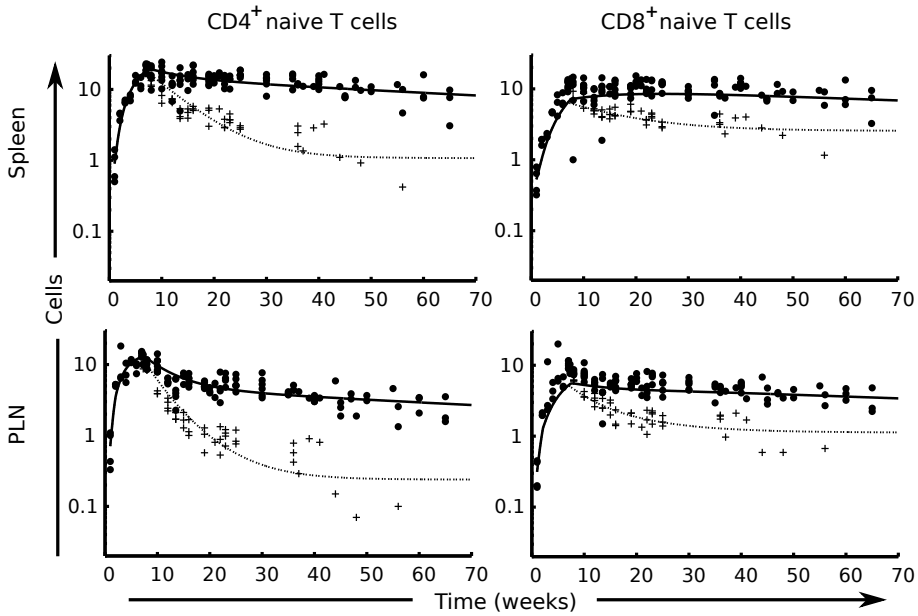

Fig. S.3.3: Size of the naive $CD4^+$ and $CD8^+$ T cell populations over age in euthymic and thymectomized mice: the homeostatic proliferation model. Best fits of the homeostatic proliferation model (model (i)) to naive $CD4^+$ and $CD8^+$ T cell counts ($\times 10^6$) in spleen (upper graphs) and PLNs (lower graphs), in control ($\bullet$) and thymectomized (+) C57Bl/6 mice. The cellular death rates were fixed to the estimates obtained with deuterium labeling (Fig. 3.1).

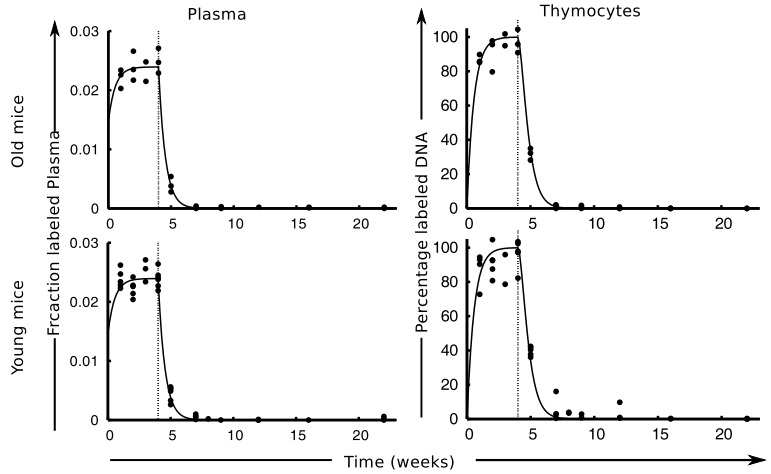

Fig. S.3.4: Deuterium enrichment in plasma and thymocytes. Best fits of plasma ^2H_2O and thymocyte deuterium enrichment in young adult and old mice[136]. Parameter values are given in Table S.3.3.

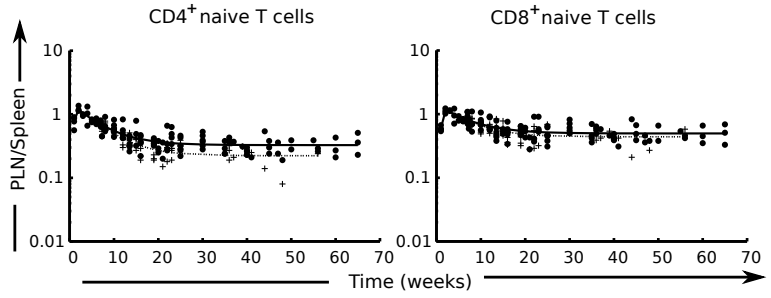

Fig. S.3.5: Proportionality function $f_2(t)$ between T cell numbers in peripheral lymph nodes (PLNs) and spleen. The proportionality function describes the proportion between naive T cell numbers in PLNs and spleen. The continuous and dotted lines represent the best fits of the proportionality function to data from control (•) and thymectomized (+) mice, respectively. Model parameters are provided in Table S.3.4.

4

No evidence for separate dynamics of recent thymic emigrants: thymus grafting experiments revisited.

Tendai Mugwagwa[1], Ineke den Braber[2], Kiki Tesselaar[2], José A.M Borghans[1,2] and Rob J. de Boer[1].

[1]Department of Theoretical Biology , Utrecht University, Utrecht, The Netherlands.
[2]Department of Immunology, University Medical center Utrecht, Utrecht, The Netherlands.

Abstract

It is generally believed that the naive T cell pool consists of a population of relatively long-lived resident naive T cells and a population of short-lived recent thymic emigrants (RTE). Both stable isotope labeling of naive T cells in mice and humans, and thymectomy studies in mice, however, have not provided any evidence for such kinetic heterogeneity in the naive T cell pool. The strongest support for the existence of a kinetically separate population of RTEs comes from thymus transplantation studies, which suggested that RTE are exempted from homeostatic control for about 3 weeks, after which they either die or become part of the resident naive T cell pool. Here, we revisit these thymus grafting experiments and show that the results from these studies are in fact fully compatible with a model in which RTE and "resident" naive T cells are kinetically identical. Taken together, there is no evidence (neither in mice, nor in men) that RTE form a kinetically distinct sub-population within the naive T cell pool.

4.1 Introduction

It is generally believed that the naive T cell pool is composed of two kinetically distinct sub-populations, RTEs and "resident" naive T cells. However, the direct assessment of RTE dynamics in mice and men is hampered by the lack of an RTE marker, which is only available in rats and chickens [64, 72]. TCR excision circles (TRECs), expression of the cell surface marker CD31, and green fluorescent protein (GFP) expressed under the RAG promoter[13, 70, 73] have been used as surrogate markers for thymic export. However, some of these measures are influenced by a combination of thymic export, cell division, and longevity of thymic emigrants and thus cannot give a strict definition of an RTE [51, 69]. Recently, in humans, protein tyrosine kinase 7 (PTK7) was introduced, as a potentially better RTE marker [44].

Although there is consensus that T cell numbers are regulated through competition for survival signals [127], some studies have suggested that RTEs are excluded from peripheral homeostatic control [7, 8]. To study the dynamics of RTEs in mice, Berzins et al. [7] grafted neonatal thymic lobes beneath the kidney capsule of 5-6 week old $C57BL/6$ mice. They found that grafting 2, 6 or 9 neonatal thymus lobes resulted in an almost linear steady state increase in total T cell numbers in the spleen of 21×10^6, 71×10^6 and 111×10^6 T cells. Based on an estimated thymic output of 10^6 cells per day, the increase in total T cell numbers corresponded to the accumulation of RTEs from the grafts over a 3 week period. In another study [7], grafting thymic lobes from congenic $Ly5.2^+$ mice into $Ly5.2^-$ mice suggested that RTEs are rapidly lost from the peripheral T cell pool, i.e. in about 4 weeks about 87% percent of $Ly5.2^+$ were lost. These studies suggested that the RTE population is composed of T cells that live on average for approximately 3 weeks, independent of the peripheral

naive T cell density [7, 8]. Berzins et al. [8] therefore claimed that during these 3 weeks, RTEs were exempted from homeostatic control.

Based on our own data described in Chapters 2 and 3, we did not find any evidence for a kinetically heterogeneous naive T cell pool. Since the thymus transplantation experiments by Berzins et al. [8] form the basis for the concept that RTEs are a kinetically separate T cell sub-population, we revisited the thymus grafting experiments [7, 8] and used mathematical models to investigate whether a separate RTE sub-population is necessary to explain this data.

4.2 Results

T cell dynamics in control and thymectomized mice.
To investigate whether the conjecture that RTEs form a dynamically separate population is necessary to explain the thymus grafting experiment data of Berzins et al [7, 8], we compare 2 mathematical models. In one model, naive T cells consist of two kinetically distinct populations (RTE model), and in another model, the naive T cell pool is kinetically homogeneous and regulated by density dependent death (homogeneous model). To parametrize these models, we counted the number of single positive (SP) $CD4^+$ and $CD8^+$ thymocytes, as well as naive and memory $CD4^+$ and $CD8^+$ T cells in the spleen (Fig. 4.1,4.2) and peripheral lymph nodes (PLNs) (Fig. S4.1,S4.2) of normal euthymic or sham-thymectomized mice and mice that had been thymectomized (Tx) at seven weeks of age. The data were subsequently fitted by the 2 different mathematical models.

First, we studied whether the "RTE model" (Fig. 4.1) is compatible with the data from control and thymectomised mice. The model describes the data well and predicts that 4% of the SP thymocytes are exported to the spleen daily, which accounts for a daily thymic output of about 1% of total thymocytes, and is in agreement with previous estimates [116]. According to the "RTE model", $CD4^+$ RTEs live on average for 8 days, $CD8^+$ RTEs for 21 days, and about 2% of the RTEs mature into resident naive T cells per day (Table 4.1). When compared to RTEs, resident naive T cells would have slower dynamics, with an average lifespan of 128 and 248 days for $CD4^+$ and $CD8^+$ naive T cells, respectively. At the time of thymectomy (week 7), about 75% of naive $CD4^+$ T cells and about 65% of naive $CD8^+$ T cells are predicted to be RTEs (Fig. 4.3c). This high fraction of RTEs together with their fast dynamics compared to resident naive T cells result in the observed biphasic loss of naive T cells after thymectomy (Fig. 4.1 and Fig. S4.1).

Next we consider a mathematical model (Eqn. 4.2) in which the naive T cell population is homogeneous and densities regulate cell numbers in the periphery. Fitting this "homogeneous" model to data from control and thymectomized mice (Fig. 4.2, Fig. S4.2 and chapter 3) we estimate that the daily contribution of $CD4^+$ and $CD8^+$ single positive (SP) thymocytes to the spleen is about 3%.

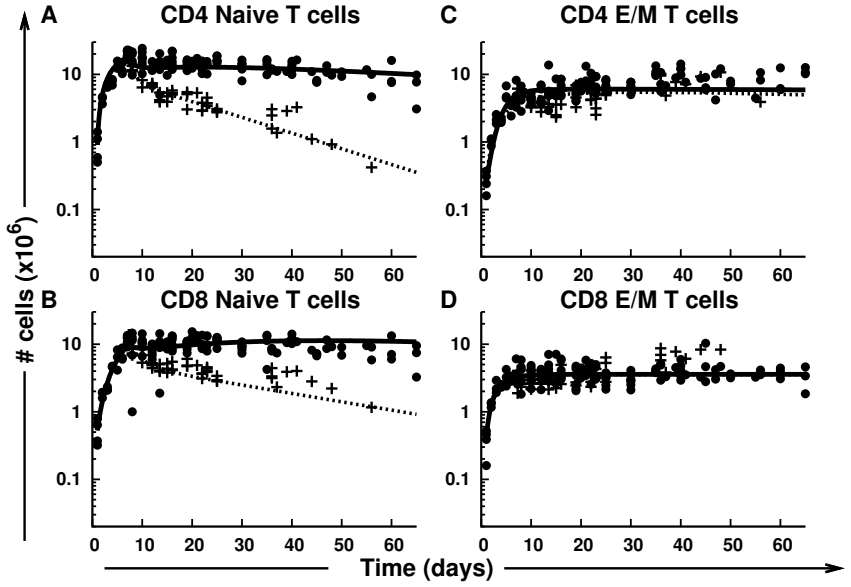

Fig. 4.1: Simulation results of fitting the "RTE model" to data on $CD4^+$ and $CD8^+$ T cell numbers from the spleen of control and thymectomised mice. Results are shown for different subsets:(a) $CD4^+$ and (b) $CD8^+$ naive T cells and (c) $CD4^+$ and (d) $CD8^+$ memory T cells from control mice (bullets) and thymectomised mice (crosses). The continuous and dotted lines show the best fit of the mathematical model with parameter values given in Table 4.1

Table. 4.1: Parameter results from fitting the "RTE model" to control and thymectomised mice data.

Parameter	**CD4**	**CD8**
d_r	0.122 (0.095−0.164)	0.047 (0.029−0.075)
d_n	0.008 (0.007−0.009)	0.004 (0.003−0.005)
a_n	0.020 (0.015−0.027)	0.016 (0.008−0.026)
a_m	0.007 (0−0.011)	0 (0−0.044)
r	0.190 (0.150−0.268)	0.856 (0.415−1.000)
h x10^5	41.610 (27.410−62.480)	2.698 (2.043−5.864)
d_m	0.086	0.06
Shared parameter		
ϵ	0.043 (0.037−0.054)	

In 12 week old control mice, naive T cells have an expected lifespan of 32 days for $CD4^+$ naive T cells and 83 days for $CD8^+$ naive T cells (Table 4.2). After thymectomy at the age of 7 weeks, the expected lifespan in 12 week old mice

increases to 56 and 121 days, for $CD4^+$ and $CD8^+$ naive T cells respectively.

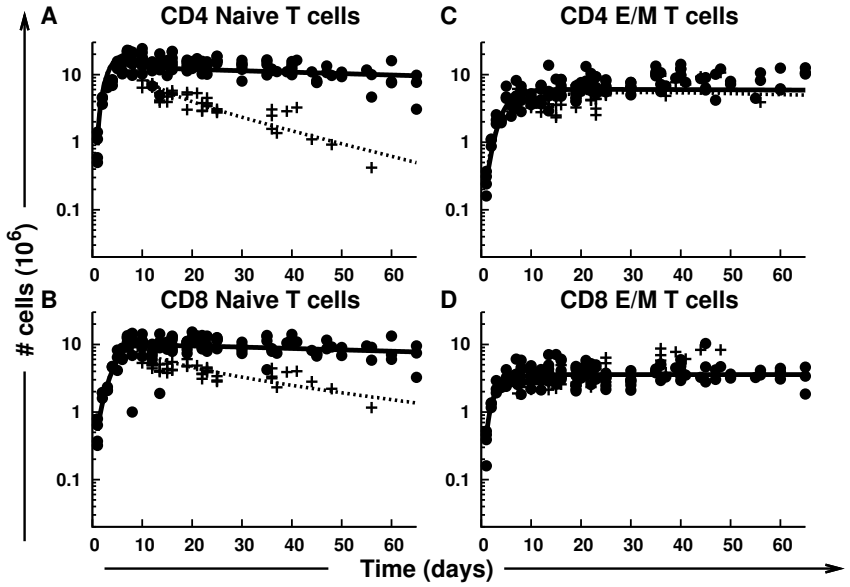

Fig. 4.2: Simulation results of fitting the "homogeneous model" to data on $CD4^+$ and $CD8^+$ T cell numbers from the spleens of control and thymectomised mice. See Fig. 4.1 legend. Parameter values given in Table 4.2

Because Berzins et al [7, 8] measured T cell totals, we also consider the dynamics of the memory T cell pool. To reduce the degrees of freedoms of the model when estimating the activation rate and renewal rates of memory T cells, models we fixed the average life-span of $CD4^+$ and $CD8^+$ memory T cells to our previous estimates from deuterium labeling experiments, i.e. 12 days and 17 days respectively (Chapter 2).

T cell dynamics during thymus grafting.
After parametrization of the mathematical models (Table 4.1,4.2), we checked for consistency of the two models with the thymus grafting experiments [7, 8]. Like Berzins et al. [8], we calculated the percentage increase in total T cell numbers in the spleen, 8 weeks after the thymus grafting. When we simulated the grafting experiments using the "RTE model", we found a similar linear increase in the total number of T cells with increasing thymic output as was found experimentally [8]. However, the linear increase resulting from the model was steeper, with increments of 38%, 115% and 172% of the total number of T cells in the spleen compared to the observed 15%, 50% and 77% after grafting 2, 6 and 9 thymic lobes, respectively [8, Fig. 4.3]. This difference

Table. 4.2: Parameter results from fitting the "homogeneous model" to control and thymectomised mice data with $k = 1$.

Parameter	**CD4**	**CD8**
d_nx10^{-9}	2.396 (2.213−2.585)	1.261 (1.124−1.396)
r	0.335 (0.268−0.389)	0.502 (0.355−0.779)
h x10^5	11.500 (8.457−15.920)	2.262 (0.564−4.188)
a_m	0 (0−0.014)	8x10^{-6} (0−0.104)
d_m	0.086	0.06
Shared parameter		
ϵ	0.032 (0.030−0.034)	
k	1.000	

suggests that the model requires homeostatic control of RTEs, or that the model overestimates the output from the grafted thymic lobes. Using the data available on the number of thymocytes from the grafted thymus [7], suggest that the grafted thymus approaches the same size as the host thymus. However, if the model assumes that the thymus graft grows to only half the size of the host thymus, the "RTE model" would correctly describe the fractional increase in total T cells from the grafting experiment data (Fig. 4.3). Thus the "RTE model" is consistent with both the thymectomy data (Fig. 4.1) and the thymic transplantation data (Fig. 4.3).

Using the "homogeneous model", the model predicted a 21%, 48% and 62% increase after grafting 2, 6 or 9 thymic lobes, respectively. The increase in the peripheral T cell pool saturates due to density dependent regulation of the death rate of naive T cells, which in turn depends on the extent to which death rates are density dependent, which is determined by the parameter k, (Fig. 4.4). This model would predict that there is a critical number of graft thymi beyond which additional grafts have no effect on total T cell numbers. However for the current range ($1 < k < 2$), the model does account for the approximately linear increase found by Berzins et al [7, 8], with the correct steepness (Fig. 4.4). Thus, the "homogeneous model" is also consistent with both the thymectomy data (Fig. 4.2) and the thymic transplantation data (Fig. 4.4).

Ly5.2 T cell dynamics.

In a separate study, Berzins et al. [7] grafted $Ly5.2^+$ thymic lobes into $Ly5.2^-$ mice and followed at the dynamics of $Ly5.2^+$ T cells in the periphery. The grafted thymus exclusively exported graft derived $Ly5.2^+$ T cells for the first 3 weeks. The fraction of $Ly5.2^+$ thymocytes in the grafted thymus then decreased such that by week four, when the grafted thymus was fully reconstituted by host derived thymocytes, all T cells exported from the grafted thymus were host derived. At week 8, Berzins et al. [7] found that only 13% of the total

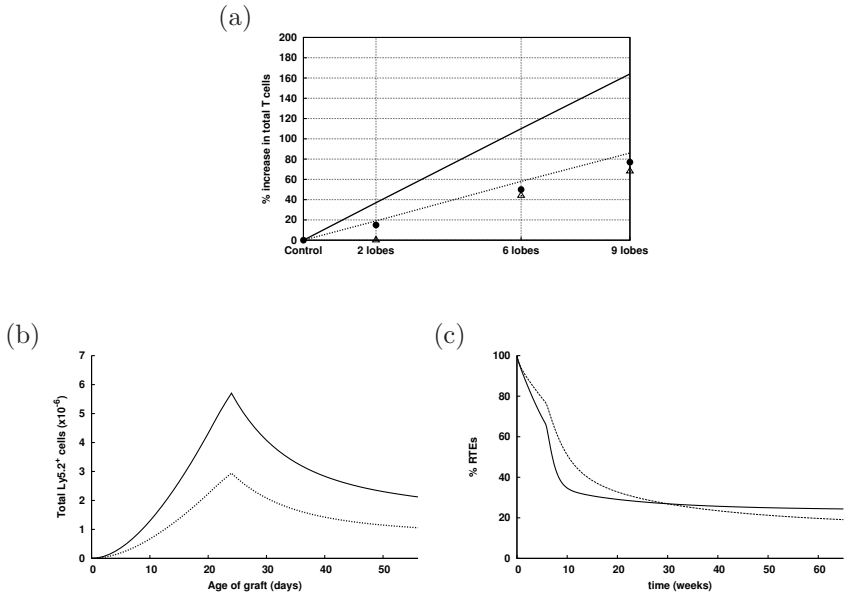

Fig. 4.3: Simulation results of the grafting experiment using the "RTE model". (a) The percentage increase in total T cell numbers in the spleen was calculated assuming that the grafted thymus grows to 100% of the size of the host thymus (continuous line) or to 50% of the size of the host thymus (dotted line). Results are compared to experimental data from Berzins et al [7, 8] (triangles and bullets). (b) The predicted total number of $Ly5.2^+$ T cells in the spleen. (c) The predicted percentage of RTEs present in total naive $CD4^+$ T cells (continuous line) and total naive $CD8^+$ T cells (dotted line).

number of $Ly5.2^+$ T cells present at week 4 remained in the periphery (9% for $CD4^+$ $Ly5.2^+$ T cells and 19% for $CD4^+$ $Ly5.2^+$ T cells).

We simulated this experiment using our models, assuming that all T cells coming from the grafted thymus for the first 3 weeks are $Ly5.2^+$. We consider a conveyor belt system of thymocyte generation and export, such that after week 3 all T cells exported by the grafted thymus are $Ly5.2^-$ T cells. Using the "RTE model", we calculate that 45% of $Ly5.2^+$ T cells present at week 4 should still be present at week 8 (Fig. 4.3b). Similarly, using the "homogeneous model", we calculated that between 25% and 42% of $Ly5.2^+$ T cells present at week 4 should still be present at week 8 (for $k = 2$ and $k = 1$ respectively) (Fig. 4.4b). Both estimates are higher than what was observed by Berzins et al. [7]

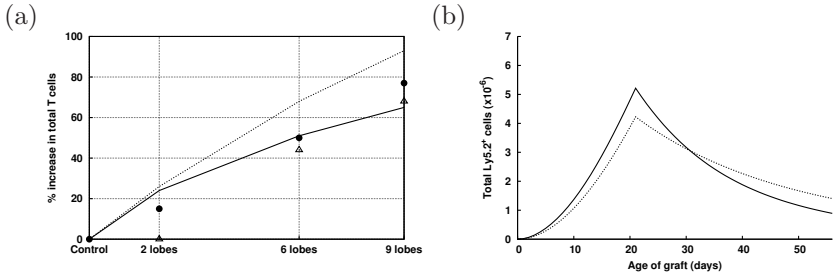

Fig. 4.4: Simulation results of the grafting experiment using the "homogeneous model". (a)The percentage increase in total T cell numbers in the spleen was calculated for the "homogeneous model" with $k = 1$ (dotted line) and $k = 2$ (continuous line) and compared to experimental data from Berzins et al [7, 8] (triangles and bullets). (b) The predicted total number of $Ly5.2^+$ T cells in the spleen from the "homogeneous model" with $k = 1$ (dotted line) and $k = 2$ (continuous line).

4.3 Discussion

Although there is a general agreement that T cell numbers are homeostatically regulated in the periphery, the mechanism behind this control remains controversial. In this study we investigated whether or not RTEs form a kinetically distinct sub-population of the naive T cell pool. Here we show that a model where RTEs form a separate sub-population provides a good description of the T cell numbers after thymectomy (described in chapter 3), as well as T cell numbers after thymus grafting [8]. For the parameter values that best describe the thymectomy data, there is a quantitative (but explainable) disagreement with the thymus grafting data. The predicted T cell numbers after thymus grafting depended strongly on the estimated thymic output from the grafted thymic lobes as compared to the host thymus. The thymus grafting data are explained well with the "RTE model" when the grafted thymus exports about 50% less T cells than the host thymus. Different grafted thymus dynamics have been reported: In rats, the grafted thymus remains smaller than the host thymus [61], however, in CBA mice grafted thymic lobes were shown to approach a similar size as the host thymus [19]. Dominguez-Gerpe and Rey-Mendez [27] also show that gender had an effect on the size of the thymus. Due to limited availability of data, and the possibility of different thymus dynamics in female mice (as used by [7]) and male mice (as used in our thymectomy experiment), we do not know the precise dynamics of the grafted thymus. Additional experiments are therefore needed to accurately determine the size of the grafted thymus and host thymus (work in progress).

Importantly, a model in which all naive T cells are kinetically similar and subject to the same density dependent death rate ("homogeneous model"), can

explain both the thymectomy data and the thymus grafting data. Despite a homeostatic control on naive and memory T cell numbers, the model predicts an approximately linear increase in peripheral T cell numbers after grafting up to 9 thymic lobes. However, the "homogeneous model" predicts that there is a ceiling beyond which additional thymic output would not result in a further increase in peripheral T cell numbers, suggesting that the T cell pool may not be as elastic as previously suggested [8].

By grafting $Ly5.2^+$ thymus lobes into $Ly5.1^+$ mice, Berzins et al. [7] were able to directly assess the dynamics of graft-derived T cells. Berzins et al. [7] found that 8 weeks post-transplantation, only 13% of the total number of $Ly5.2^+$ T cells present at 4 weeks remained in the periphery. In contrast, both the "RTE model" and the "homogeneous model" predicted that 25-45% of the total $Ly5.2^+$ T cells would remain over the same period. This discrepancy cannot easily be explained. Assuming an exponential death rate of RTEs, these data suggest that $Ly5.2^+$ T cells have an average lifespan of 14 days (11 days for $CD4^+$ $Ly5.2^+$ T cells and 17 for $CD4^+$ $Ly5.2^+$ T cells). In the current study, the "RTE model" estimated that $CD4^+$ and $CD8^+$ RTEs live on average for 8 (6-11 days, 95% confidence interval) and 21 days (13-34 days, 95% confidence interval), respectively, which is similar to the turnover rates calculated from the dynamics of $Ly5.2^+$ T cells [7]. However, we cannot directly compare these turnover rates because after 8 weeks, some of the graft derived $Ly5.2^+$ T cells have matured into "resident" naive T cells and effector/memory T cells that may have different turnover rates compared to RTEs. In that sense, the $Ly5.2^+$ T cells measured by Berzins et al. [7] are not exclusively RTEs. When we calculated the turnover rate of $Ly5.2^+$ T cells, both the "RTE model" and the "homogeneous model" predicted that $Ly5.2^+$ T cells live 2-fold longer than the experiment suggested [7]. Since the 14-17 day estimated lifespan of $Ly5.2^+$ T cells is based upon just two data points, it is essential to repeat the experiments and at least separate naive T cells from memory T cells (work in progress).

Mice expressing GFP under the recombination activating gene 2 promoter (Rag2p-GFPtg mice), have been used to follow RTE dynamics. After RAG expression is extinguished, GFP lingers on in the thymus as well as in the periphery with a half-life of 54 hours [13, 45, 85]. Although the short half-life of GFP expression allows for a more strict definition of RTEs, and makes it possible to study their phenotypic features [13, 82], it also hinders its use to study the turnover of RTEs because the data may in fact show the dynamics of GFP expression, rather than that of RTEs [Mugwagwa et al, unpublished result] if the marker disappears faster than the RTEs themselves. This calls for a more stable marker for RTEs, like the recently proposed protein tyrosine kinase 7 (PTK7) [44].

The relative contribution of self renewal of memory T cells versus an input by activation and expansion of naive T cells to the memory T cell pool is un-

known. Currently the only data available suggests that about 35% of $Ly5.2^+$ T cells at 16 weeks post-transplantation are memory T cells [8]. In mice with additional thymic lobes, increasing thymic output allows for increased repertoire diversity in the periphery. If memory T cells are largely independent of naive T cells in adult mice, as suggested by our parameter estimates (Table 4.1 and 4.2), the diversity of the memory T cell repertoire would fail to increase when thymic output is boosted. Since so little is known about the relative contribution of naive T cells to the memory T cell pool, we plan to investigate the accumulation of $Ly5.2^+$ T cells in individual T cell subsets after grafting $Ly5.2^+$ thymus lobes into $Ly5.1^+$ mice.

In summary, both the "RTE model" and the "homogeneous model" are consistent with both the thymectomy experiment data and the thymus grafting experimental data. Therefore, the data that are currently available provide no evidence for the existence of a dynamically separate RTE sub-population. Using deuterium labeling in 12 week old mice, we preciously showed that the naive T cell pool in mice is kinetically homogeneous (den Braber et al, submitted and chapter 2). Similarly in humans, we previously showed that naive T cells are kinetically homogeneous [136]. While the incorporation of RTEs into an established T cell pool may be important to maintain the diversity of the T cell repertoire, RTEs need not have different dynamics from resident naive T cells to achieve this.

4.4 Methods

Mathematical modeling of thymic output.
To simulate the thymus grafting experiments of Berzins et al [7, 8], we compared the limited data available on the number of thymocytes in the grafted thymuses [7] and thymocyte numbers from control mice (Chapter 3, see Fig. 4.5). This suggests that a neonatal thymus implanted into a 5 week old mouse grows to reach the same size as the host thymus within 3 weeks after transplantation. Subsequently the grafted thymus follows the same thymic involution dynamics as the host thymus. In cases where more than one thymus is implanted, each thymus graft grows to the size of the host thymus independent of the number of thymi grafted [87]. In addition, each of these grafts exports the same fraction of thymocytes as the host thymus [7]. We describe thymic output from the host thymus with the function $f(t)$ as described earlier (Chapter 3) and assume an exponential growth of the grafted thymus for 3 weeks, after which it follows the same dynamics as the host thymus, until thymocyte numbers from the graft are equal to those from the host (see insert of Fig. 4.5).

RTE model: *Mathematical modeling of a T cell population with RTEs.*

Considering that RTEs form a separate population from resident naive T cells, we write a mathematical model with three populations, RTEs R, resident naive T cells N, and memory cells M. Input of RTEs into the spleen comes

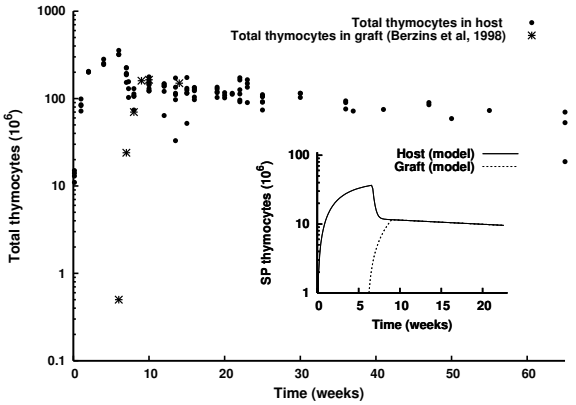

Fig. 4.5: An overlay of total thymocyte data (bullets) from control male B6 mice (Chapter 3) and the total number of thymocytes from neonatal female B6 thymus grafts [7] (asterisks). The insert shows the thymic output function $f(t)$ of the host thymus (continuous line) and the grafted thymus (dashed line) used in the mathematical model.

from the thymus at a rate $\epsilon f(t)$ cells per day. RTEs mature into resident naive T cells at a rate a_n, and are lost either due to death or transition into resident naive T cells at a constant rate d_r. Resident naive T cells in turn are lost either due to death or priming into memory T cells at a constant rate d_n. Resident naive T cells can be activated into memory T cells at a rate $\frac{a_m N}{1+M/h}$ cells per day. Memory T cells are self-renewed at a rate $\frac{rM}{1+M/h}$ cells per day. Both activation and renewal rates depend on the density of memory T cells with a saturation constant h. Memory cells are lost at a constant death rate d_m. The dynamics of RTEs, resident naive T cells and memory T cells are thus given by:

$$\begin{aligned} R^{'} &= \epsilon f(t) - d_r R, \\ N^{'} &= a_n R - d_n N, \\ M^{'} &= \frac{a_m N + rM}{1 + \frac{M}{h}} - d_m M. \end{aligned} \tag{4.1}$$

"Homogeneous model": *Mathematical modeling of the naive T cell population without RTE.*

Assuming that RTEs do not form a kinetically distinct T cell sub-population, we also write a mathematical model with two T cell populations, i.e. naive and memory T cells. Naive T cells, N, enter a peripheral niche, such as the spleen, at a rate $\epsilon f(t)$ per day. At lower cell densities, survival signals are abundant and naive T cells live long, while at higher cell densities they are shorter lived due to scarce survival signals. Thus, in the spleen RTEs are subjected to the

same survival signals as "resident" naive T cells, such that their death rate, $d_n N^k$, is regulated by the total naive T cell population density, where k is the strength of the density dependent regulation. Since we cannot distinguish between death and priming of naive T cells, the term $d_n N^k$ denotes a composite loss rate. Like in the RTE model, naive T cells are activated into memory T cells at a rate $\frac{a_m N}{1+M/h}$. Memory T cells have the same dynamics as in Eqn 4.1. The dynamics of the total naive and memory T cell population is thus given by:

$$\begin{aligned} N^{'} &= \epsilon f(t) - d_n N^{k+1}, \\ M^{'} &= \frac{a_m N + rM}{1 + \frac{M}{h}} - d_m M. \end{aligned} \tag{4.2}$$

4.5 Supplementary information.

Table. S4.1: Parameter results from fitting the homogeneous model to control and thymectomised mice data with $k = 2$.

Parameter	**CD4**	**CD8**
d_nx10^{-16}	3.087 (2.736−3.498)	2.339 (2.020−2.690)
r	0.213 (0.148−0.235)	0.512 (0.324−0.750)
h x10^5	27.380 (22.950−50.600)	2.165 (0.641−4.935)
a_m	4x10^{-4} (0−0.007)	0 (0−0.093)
d_m	0.086	0.06
Shared parameter		
ϵ	0.045 (0.040−0.050)	
k	2	

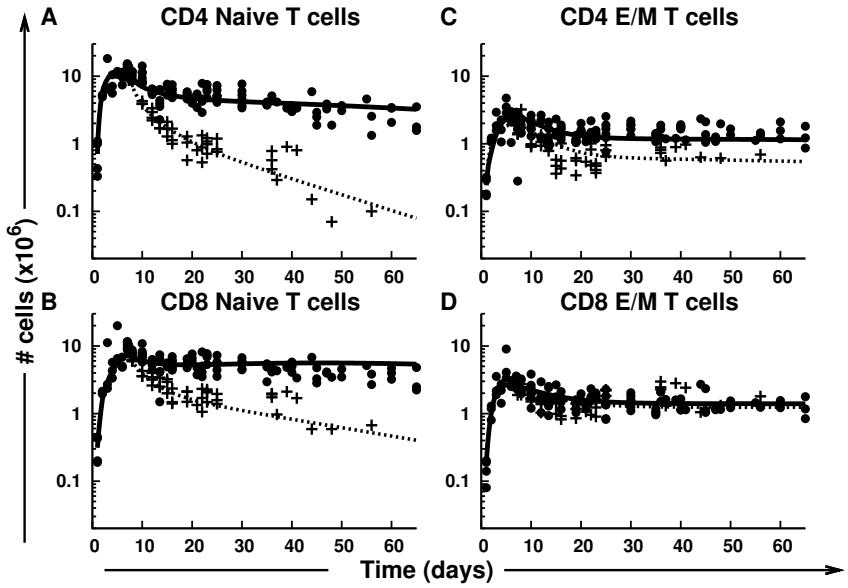

Fig. S4.1: Simulation results of fitting the RTE model to data on $CD4^+$ and $CD8^+$ T cell numbers from the peripheral lymph nodes of control and thymectomised mice. See Fig. 4.1 legend. Parameter values given in Table 4.1

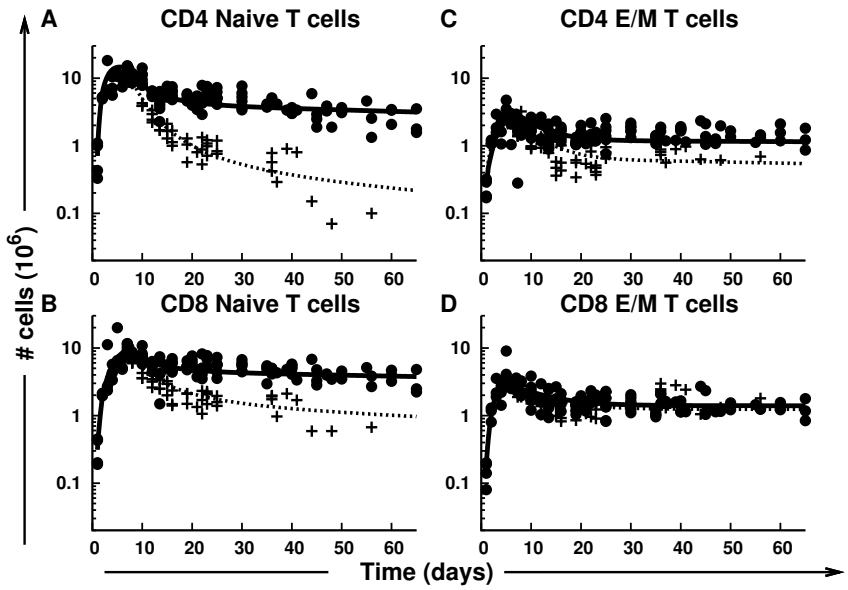

Fig. S4.2: Simulation results of fitting the homogeneous model to data on $CD4^+$ and $CD8^+$ T cell numbers from the peripheral lymph nodes of control and thymectomised mice. See Fig. 4.1 legend. Parameter values given in Table 4.2

5

T cell exhaustion and depletion in mice with chronic immune activation via CD27/CD70 costimulation.

Ineke den Braber[1,*], Tendai Mugwagwa[2,*], Elise H.R. Schrijver[1], Erik Mul[3], Floris van Alphen[3], Rob J. de Boer[2,#], José A.M Borghans[1,2,#], and Kiki Tesselaar[1,#].

[1] Department of Immunology, University Medical Center Utrecht,Utrecht, The Netherlands

[2] Department of Theoretical Biology, Utrecht University, Utrecht, The Netherlands

[3] Department of Clinical Viro-immunology, Sanquin Research, Amsterdam, The Netherlands

[*,#] These authors contributed equally to this work

Abstract

It has recently become generally accepted that chronic immune activation in HIV-1 infection plays an important role in $CD4^+$ T cell depletion. The role of thymic impairment by HIV-1 is however still debated. We here show that even in the context of substantial thymic output, chronic immune activation can lead to severe naive T cell depletion. In CD70Tg mice, excessive immune activation via CD27/CD70 results in the accumulation of T cells with an effector/memory phenotype and depletion of naive T cells. We studied T cell numbers in normal and hyper-immune mice with different amounts of thymic output. Our data show that hyper-activation on its own is sufficient to cause naive T cell depletion, and reduced thymic output accelerates this. Fitting the data with a mathematical model confirmed the impact of hyper-activation on naive T cell depletion. Continuous immune activation also induced enhanced PD-1 expression, and administration of IL-7 to the transgenic mice killed the mice within a few days. Administration of immune stimulatory mediators to untreated HIV patients could therefore also have adverse effects.

5.1 Introduction

$CD4^+$ T cell depletion is the hallmark of HIV-1 infection. Thanks to decades of intensive research it has become accepted that chronic immune activation is one of the main drivers of naive $CD4^+$ T cell depletion in HIV-1 infection, and that direct killing of naive $CD4^+$ T cells by the virus plays a minor role [30, 98]. The topical question addresses the mechanism by which immune activation drives naive T cell depletion. Continuous priming of naive T cells either by HIV-1 or by an increased microbial pressure might be involved in this process [14, 97]. The role of impairment of de novo thymic production of T cells in $CD4^+$ T cell depletion is still a matter of debate [26, 29, 107]. Loss of lymphoid cells and profound stromal damage has been observed in the thymus of HIV-1 infected patients [63]. Since thymic output in human adults contributes only marginally to the maintenance of the peripheral T cell pool (Vrisekoop et al, manuscript in preparation), the effect of thymus dysfunction on naive T cell depletion remains questionable however.

Exhaustion or functional impairment of the T cell compartment also hampers T cell immunity in HIV-1 infected individuals. Loss of functional capacity, like cytotoxicity, cytokine production and proliferative capacity, is thought to reflect prolonged excessive immune activation and to correlate with disease progression. Enhanced expression and function of inhibitory receptors like CTLA4 and PD-1 might reflect this dysfunction, and blockade of these receptors improves in vitro T cell function and vaccination responses in SIV-infected macaques [20, 66, 68, 133, 134]. Based on these observations PD-1 blockade is being considered as a treatment option in HIV infection.

Upon highly active antiretroviral therapy (HAART) of HIV infected in-

dividuals, the viral load usually decreases and naive T cell numbers slowly increase [96, 138]. Slow T cell recovery is a problem in some HIV patients, and stimulation of T cell reconstitution might therefore be beneficial. So far IL-2 and GH treatment have been used in HIV patients. IL-2 treatment typically increased $CD4^+$ regulatory T cells [74, 76]; in contrast, GH treatment significantly increased T cell numbers and had little adverse effects [91]. IL-7 has potent stimulatory effects on T cell numbers and T cell diversity in healthy humans [121], but has not yet been tested in HIV patients.

In this study we addressed the effect of chronic immune activation and thymic output on naive T cell depletion in mice. We studied wild-type mice and two CD70Tg mouse lines in which continuous CD27/CD70 interaction induces chronic immune activation. We used a mathematical model to investigate the main effects of CD27/CD70, eventually leading to T cell depletion. We found that CD70Tg mice have a reduced but functional thymic output, because further reducing their thymic output caused substantial naive T cell loss. The hyper-activation in CD70Tg mice is also responsible for naive T cell depletion, and induces naive T cell depletion in mice with normal thymic output. Continuous immune stimulation enhanced PD-1 expression, which might be a protective mechanism against immunopathology by excessive amounts of effector cells, as suggested by the lethal effect of IL-7 administration. In conclusion our data suggest that immune activation by itself may induce severe immune depletion in situations of marginal thymic output, as found in human adults.

5.2 Results

Chronic stimulation of murine T cells *via* CD27 in CD70Tg-F13 mice induces excessive differentiation of naive $CD4^+$ and $CD8^+$ T cells into effector-memory T cells and accelerates thymic involution (Fig. 5.1) [128]. To investigate to what extent both effects contribute to the observed naive T cell decline in CD70Tg-F13 mice, we measured thymocyte and T cell subset numbers in the spleen of control and thymectomized wild-type and CD70Tg-F13 mice, and applied mathematical modeling to interpret the data.

Thymectomy of 7-week old mice resulted in a rapid decline of naive T cell numbers, both in wild-type C57Bl/6 and CD70Tg-F13 mice (Fig. 5.1, Fig. S.5.2 and chapter 3), demonstrating that also in transgenic mice thymic output plays an important role in the maintenance of the naive T cell compartment, despite the observed thymic involution. The loss of naive T cells was however most rapid in thymectomized CD70Tg-F13 mice, and the naive T cell decline in these mice markedly exceeded the naive T cell decline in wild-type thymectomized mice, demonstrating that next to accelerated thymic involution, continuous immune activation further decreased naive T cell numbers in these mice (Fig. 5.1).

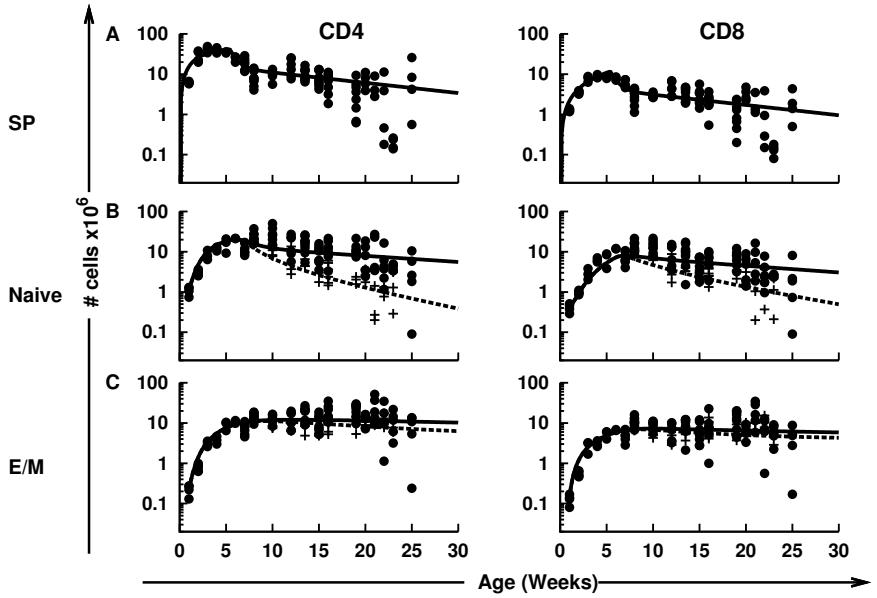

Fig. 5.1: Decline in naive T cell numbers after thymectomy of CD70Tg-F13 mice. (A) Age-dependent number of single positive (SP) thymocytes in CD70Tg-F13 mice of different ages (dots). The number of SP thymocytes was described by a phenomenological model (see methods): the solid line represents the best fit to the number of SP thymocytes from CD70Tg-F13 mice. (B, C) Total number of (B) naive and (C) effector/memory (E/M) $CD4^+$ and $CD8^+$ T cells in the spleen of thymectomized (crosses) and control (dots) CD70Tg-F13 mice. The solid line and the dashed line represent the best fits of control and thymectomized CD70Tg-F13 mice. Model parameters are provided in Table 5.1 and Table 5.2.

To quantify the effect of the decline in thymic output and the increase in immune activation, we fitted the data to a mathematical model. In this model naive T cells are maintained by export of a daily fraction (ϵ) of the total number of single positive (SP) thymocytes ($f(t)$), and are lost via cell death and a constant rate of cell priming. Since both priming and peripheral self-renewal are taken to occur at a fixed rate, i.e. are density-independent, the resultant priming rate (r_n) is a net rate, combining both characteristics. Naive T cell homeostasis is accounted for by introducing density-dependent cell death in the model, where naive T cells are thought to live longer at low T cell densities when survival factors are more abundant. Effector/memory T cells are produced by peripheral renewal and naive T cell priming, followed by subsequent clonal expansion. Effector/memory T cells are lost by density-

dependent death. We fitted the wild-type and CD70Tg data simultaneously allowing for different priming rates (r_n) and clonal expansion rate (a) between the two data sets. All other parameters were assumed to remain unaffected in CD70Tg-F13 mice (allowing other parameters to vary, failed to improve the quality of the fits).The estimated parameter values for the best fit of the model to the data are shown in Table 5.1.

Table. 5.1: Parameter estimates for C57Bl/6, CD70Tg-F12 and CD70Tg-F13 mice as estimated by the mathematical model. The 95%-confidence intervals are given between parentheses and were determined by the bootstrapping method [60].

		CD4	**CD8**
C57Bl/6	r_n (day^{-1})	0.000 (-0.003-0.002)	-0.003 (-0.006-0.000)
	a (day^{-1})	0.012 (0.007-0.021)	0.000 (-0.029-0.021)
CD70TG-F12	r_n (day^{-1})	0.059 (0.052-0.078)	0.021 (0.017-0.029)
	a (day^{-1})	0.038 (0.026-0.046)	0.089 (0.042-0.117)
CD70TG-F13	r_n (day^{-1})	0.015 (0.012-0.018)	0.012 (0.010-0.015)
	a (day^{-1})	0.080 (0.056-0.137)	0.221 (0.149-0.616)
Shared	$d_n(10^{-9}$ day$^{-1})$	2.894 (2.501-3.385)	2.103 (1.623-2.678)
	r_m (day^{-1})	0.057 (0.033-0.099)	0.288 (0.224-0.537)
	$h(10^6)$	2.008 (0.869-4.280)	1.082 (0.264-3.320)
	d_m (day^{-1})	0.018 (0.010-0.032)	0.065 (0.037-0.013)
	ϵ (day^{-1})	0.041 (0.038-0.045)	

By the best fit of the model we estimate that in both wild-type and CD70Tg-F13 mice 4% of the number of SP thymocytes was exported on a daily basis (Table 5.1: $\epsilon = 0.041$ per day). Since the size of the thymus was different between C57Bl/6 and CD70Tg-F13 mice (Fig. S.5.1), the absolute number of emigrating SP thymocytes per day was reduced in CD70Tg-F13 mice (e.g., in 12-week old CD70Tg-F13 mice this amounts to a 15% and 25% reduction for $CD4^+$ and $CD8^+$ RTE, respectively). Thus, reduced thymic output is partially responsible for the decreased naive T cell numbers in CD70Tg-F13 mice, but thymic output continues to contribute to the maintenance of the naive T cell pool in these mice. In CD70Tg-F13 mice we estimate a daily loss of 1.5% and 1.2% of the naive $CD4^+$ and $CD8^+$ T cells, respectively, by priming only ($r_n = 0.015$ and 0.012; Table 5.1). Indeed the average life span of naive T cells in 12-week old CD70Tg-F13 mice are 15% to 30% shorter than those in wild type mice (Table 5.2). The increased naive T cell priming was also reflected in the memory pool. Compared to the wild-type situation in 12-week old mice there were at least 2,5 fold more E/M T cells produced by T cell differentiation . As a result, 60% of the $CD4^+$ and 47% of the $CD8^+$ T memory cells in CD70Tg-F13 mice were produced by naive T cell activation and their subsequent expansion. In contrast, in wild-type mice more than 60% of the memory T cells were formed by renewal. Summarizing, continuous activation in CD70Tg-F13 mice decreased thymic output and increased naive T

cell priming, and both contributed about equally to the naive T cell depletion in these mice.

Table. 5.2: Effects of immune activation on naive $CD4^+$ and $CD8^+$ T cell life span. Life spans (in days) of naive $CD4^+$ and $CD8^+$ T cells were calculated for 12-week old mice.

	C57Bl/6 mice		**CD70Tg-F13 mice**	
	Naive CD4	Naive CD8	Naive CD4	Naive CD8
Control	26	56	22	40
Thymectomized	59	104	39	53

Strength of immune activation correlates with the amount of T cell depletion. For our initial analysis of CD27 function we generated two CD70Tg lines [3]. The second CD70Tg strain, F12, also constitutively expresses CD70, but at a lower level. The F12 line has more physiological levels of CD70 expression, and these mice have increased fractions of effector/ memory T cells, but less than CD70Tg-F13 mice(Fig. S.5.2). Additionally, CD70Tg-F12 mice show no signs of enhanced thymic involution compared to wild-type mice (Fig. 5.2,Fig. S.5.2), suggesting a normal thymic output [8]. The main dynamic difference between C57Bl/6 mice and CD70Tg-F12 mice would therefore be the peripheral activation rates. To address the effect of continuous immune activation in the context of a fairly normal thymic output we measured thymocyte and T cell numbers in CD70Tg-F12 mice and fitted the same mathematical model combining the data sets of all three types of mice (Fig. 5.2). The naive and effector/memory T cell numbers in CD70Tg-F12 mice can again be explained by an increased priming and clonal expansion rate (Table 5.1). Since thymic output is normal in the F12 mice, this shows that enhanced priming is sufficient to decrease naive T cell numbers. Comparison of the parameters of CD70Tg-F12 and CD70Tg-F13 mice showed that the clonal expansion rate, a, was highest in CD70Tg-F13 mice, but the priming rate, r_n, was highest in F12 mice. Since the clonal expansion rate, a, combines naive T cell priming with their subsequent clonal expansion, this suggests a much more extensive clonal expansion in CD70Tg-F13 mice.

Increased fraction of PD-1 expressing memory cells in CD70Tg mice. Remarkable differences were observed when evaluating the life span of the different animals: control C57Bl/6 mice lived on average 24 months, CD70Tg-F13 mice lived only 5-6 months, and thymectomy had no influence on these life spans (data not shown). Since thymectomy does lower naive T cell numbers in CD70Tg-F13 mice, low naive T cell numbers by themselves fail to explain the short life span of F13 mice. We therefore tested whether continuous immune activation has additional effects on immune-function. Regulatory T cells were measured by the number of $CD4^+$ $CD25^+$ $CD103^+$ $GITR^+$ T cells, and we measured exhaustion of memory cells by analysing the fraction of PD-1

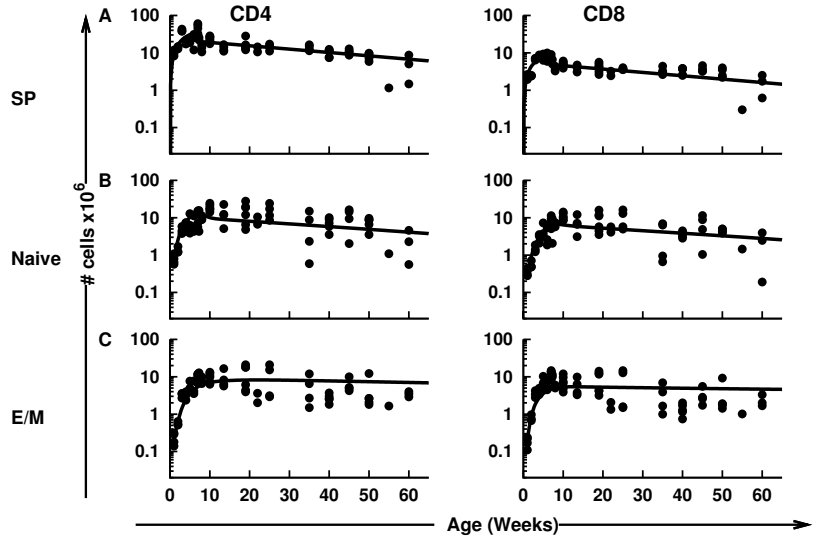

Fig. 5.2: Thymocyte and T cell counts in CD70Tg-F12 mice. Best fits (solid lines) through the number of (A) SP thymocytes, (B) naive and (C) effector/memory T cell numbers (dots). Model parameters are given in Table 5.1 and Table 5.2.

expressing cells within this compartment. Continuous expression of CD70 at young age increased the fraction and the number of regulatory T cells in both spleen (Fig. 5.3A) and peripheral lymph nodes (data not shown). In older mice this effect seemed to revert, as the number of regulatory T cells was two-fold decreased in old F12 mice. PD-1 expression was increased in the $CD4^+$ and $CD8^+$ memory compartment in the spleen (Fig. 5.3B) and in the PLN (data not shown). This increase of PD-1 expression was seen in both transgenic lines, but was most pronounced in the spleen of the CD70Tg-F13 line. In both lines the effect was stronger in older mice. This permanently increased expression of PD-1 within the memory compartment may indicate immune exhaustion and may partially explain the immune dysfunction at old age.

IL-7 treatment is lethal for CD70Tg-F13 but not C57Bl/6 mice. IL-7 administration has been used as treatment for T cell depleted patients. IL-7 enhances thymic function and restoration of naive T cell pool [103, 117], and IL-7 can down-regulate PD-1 expression [6]. We aimed to treat six C57Bl/6 and six CD70Tg-F13 mice for three weeks with hIL-7 to investigate whether we could improve their T cell numbers and immunity to enhance their life span. Unexpectedly, all CD70Tg-F13 mice died between two to fifteen days after start of the experiment, while the C57Bl/6 mice remained healthy. Repeating

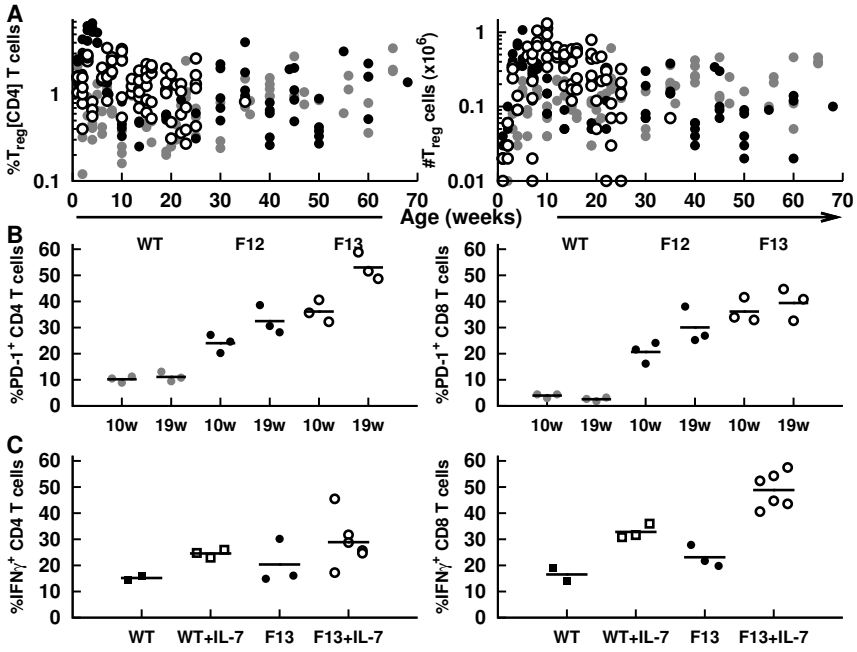

CD8

Fig. 5.3: Functional characteristics of CD70Tg mice. (A) The percentage CD4$^+$ CD25$^+$ CD103$^+$ GITR$^+$ regulatory T cells within the CD4$^+$ T cell population, the absolute number of regulatory T cells, and (B) the percentage of PD-1$^+$ cells within the CD4$^+$ and CD8$^+$ T cell pool were determined in the spleen of C57Bl/6 (grey dots), CD70Tg-F12 (black dots), and CD70Tg-F13 mice (open circles) of different ages. ((C) Splenocytes were isolated from 19-week old control (solid squares) and IL-7 treated C57Bl/6 (open squares) and control (closed circles) and IL-7-treated CD70Tg-F13 mice (open circles). The cells were stimulated for 4h with PMA/ionomycin in the presence of Brefeldin A, and subsequently intracellularly stained with IFNγ. The symbols depict the percentage of positive cells within the CD4 or CD8 gated cells.

the experiment with a two-day treatment period, we could not find any evidence for an enlarged thymus, or enhanced T cell numbers. However, despite the short treatment period, hIL-7 appeared to improve T cell function as the percentage of IFN-γ producing $CD8^+$ cells in CD70Tg-F13 mice tended to be increased (Fig. 5.3C).

5.3 Discussion

In this study we addressed the effect of continuous immune activation in mice constitutively expressing CD70. Although enhanced immune activation by itself was sufficient to reduce naive T cell numbers, we only observe severe depletion in young mice in the context of accelerated thymic involution. In these mice thymic output plays an important role in the maintenance of naive T cell numbers, and in young mice there seems to be an overproduction of naive T cells by the thymus that is compensated for by a transient increase of the death rate (see chapter 3). Total naive T cell depletion is therefore difficult to achieve, and seems unfeasible in our model because of the limited number of cells expressing CD70. In human adults with a much lower thymic output, however, even moderately enhanced priming rates may lead to severe T cell depletion.

The estimated priming rates, r_n, in CD70Tg mice were around 1 to 6% per day, but this might be an underestimation of the true priming rate in CD70Tg mice as in our mathematical model the priming rate is the net result of a positive renewal rate and a negative priming rate. Analysis of Ki-67 expression indeed showed increased fractions of proliferating cells within the naive and memory compartments in CD70Tg mice. This might indicate that in the CD70Tg system increased renewal compensates somewhat for the naive T cell loss by increased priming. The increased Ki67 expression in the naive compartment is also readily explained by the increased clonal expansion however, i.e., by phenotypically-naive proliferating transitional cells that are on their way to the memory compartment.

Despite an overall similarity, careful analysis of F12 and F13 transgenic mice revealed several differences. In line with our expectations based on the level of CD70 expression, we saw a higher number and more differentiated phenotype of memory cells in F13 mice, an increased fraction of memory cells expressing PD-1, and estimated the largest contribution of clonal expansion on memory T cell production in CD70Tg-F13 mice. The most striking difference was the difference in life spans of the mice. Both failing immunity and disturbed haematopoiesis could be the explanation for this difference. At the time of death (at 5-6 months), T cell numbers are so much reduced in CD70Tg-F13 mice that opportunistic infections are to be expected. This need not be the explanation however, because individuals and mice with extremely low (naive) T cell numbers can live without clinical complications. Nef-transgenic mice have dramatically reduced T cell numbers, but have a normal life span, with-

out overt increases in infection incidence [71]. In addition, healthy Ethiopians, that are reported to have several features of chronic immune activation, exhibit reduced proportions of naive T cells and a diminished TREC content, but do not die prematurely as a consequence of aids-like symptoms [Tsegaye et al, manuscript in preparation]. Chronic immune activation does lead to exhaustion of the memory pool in HIV-1 infection, and our PD-1 and cytokine data suggest that this is also the case in the transgenic mice. It might thus be that it is the combination of low naive numbers and an exhausted memory compartment causing the immune failure and death in CD70Tg mice. We indeed observed CD70Tg-F13 mice suffering and dying from opportunistic infections [128]. Alternatively, the enormous numbers of IFN-γ producing effector cells in the CD70Tg mice [3] could indirectly cause immuno-pathology, and the premature death of these mice. Severe anaemia is observed in some old CD70Tg mice, and IFN-γ inhibits erythropoiesis [35]. Enhancement of T cells numbers producing IFN-γ and TNF-α has been implicated in hematopoietic destruction in aplastic anemia [31]. When we treated CD70Tg-F13 mice with hIL-7, with the idea that this would increase their life span, the result was dramatic. None of the mice survived the treatment. Studies on the role of Fas-induced death in CD70Tg mice have shown that increased numbers of effector cells leads to immunopathology, and an even more premature death of the mice [2]. IL-7 is known to induce $CD8^+$ memory T cell proliferation, and in combination with TCR triggering, is known to abate PD-1 expression [6]. Administration of this cytokine to the CD70Tg mice could thus have led to a massive increase of functional memory T cells causing the death of the mice. Additionally, if the IL-7 were to down-regulate PD-1 expression these results would suggest that the increased PD-1 expression in CD70Tg mice is a negative feedback mechanism preventing the excessive formation of functional effector T cells. In untreated CD70Tg mice the enhanced PD-1 expression may thus protect the mice from immunopathology and prolongs their life expectancy.

In conclusion we show that enhanced immune activation can drive naive T cell depletion, especially in the context of low thymic output. IL-7 treatment of CD70Tg mice resulted in their death, possibly caused by immunopathology of large numbers of cytokine producing effector/memory T cells. In analogy, treatment of HIV-1 patients with IL-7 or PD-1 might have adverse effects.

5.4 Materials and Methods

Mice.
C57Bl/6, heterozygous CD70Tg-F12, and hemizygous CD70Tg-F13 mice [3], all on a C57Bl/6 background, were maintained by in-house breeding at the Netherlands Cancer Institute (Amsterdam) or the Central Animal Facility of the Utrecht University (Utrecht) under specific pathogen-free conditions in accordance with institutional and national guidelines. The phenotype of C57Bl/6 and CD70Tg mice was comparable in both animal facilities (data not shown).

Thymectomy was performed as described previously [136]. Mice were i.p. injected with 10 μg hIL-7 (Cytheris, Vanves, France) in PBS on a daily basis for 3 weeks.

Antibodies.
FITC-labeled antibodies against IFN-γ (clone XMG1.2), Ki-67 (clone B56), CD4 (clone RM4-5)and CD8a (clone 53-6.7), PE-conjugated antibodies recognizing CD43 (clone 1B11) and CD62L (clone MEL-14), PerCP-labeled CD4 (clone RM4-5) and CD8 (clone 53- 6.7), APC-labeled CD44 (clone IM7) were purchased from BD Biosciences PharMingen (San Diego, CA). Anti-CD25 (PE) antibodies (clone PC61 5.3) were purchased from Caltag laboratories (Burlingame, CA). FITC-conjugated antibodies against CD103 (clone 2E7) and biotinylated GITR (clone DTA-1) were purchased from eBioscience (San Diego, CA).

Cell preparation and flow cytometry.
Spleen, (axillary, branchial, inguinal and superficial cervical) lymph nodes and (if present) thymus were isolated from C57Bl/6 and CD70Tg mice of different ages. Single cell suspensions were obtained by mechanical disruption. Red blood cells were lysed with ammonium chloride solution (155 mM NH4Cl, 10 mM KHCO3 and 0.1 mM EDTA, pH 7.4). Cells were washed, resuspended in IMDM/7% FCS and counted. FACSstaining was performed as described previously [136]. Intracellular staining for IFN-γ was performed after 4h stimulation with 10 ng/ml PMA and 100 μg/ml ionomycin in the presence of 1 μg/ml of the protein-secretion inhibitor Brefeldin A (BD Biosciences PharMingen, San Diego, CA).

Mathematical modeling.
Using a mathematical model to quantify naive T cell dynamics in control and thymectomized mice, we consider a naive T cell pool that is maintained by input from the thymus. We describe thymic output with a phenomenological function $f(t)$ which is proportional to the number of single positive (SP) thymocytes (Fig. 5.2; see chapter 3 for a detailed description). The rates of thymic involution are the same for $CD4^+$ and $CD8^+$ SP thymocytes, but their population kinetics (σ and v_1) are allowed to be different. Parameter estimates of the best fit of this model to the data are given in Supplementary Table S.5.1.

In addition to an input of naive T cells from the thymus, the mathematical model allows for maintenance of naive T cells by self renewal, or loss by priming and a density dependent death rate ($d_n N$), allowing cells to live longer when the population density is low (see chapter 3). However, because the model has too many degrees of freedom to separately estimate self renewal and priming rates, we lump these to rates together into a net rate r_n per day. r_n can be positive or negative depending on the magnitude of the renewal rate relative to the priming rate. Naive T cell dynamics are described by the equation:

$$N' = \epsilon f(t) - r_n N - d_n N^2.$$

5. T cell exhaustion and depletion in mice with chronic immune activation via CD27/CD70 costimulation.

Memory T cells are produced from either density dependent activation of naive T cells at a rate $\frac{a}{1+M/h}$ or by density dependent renewal at a rate $\frac{r_m}{1+M/h}$ where h is the half saturation constant, i.e. when $M = h$ the production of memory cells is half maximal. Memory T cell dynamics are described by the equation:

$$M' = \frac{aN + r_m M}{1 + M/h} - d_m M$$

Due to their continuous recirculation around the body, naive T cell dynamics should be averaged over different body organs, and we simultaneously model dynamics in the spleen and peripheral lymph nodes (PLN) by fitting a function, ψ(t), relating the number of cells in PLN to those in the spleen. In the first weeks, when $t \leq \varsigma$, the ratio of cells in PLN to spleen increases, which is described by $\psi(t) = \theta(1-e^{x_1 t})$. Hereafter this ratio decreases, which in control mice is described by

$$\psi(t) = \psi(\varsigma)\left[z_1 e^{-x_2(t-\varsigma)} + (1-z_1)e^{-x_3(t-\varsigma)}\right].$$

At the time of thymectomy the ratio changes and we describe the PLN/spleen ratio by the same function with new parameters, i.e.,

$$\psi(t) = \psi(\mathrm{T}_{off})\left[z_1 e^{-x_2(t-\mathrm{T}_{off})} + (1-z_1)e^{-x_3(t-\mathrm{T}_{off})}\right], \text{ where} \mathrm{T}_{off} > \varsigma.$$

The function $\psi(t)$was fitted to the data of each mouse strain separately, and the parameter estimates of the best fits (Fig. S.5.1) are given in Supplementary Table S.5.2.

Statistical analysis.
All statistical analyses were performed using the software program SPSS 15.0 (SPSS Inc, Chicago, Illinois). Differences with p $\leq$ 0.05 were considered significant.

*A*cknowledgments
We thank Sjaak Greeven and Linda Nijdam for biotechnical assistance. This research has been funded by the Landsteiner Foundation for Blood Research (LSBR grant #0210).

5.5 Supplementary information.

Table. S.5.1: Parameters values and 95% confidence intervals for the best fit of the thymic output function to $CD4^+$ and $CD8^+$ single positive thymocytes from C57Bl/6 mice, CD70Tg-F12 mice and CD70Tg-F13 mice.

	C57Bl/6	**CD70Tg-F12**	**CD70Tg-F13**
CD4			
$\sigma(10^7$ cells)	3.459(3.224-3.772)	4.555 (3.580-10.820)	4.741 (3.925-6.058)
v_1 (day^{-1})	0.084 (0.065-0.106)	0.032 (0.010-0.056)	0.056 (0.035-0.087)
CD8			
$\sigma(10^7$ cells)	1.679 (1.074-9.786)	0.995 (0.692-3.508)	241.8 (0.944-697.6
v_1 (day^{-1})	0.023 (0.003-0.056)	0.041 (0.006-0.507)	0.000 (0.000-0.093)
Shared			
v_2 (day^{-1})	0.001 (0.001-0.002)	0.003 (0.002-0.004)	0.201 (0.097-0.415)
v_3 (day^{-1})	0.524 (0.187-2.961)	1.846 (0.132-36.71)	0.008 (0.003-0.012)
T_{off} (days)	46.88 (42.00-48.58)	50.21 (47.85-50.97)	37.79 (34.25-40.38)
γ	0.352 (0.313-0.384)	0.555 (0.437-0.652)	0.655 (0.579-0.760)

Table. S.5.2: Parameters values and 95% confidence intervals the best fit of the function $\psi(t)$ expressing the ratio of $CD4^+$ and $CD8^+$ naive T cells in PLN to those in the spleen for both control and thymectomized C57Bl/6, CD70Tg-F12, and CD70Tg-F13 mice.

	C57Bl/6	**CD70Tg-F12**	**CD70Tg-F13**
CD4			
α	1.578 (1.197-2.373)	3.880 (2.212-22.99)	3.500 (1.425-15.84)
x_1	0.098 (0.049-0.168)	0.064 (0.006-2.915)	0.0422 (0.007-0.202)
x_2	0.024 (0.020-0.030)	0.125 (0.055-0.480)	0
x_3	0 0 0.017 (0.013-0.022)		
y_2	0.025 (0.016-0.0408)	0.025 (0.016-0.041)	0.004 (0.000-0.007)
y_3	0	0	0
z_1	0.723 (0.692-0.750)	0.929 (0.873-0.957)	0
z_2	0.679 (0.597-0.784)	0	0
ς	14.00 (11.56-18.16)	40.16 (28.00-49.00)	14.00 (8.692-26.23)
CD8			
α	5.401 (1.399-18.58)	3.952 (2.304-30.90)	3.427 (1.441-13.34)
x_1	0.017 (0.004-0.096)	0.062 (0.005-2.961)	0.047 (0.009-0.322)
x_2	0.022 (0.015-0.030)	0.141 (0.066-0.810)	0
x_3	0	0	0.014 (0.009-0.021)
y_2	0.024 (0.011-0.054)	0.024 (0.011-0.054)	0.002 (0.000-0.006)
y_3	0	0	0
z_1	0.576 (0.523-0.618)	0.927 (0.877-0.959)	0
z_2	0.459 (0.363-0.589)	0	0
ς	14.72 (11.56-19.50)	41.70 (33.98-49.00)	14.00 (7.442-33.70)

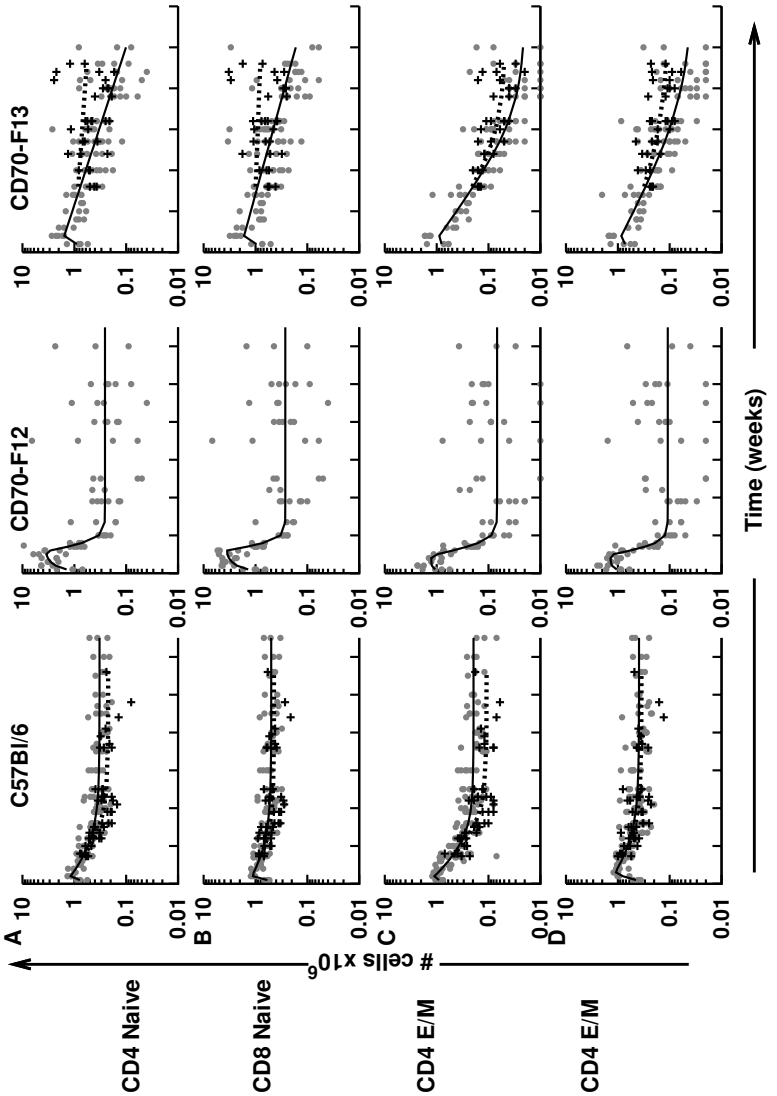

Fig. S.5.1: Proportionality function $\Phi(t)$ correlating T cell dynamics in spleen and peripheral lymph nodes, based on cell densities in the two organs. Proportionality functions of Naive (A) $CD4^+$, (B) $CD8^+$, memory (C) $CD4^+$ and (D) $CD8^+$ from C57Bl/6 mice, CD70Tg-F12 mice, and CD70Tg-F13 mice. Black solid and dotted lines represent the best fits of the proportionality function to data from control mice (grey dots) and thymectomized mice (black crosses), respectively. Model parameters are provided in Table S.5.2.

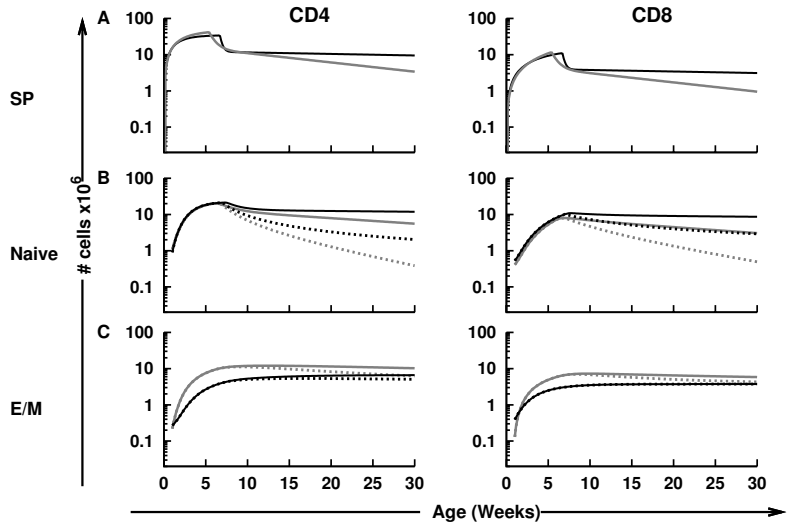

Fig. S.5.2: Comparison of thymocyte and T cell counts from C57Bl/6 mice (black lines) and CD70Tg-F13 mice (grey lines).(A) The lines represents the best fit to the number of single positive (SP) thymocytes in mice of different ages. The number of SP thymocytes was described by a phenomenological model (see material and methods). For clarity the data points from C57Bl/6 and CD70Tg-F13 mice are not shown; data points from C57Bl/6 and CD70tg-F13 mice are shown in chapter 3 and Fig. 5.1 respectively. (B, C) The lines represents the best fit to the total number of (B) naive and (C) effector/memory (E/M) $CD4^+$ and $CD8^+$ T cells in the spleen of thymectomized (dashed lines) and control (solid lines) C57Bl/6 and CD70Tg-F13 mice. Model parameters are provided in Table 5.1 and Table 5.2.

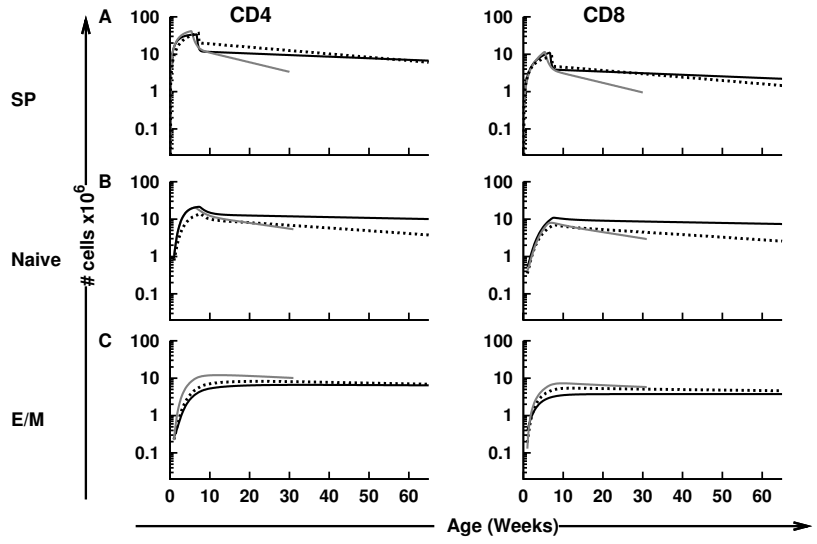

Fig. S.5.3: Comparison of thymocyte and T cell counts from C57Bl/6 mice (black lines), CD70Tg-F12 mice (dashed black lines) and CD70Tg-F13 mice (grey lines).(A) The lines represents the best fit to the number of single positive (SP) thymocytes in mice of different ages. The number of SP thymocytes was described by a phenomenological model (see material and methods). Data points from C57Bl/6, CD70tg-F12 and CD70tg-F13 mice are shown in chapter 3, Fig. 5.2 and Fig. 5.1 respectively. (B, C) The lines represents the best fit to the total number of (B) naive and (C) effector/memory (E/M) $CD4^+$ and $CD8^+$ T cells in the spleen of control C57Bl/6, CD70Tg-F12 and CD70Tg-F13 mice. Model parameters are provided in Table 5.1and Table 5.2.

6

Qualitative changes in T cell turnover during HIV-1 infection.

Nienke Vrisekoop[1], Rogier van Gent[1], Tendai Mugwagwa[2], Anne Bregje de Boer[1], Sigrid A. Otto[1], An F.C. Ruiter[3], Mariëtte T. Ackermans[3], Joost N. Vermeulen[4,6], Hidde H. Huidekoper[5], Koos Gaiser[1], Hans P. Sauerwein[5], Jan M. Prins[6], Frank Miedema[1], Rob J. de Boer[2], Kiki Tesselaar[1] and José A.M. Borghans[1,2].

[1]Department of Immunology, University Medical Center Utrecht, Utrecht;
[2]Theoretical Biology, Utrecht University, Utrecht;
[3]Department of Clinical Chemistry, Laboratory of Endocrinology, Academic Medical Center, Amsterdam;
[4]IATEC, Academic Medical Center, Amsterdam;
[5]Department of Endocrinology and Metabolism, Academic Medical Center, Amsterdam;
[6]Department of Internal Medicine, Academic Medical Center Amsterdam, TheNetherlands.

Abstract

The cause of the progressive decline of $CD4^+$ T cell numbers during human immunodeficiency virus (HIV) infection remains debated. Based on different markers and labeling strategies, several studies have shown that T cell turnover rates are increased during HIV infection. Using long-term *in vivo* ^2H_2O labeling, we show that during HIV infection, naive $CD4^+$ and $CD8^+$ T lymphocytes live on average 618 and 271 days, while memory $CD4^+$ and $CD8^+$ T lymphocytes have average life spans of 53 and 43 days, respectively. We show that these average life spans are at least three-fold shorter than in healthy volunteers. Our analyses also show that while the naive T cell pool in healthy individuals forms a kinetically homogeneous population of long-lived cells, upon HIV infection a significant subset of naive T cells acquires a much higher rate of turnover. Such a shift towards faster turnover, even within the naive T cell population, supports the conjecture that changes in the naive and memory T cell populations during HIV infection are caused by chronic immune activation.

6.1 Introduction

The cause of the progressive decline of $CD4^+$ T cell numbers during human immunodeficiency virus (HIV) infection remains debated. There is increasing evidence that the state of chronic immune activation induced by HIV plays a key role in disease progression. Major controversies remain, however, on the role of impaired thymic output in HIV infection. Several studies have shown increased production rates of $CD4^+$ and $CD8^+$ T cells during HIV-infection, measured by different labeling techniques or markers for T cell proliferation [36, 55, 75, 86, 88, 100]. It is also clear that these increased turnover rates are not merely due to shifts in the percentages of naive and memory T cells [110], because studies in separated naive and memory T cell populations have shown that both naive and memory $CD4^+$ and $CD8^+$ T cells are turning over more rapidly in HIV-infected individuals [57].

The major challenge in the field remains to understand how the depletion of naive $CD4^+$ and $CD8^+$, and memory $CD4^+$ T cells can be made consistent with increased *per capita* production rates. Here we compare *per capita* production rates (i.e., fractions of cells turning over per day) and total daily production rates (i.e., numbers of cells produced per day) between healthy volunteers and HIV-1 infected individuals. The recently introduced technique of stable isotope labeling has paved the way to analyze T cell dynamics in healthy and HIV-infected individuals in much detail. A few studies based on ^{2}H-glucose or ^2H_2O labeling have been performed in healthy and HIV-infected individuals [55, 57, 80, 81, 86, 88, 108, 110, 136, 139], but until now complete up- and down-labeling curves, which are required to reliably estimate average turnover rates, in HIV infection are lacking. Here we performed long-term *in*

vivo labeling with deuterated water (^2H_2O) in 4 HIV patients and 5 healthy volunteers, and followed the fate of labeled naive and memory $CD4^+$ and $CD8^+$ T cells after label cessation. Mathematical analysis of these data confirms that *per capita* production and death rates of naive and memory $CD4^+$ and $CD8^+$ T lymphocytes are significantly increased during HIV infection, and shows that the naive T-lymphocyte population, which is kinetically homogeneous in healthy individuals, becomes kinetically heterogeneous upon HIV infection. We discuss why our data are fully compatible with the concept that changes in the T cell population of HIV-infected individuals are caused by chronic immune activation, rather than by impaired thymic output.

6.2 Results

A steady-state model for label enrichment

During the entire protocol, absolute $CD4^+$ T cell counts and fractions of naive $CD4^+$ and $CD8^+$ T cells remained fairly constant in all HIV patients (data not shown). Absolute $CD4^+$ T cell counts were about 3.5-fold lower in HIV-infected individuals compared to healthy volunteers, and numbers of naive $CD4^+$ and $CD8^+$ T cells were about 5-fold and 2-fold lower, respectively (Table 6.1). Fractions of $Ki67^+$ $CD4^+$ and $CD8^+$ T cells in HIV patients were also constant during the execution of the study and were 2-3 fold higher compared to healthy volunteers (Table 6.1). Because naive and memory $CD4^+$ and $CD8^+$ T cell counts hardly changed during the analyses, we fitted the label enrichment data of naive and memory $CD4^+$ and $CD8^+$ T cells with a mathematical model assuming that the size of the cell population under investigation remained in steady-state. In the model we allowed for kinetic heterogeneity within T cell populations, i.e. each cell population was modeled as a combination of subpopulations i, with size α_i, an turnover rate p_i (see Material and Methods). From the best fit to the data, we subsequently calculated the average lymphocyte turnover rate (p) of the whole cell population under investigation. To determine the maximum level of label enrichment in the DNA that could potentially be attained, we measured the label enrichment in granulocytes, a cell population that is thought to turnover completely during the labeling period [93]. The granulocytes of the HIV-infected study subjects reached similar enrichment levels as those of healthy volunteers [136]. To correct for the actual availability of deuterium for the different cell populations at any point in time, we also determined the label enrichment in urine of the study participants at different time points (see Material and Methods and Fig. S.6.2) [136].

$CD4^+$ and $CD8^+$ T cell turnover in healthy volunteers

We have previously measured T-lymphocyte turnover rates in 5 healthy volunteers by heavy water labeling [136]. After 9 weeks of labeling, enrichment levels reached were about 1-5% for naive and 10-20% for memory $CD4^+$ and $CD8^+$ T cells. During the down-labeling phase of 16 weeks we observed no

Table. 6.1: Characteristics of HIV-infected individuals

	A	**B**	**C**	**D**	**Healthy**[a]
Age at start protocol (yrs)	47	63	54	25	22
$CD4^+$ count (cells/μl blood)	306[b] (283-354)	182 (165-221)	189 (165-243)	450 (425-503)	890
$CD8^+$ count (cells/μl blood)	667 (558-816)	1612 (1574-1798)	296 (259-384)	532 (489-548)	470
%naive $CD4^+$	52.8 (51.0-64.5)	23.7 (20.3-26.9)	23.9 (22.4-24.4)	49.0 (45.6-56.5)	68
%memory $CD4^+$	42.7 (33.9-46.2)	74.7 (71.6-78.8)	74.6 (74.0-76.6)	42.6 (35.0-45.9)	32
%naive $CD8^+$	17.3 (15.4-17.4)	8.1 (6.9-10.2)	14.0 (13.0-14.6)	25.6 (22.8-29.2)	59
%memory $CD8^+$	29.6 (28.4-35.5)	67.0 (65.1-69.1)	58.5 (57.2-63.0)	24.9 (20.2-26.7)	18
%$Ki67^+$ in $CD4^+$	4.7 (3.60-6.40)	7.2 (6.30-8.40)	6.4 (4.70-8.30)	2.8 (2.00-3.60)	1.9
%$Ki67^+$ in naive $CD4^+$	1.3 (0.80-1.60)	3.8 (3.10-4.30)	4.1 (2.90-4.80)	1.4 (0.70-2.00)	0.8
%$Ki67^+$ in memory $CD4^+$	7.0 (6.20-10.20)	7.7 (6.90-9.70)	6.4 (4.70-7.90)	4.6 (3.00-6.50)	3.4
%$Ki67^+$ in $CD8^+$	2.4 (1.40-3.60)	2.6 (2.50-3.40)	8.3 (6.30-10.20)	4.1 (3.40-6.40)	1.5
%$Ki67^+$ in naive $CD8^+$	1.9 (0.90-2.30)	2.2 (2.10-3.00)	4.7 (4.00-5.60)	4.4 (2.20-6.90)	0.7
%$Ki67^+$ in memory $CD8^+$	3.8 (2.10-5.90)	2.8 (2.50-3.70)	9.4 (6.80-11.10)	10.8 (8.20-13.90)	2.1

[a] Median values from healthy individuals described in Vrisekoop et al. [136].
[b] Depicted are median values and inter-quartile ranges during the entire follow-up.

significant loss of label from the naive T cell populations. To reconfirm our conclusion that naive T cells in healthy volunteers are extremely long-lived [136], 4 of the 5 healthy volunteers donated blood once again approximately 3 years after label cessation. When these samples were analyzed along with a few historic samples, we found that indeed, even 3 years after label cessation, labeled DNA could still be detected in the naive T cell pools of these individuals. When fitting the full data-sets of each healthy individual, we found no statistical evidence for kinetic heterogeneity in the naive T cell pool, i.e. the labeling kinetics of the naive T cell pool could perfectly be described by a model in which all naive T cells have the same rate of turnover (Fig. 6.1 and Fig. 6.2). The fits reconfirmed the very low rate of turnover of naive T cells that we previously reported [136] (see Table 6.2), while they also described the late data points (Fig. 6.2), strengthening our conclusion that naive T cells in

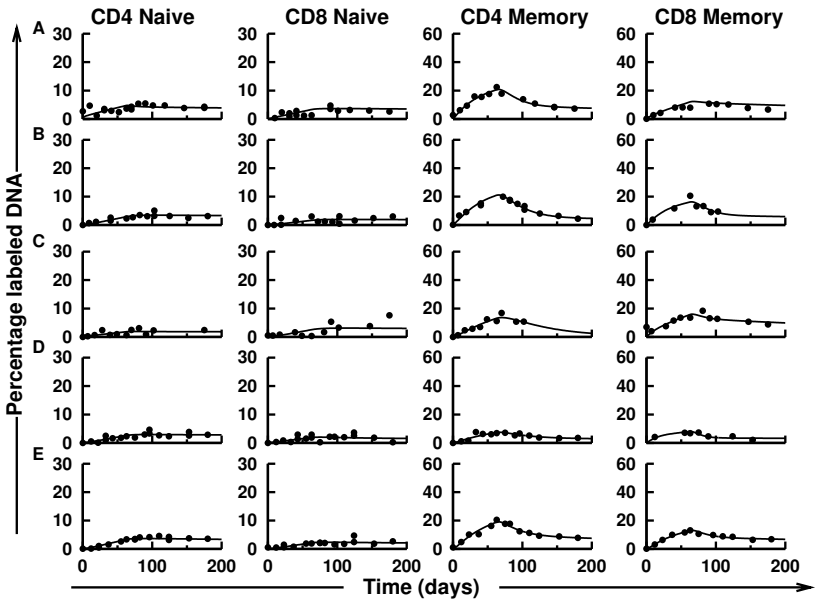

Fig. 6.1: ^{2}H enrichment of naive and memory T cells of healthy individuals described in Vrisekoop et al. [136]. Best fits of the percentage of labeled DNA in naive and memory $CD4^+$ and $CD8^+$ T cells of 5 healthy volunteers. The curves show the best fit of the two-compartment model to the full experimental data-set, including the long-term follow-up points whenever available. For clarity, the quality of fit to the long-term follow-up points is shown separately in Fig 6.2. Label enrichment in the DNA of the different cell populations was scaled between 0 and 100% by normalizing for the estimated maximum percentage labeled DNA obtained in granulocytes (see Material and Methods).

healthy adults undergo very little turnover and do not contain a substantial pool of short-lived recent thymic emigrants (RTE). The labeling kinetics of the $CD4^+$ and $CD8^+$ memory T cell populations, in contrast, were significantly better described when the model allowed for heterogeneity in turnover rates of memory T cells. Summarizing, naive T cells in healthy adults are long-lived (with expected life spans of 5.6 and 8.8 years for $CD4^+$ and $CD8^+$ T cells, respectively, see Table 6.2) and form a kinetically homogeneous population, while memory T cells have a shorter expected life span (with expected life spans of 0.45 and 0.33 years for $CD4^+$ and $CD8^+$ T cells, respectively, see Table 6.2) and are kinetically heterogeneous.

$CD4^+$ and $CD8^+$ T cell turnover in HIV-infected individuals

After 9 weeks of ^2H_2O administration, HIV-infected patients reached significantly higher labeling levels (of about 5-20% for naive $CD4^+$ and $CD8^+$ T cells, and 30-50% for memory $CD4^+$ and $CD8^+$ T cells, respectively) compared to

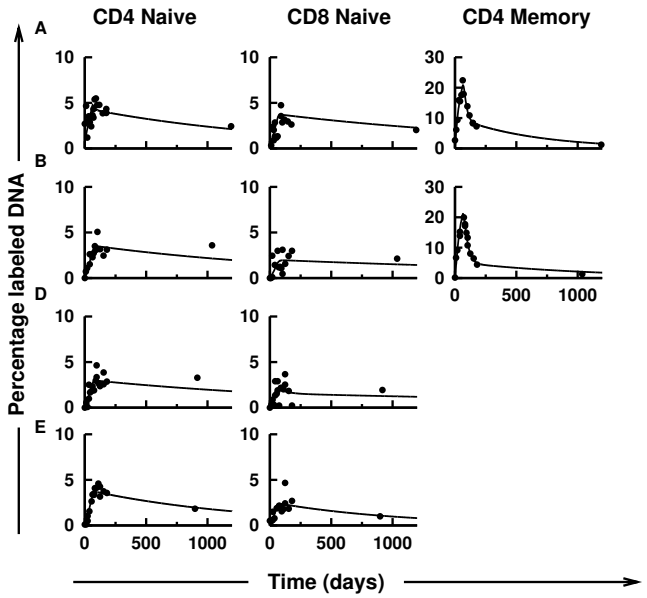

Fig. 6.2: Long-term ^{2}H enrichment of naive and memory T cells of healthy individuals. Best fits of the percentage of labeled DNA in naive and memory $CD4^+$ and $CD8^+$ T cells of 4 healthy volunteers. he curves show the best fit of the two-compartment model to the full experimental data-set, and visualize the quality of fit to the long-term follow-up points. (See legend of Fig. 6.1 for details.)

Table. 6.2: Average *per capita* turnover rates (p day$^-$1) of healthy individuals

	Naive $CD4^+$	Naive $CD8^+$	Memory $CD4^+$	Memory $CD8^+$
A	0.0013	0.0006	0.0141	0.0108
	(0.0008-0.0015)[b]	(0.0004-0.0009)	(0.0103-0.0290)	(0.0035-0.0213)
B	0.0005	0.0002	0.0079	0.0084
	(0.0003-0.0008)	(0.0001-0.0004)	(0.0062-0.0153)	(0.0055-0.0181)
C	0.0003	0.0001	0.0035	0.0064
	(0.0002-0.0005)	(0.00-0.0004)	(0.0025-0.0103)	(0.0261-0.0280)
D	0.0004	0.0003	0.0020	0.0637
	(0.0002-0.0006)	(0.0002-0.00-5)	(0.0014-0.0081)	(0.0026-0.0280)
E	0.0006	0.0004	0.0061	0.0048
	(0.0003-0.0008)	(0.0003-0.0006)	(0.0048-0.0098)	(0.0028-0.0133)
Θ[a]	**0.0005**	**0.0003**	**0.0061**	**0.0084**

[a] Median values of the 5 healthy individuals

[b] 95%-confidence intervals (given in parentheses) were determined by a bootstrap method [33, 60]

healthy individuals, in line with previous data from HIV-infected subjects [57]. In order to follow the fate of the newly produced T cells in HIV infection, we

also measured the percentage of labeled DNA within each T cell population during the subsequent 16 weeks after label cessation. The data of (3 out of 4) HIV-infected individuals turned out to be significantly better described by a model that allowed for kinetic heterogeneity, not only for memory but also for naive T cells, (Fig. 6.3). The dynamics of the naive T cell pool thus became

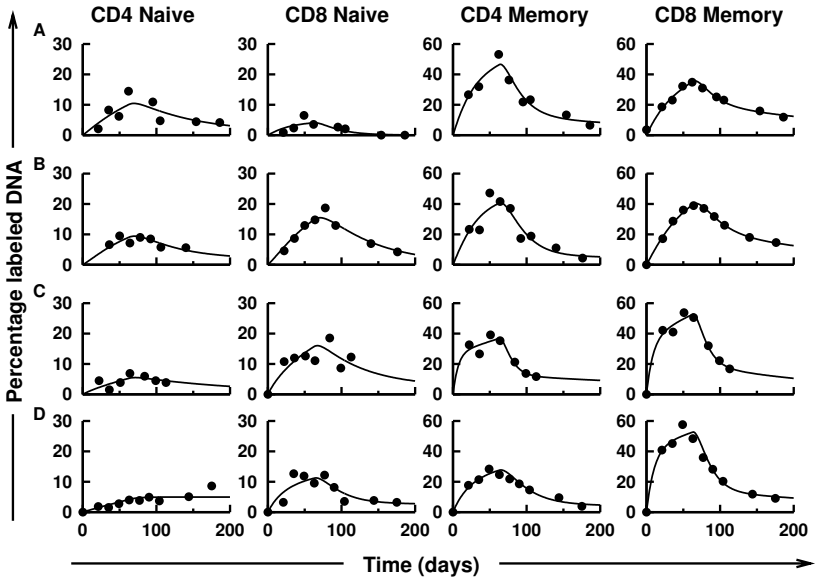

Fig. 6.3: ^{2}H enrichment of naive and memory T cells of HIV-infected individuals. Best fits of the percentage of labeled DNA in naive and memory CD4$^+$ and CD8$^+$ T cells of 4 HIV-infected individuals. The curves show the best fit of the two-compartment model to the experimental data. Label enrichment in the DNA of the different cell populations was scaled between 0 and 100% by normalizing for the estimated maximum percentage labeled DNA obtained in granulocytes (see Material and Methods).

qualitatively different upon HIV infection; instead of the homogeneous behavior of naive T cells in healthy humans, naive T cells in HIV-infected individuals become kinetically heterogeneous. The average turnover rates of naive CD4$^+$ and CD8$^+$ T cells were $\sim$0.16% and 0.37% of the naive CD4$^+$ and CD8$^+$ T cell pool per day, corresponding to expected lifespans of 618 and 271 days, respectively, which is 3 and 12 times shorter than in healthy volunteers. The average turnover rates of memory CD4$^+$ and CD8$^+$ T cells were 1.9% and 2.3% of the memory CD4$^+$ or CD8$^+$ T cell pool per day, corresponding to expected lifespans of 53 and 43 days, respectively, i.e. 3 times shorter than in uninfected individuals (Table 6.3 and Fig. 6.4A,B).

Although average *per capita* T cell turnover rates of all T cell subsets

Table. 6.3: Average *per capita* turnover rates (p day^{-}1) of HIV-1 infected individuals.

	Naive CD4$^+$	Naive CD8$^+$	Memory CD4$^+$	Memory CD8$^+$
A	0.0023	0.0017	0.0190	0.0124
	(0.0015-0.0033)[b]	(0.0009-0.0031)	(0.0139-0.0290)	(0.0081-0.0319)
B	0.0024	0.0038	0.0186	0.0140
	(0.0016-0.0034)	(0.0031-0.0048)	(0.0150-0.025)	(0.0103-0.0426)
C	0.0010	0.0036	0.0291	0.0328
	(0.0005-0.0016)	(0.0024-0.0054)	(0.0148-0.1210)	(0.0194-0.1060)
D	0.0006	0.0039	0.0096	0.0344
	(0.0005-0.0008)	(0.0027-0.0061)	(0.0077-0.0142)	(0.0256-0.0508)
Θ[a]	**0.0016**	**0.0037**	**0.0188**	**0.0234**

[a] Median values of the 4 HIV infected individuals.
[b] 95%-confidence intervals (given in parentheses) were determined by a bootstrap method [33, 60]

were increased in HIV infection, total naive CD4$^+$ T cell production rates, expressed in cells per day, were found to be reduced in 3 out of 4 HIV-infected individuals when compared to healthy volunteers (Fig. 6.4C). This was a direct consequence of the dramatically reduced naive CD4$^+$ T cell counts of the HIV-infected individuals included in this study (Table 6.1). Total memory CD4$^+$ T cell production was similar in HIV-infected and healthy individuals (Fig. 6.4D). Total naive and memory CD8$^+$ T cell production expressed in cells per day were found to be significantly increased during HIV infection (Fig. 6.4C,D) even though naive CD8$^+$ T cell counts were significantly decreased in HIV-infected individuals (Table 6.1).

6.3 Discussion

Long-term administration of ^2H_2O and follow-up of labeled T cells after label cessation enabled us to measure T cell turnover rates even in the naive T cell pool of healthy and HIV-infected individuals. Our data suggest that both naive and memory CD4$^+$ and CD8$^+$ average T cell life spans are at least 3-fold shortened during HIV infection, and point at qualitative changes in the kinetics of the naive T cell pool of HIV-infected individuals. Whereas in healthy individuals, naive T cells form a kinetically homogeneous pool of cells that are extremely long-lived, upon HIV infection the naive T cell population becomes kinetically heterogeneous, and a significant subset of naive T cells acquires a high rate of turnover. During the entire follow-up period, naive T cell numbers nevertheless stayed relatively constant in all HIV-infected individuals, suggesting that the naive T cells that acquired a short expected life span were also produced at high rates. Although the ages of HIV-infected and healthy subjects differed, it is highly unlikely that the observed differences in T cell turnover are due to age differences, because T cell turnover rates in healthy individuals have previously been shown to be hardly influenced by age [139].

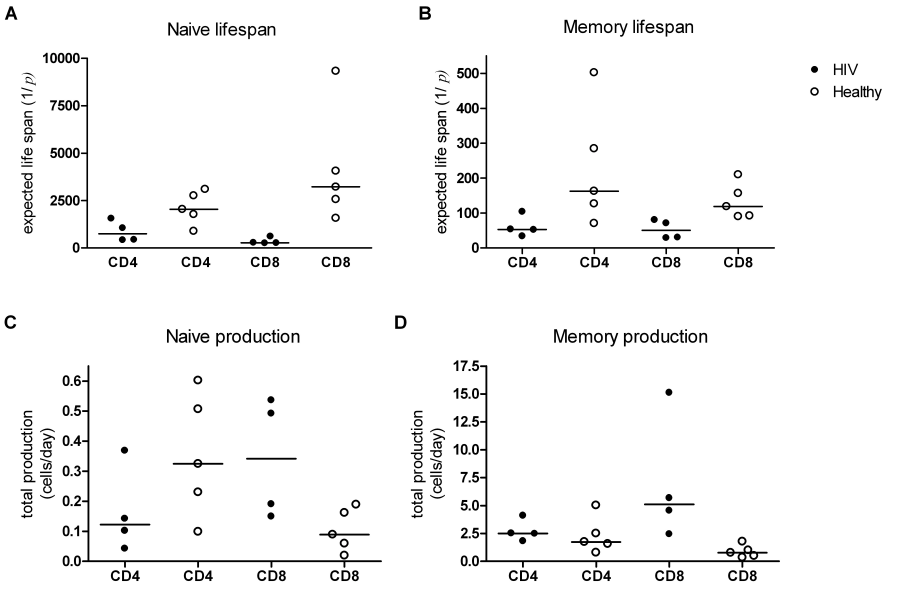

Fig. 6.4: Estimated T cell life spans and total daily production in healthy and HIV-infected individuals. Estimated life spans of (A) naive and B) memory $CD4^+$ and $CD8^+$ T cells in HIV-infected (closed symbols) and healthy (open symbols) individuals, calculated from the average T cell turnover rate (p) resulting from fitting a two-compartment model to the data. Total daily production (expressed in cells per day) of (C) naive and (D) memory $CD4^+$ and $CD8^+$ T cells in HIV-infected (closed symbols) and healthy (open symbols) individuals, calculated by multiplying the estimated average T cell turnover rate (p), based on the two-compartment model) with the number of T cells in the population under investigation.

Elevated T cell production rates in HIV-infected patients have been proposed to reflect either a homeostatic response to compensate for the progressive loss of $CD4^+$ T cells [26, 62], or to be driven by immune activation [50, 54]. It has previously been shown that HIV-infected patients suffering from AIDS have increased levels of IL-7 production in lymphoid tissue [90], and that naive T cells can divide in response to IL-7 while retaining the naive phenotype [120, 123], suggesting that homeostatic T cell proliferation may occur in HIV infection. However, the observation that HAART strongly decreases the percentage of Ki67-expressing $CD4^+$ T cells long before $CD4^+$ T cell numbers have recovered to normal values provides a very strong argument that increased T cell production rates in HIV infection are driven by the effects of the virus, rather than by a homeostatic response to low $CD4^+$ T cell numbers [54].

The role of the thymus in the altered dynamics of naive T cells during

6. Qualitative changes in T cell turnover during HIV-1 infection.

HIV-1 infection is vigorously debated [26, 29, 51, 86]. Using mathematical modeling we have shown that the observed relatively rapid dilution of the average T cell receptor excision circle (TREC) content of naive T cells in HIV-infected individuals [29] cannot be explained by changes in thymic output alone [51] when naive T cells are long-lived. TREC dilution in HIV infection is therefore presumably caused by the state of chronic immune activation induced by the virus [51]. This conclusion is confirmed by our long-term follow-up of ^2H_2O-labeled individuals, demonstrating that under healthy circumstances naive $CD4^+$ and $CD8^+$ T cells are kinetically homogeneous and have expected life spans as long as 5.6 and 8.8 years, respectively.

Our original proposal that rapid dilution of the TREC content in naive T cells during HIV infection is caused by increased rates of naive T-lymphocyte turnover [51] was criticized for several reasons. Firstly, it was argued that if the naive T cell pool comprises a sub-population of short-lived RTE, as has been suggested in mice [7, 8], the average TREC content of naive T cells may be rapidly affected when thymic output is blocked [26]. Our analysis of ^2H_2O labeling data demonstrates that human naive T cells are very long-lived and form a kinetically homogeneous population, arguing against the presence of a substantial RTE population with rapid kinetics in healthy adults (see Dion et al. [26], Vrisekoop et al. [136]. Secondly, the fact that increased Ki67 expression of naive T cells in HIV infection was taken as support for the immune activation hypothesis, has been criticized because Ki67 expression may be high due to cell cycle arrest [18]. Here we show that naive and memory *per capita* production and death rates in HIV infection are significantly increased, which is perfectly consistent with their increased Ki67 expression. Importantly, we also show that the increased turnover in the naive T cell population during HIV infection is probably caused by sub-populations of naive T cells obtaining higher production and loss rates. Apparently these cells retain the $CD45RA^+CD27^+$ phenotype of naive T cells, and readily explain the observed dilution of the naive T cell TREC content during HIV infection. This result refutes the third criticism, that the generation of a population of transitional naive T cells, which are about to enter the memory T cell pool, would not reduce the average naive T cell TREC content [42].

By gradually building up the mathematical model, from a one-compartment model in which every cell is produced and lost at the same rate, to a two-compartment model, we found that adding a second compartment did not significantly improve the quality of the fit of the naive T cell labeling data from healthy volunteers. This suggests not only that there is no substantial pool of short-lived RTE in healthy humans, in contrast to what was previously suggested by others [26], but also that recently-produced naive T cells have the same life expectancy as resident naive T cells, in contrast to what we proposed based on our previous modeling approach [136]. Interestingly, despite much higher rates of naive T cell turnover in mice compared to humans, we found that even in mice there is no evidence for kinetic heterogeneity in the naive T

cell pool (Den Braber et al. unpublished).

The current data are fully in line with the idea that changes in the T-lymphocyte populations of HIV-infected individuals are to a large extent caused by the immune activation induced by the virus. Other lines of evidence for the critical role of immune activation in HIV-1 infection include i) the finding that the level of T cell activation is the strongest prognostic factor for disease progression, even independent of plasma viral load [24, 39, 52], and ii) the observation that both SIV-infected sooty mangabeys, which do not develop AIDS despite high HIV loads [119], and rare, long-term asymptomatic HIV-infected patients with high plasma loads of pathogenic HIV [17] have low levels of immune activation. The acute, drastic loss of memory $CD4^+$ T cells from the gastro-intestinal tract which causes translocation of microbial products from the gut into the blood in HIV-infected individuals may be the driver of chronic immune activation during HIV-infection [14].

Summarizing, mathematical modeling of the longest human labeling time series published so far suggests that naive T cell populations become kinetically heterogeneous during HIV-1 infection, probably by adding a compartment of naive T cells with rapid turnover. At present it remains unclear how one should interpret the biological nature of the naive T cells comprising this compartment. The fact that treatment normalizes naive turnover rates long before $CD4^+$ T cell counts have normalized [54] demonstrates that the rapid naive T cell compartment is not reflecting a homeostatic response, and is more likely a consequence of the state of chronic immune activation induced by the virus.

*A*cknowledgments
The authors greatly acknowledge Marc Hellerstein and Rich Neese for sharing the ^2H_2O labeling and GC MS protocols, and Mette D. Hazenberg for her help in designing and implementing the study protocol. This research has been funded by AIDS Fonds Netherlands (grants 4025, 4024, 7010) and the Netherlands Organization for Scientific Research (NWO, grants 016.048.603, 917.96.350, 836.07.002).

6.4 Material and Methods

Subjects and *in vivo* ^2H_2O labeling protocol
Four HIV-infected and five healthy male volunteers were admitted to the AMC hospital, Amsterdam, the Netherlands to receive the initial dose of 10 ml ^2H_2O per kg body water in small portions throughout the day. Body water was estimated to be 60% of body weight. As a maintenance dose, the subjects drank 1/8 of their initial dose daily for nine weeks. Blood and urine were collected before labeling, at the end of the first labeling day, four to six times during the rest of the nine-week labeling phase, five to seven times during the down-label phase of 16 weeks, and approximately 3 years after stop of label in healthy individuals. All HIV-patients were treatment-naive at inclusion and did not receive

antiretroviral therapy during the whole protocol (CDC class A). Patient B experienced bronchitis (diagnosed and treated by the general practitioner) which started a few days prior to the second visit at day 22. Patient C withdrew from the protocol from day 113 onward, because he was advised to start treatment, and developed a disseminated Varicella shortly after withdrawal. Patient D developed gastro-enteritis (light fever and diarrhea) a few days prior to the visit at day 63. All healthy volunteers were asked to answer a questionnaire to exclude (a high risk of) infections and immunomodulatory medication. Details about the HIV-infected patients are shown in Table 6.1, while those about the healthy volunteers have been described previously [136]. This study was approved by the medical ethical committee of the AMC and written informed consent was obtained from all participants [136].

Flow cytometry and cell sorting
Absolute $CD4^+$ and $CD8^+$ T cell counts were determined by dual-platform flow cytometry. Peripheral blood mononuclear cells (PBMC) were obtained by Ficoll-Paque density gradient centrifugation from heparinized blood and cryopreserved until further processed. T cell proliferation in $CD4^+$ and $CD8^+$ T cell subsets was studied by flow-cytometric measurements of the Ki67 nuclear antigen, as described previously [54]. To measure the fraction of labeled cells within the naive ($CD45RO^-CD27^+$) and memory ($CD45RO^+$) $CD4^+$ and $CD8^+$ T cell population, these subsets were isolated by cell sorting on a FACSAria (BD) as previously described [136]. Purity of the sorted cells was on average 99.2% for naive $CD4^+$, 98.7% for naive $CD8^+$ T cells, 98.1% for memory $CD4^+$ T cells and 97.1% for memory $CD8^+$ T cells.

Measurement of ^2H_2O enrichment in body water and DNA and mathematical modeling
Deuterium enrichment in urine was measured by a method adopted from Previs et al. [106]. The isotopic enrichment of DNA was measured according to the method described by Neese et al. [93] with minor modifications [136]. We first fitted a simple label enrichment/decay curve to the urine enrichment data of each individual:
During label intake ($t \leq \tau$):

$$U(t) = f(1 - e^{-\delta t}) + \beta e^{-\delta t} \tag{6.1}$$

After label intake ($t > \tau$):

$$U(t) = \left[f(1 - e^{-\delta t}) + \beta e^{-\delta t}\right] e^{-\delta(t-\tau)}. \tag{6.2}$$

as described previously [136] (see Fig. S.6.2, Table S.6.3 and Table S.6.1), where $U(t)$ represents the fraction of ^2H_2O in plasma at time t (in days), f is the fraction of ^2H_2O in the drinking water, labelling was stopped at $t = \tau$ days, δ represents the turnover rate of body water per day, and β is the plasma enrichment attained after the boost of label by the end of day 0. We incorporated these best fits when analyzing the enrichment in the different

cell populations. Up- and down-labeling of the granulocyte population of each individual was analyzed as described previously [136] (see Fig. S.6.2, Table S.6.4 and Table S.6.2), to estimate the maximum level of label intake that cells could possibly attain. The label enrichment data of all cell subsets were subsequently scaled by the granulocyte asymptote of each individual [136].

Labeling data of the different T cell subsets were fitted with mathematical models that did or did not allow for kinetic heterogeneity between cells of the same population. Each kinetic sub-population i was modeled to contain a fraction α_i of cells with turnover rate p_i. Assuming a steady state for each kinetic sub-population, label enrichment of adenosine in the DNA of each sub-population i was modeled by the following differential equation:

$$l_i' = p_i c U(t) \alpha_i A - P_i l_i \tag{6.3}$$

where l_i is the total amount of labeled adenosine in the DNA of sub-population i and A is the total amount of adenosine in the cell population under investigation , c is an amplification factor that needs to be introduced because the adenosine deoxyribose (Dar) moiety contains seven hydrogen atoms that can be replaced by deuterium, and p_i is the average turnover rate of sub-population i. Basically, labeled adenosines in sub-population i are gained when a deuterium atom is incorporated with probability $cU(t)$ into the DNA of cells that replicate at rate p_i, and they are lost when cells of sub-population i are lost at rate p_i. For naive T cells this replication may occur both in the periphery and in the thymus. Scaling this equation by the total amount of adenosine in the DNA of sub-population i, i.e., defining $L_i = l_i/(\alpha_i A)$, yields

$$L_i' = p_i c U(t) - P_i L_i \tag{6.4}$$

throughout the up- and down-labeling period, where L_i represents the fraction of labeled adenosine dR moieties in the DNA of sub-population i. The corresponding analytical solutions are

$$L_i(t) = \frac{c}{\delta - p_i} \left[p_i \left(\beta e{-}p_i t - U(t) \right) + f(1 - e^{-p_i t}) \right] \tag{6.5}$$

during label intake ($t \leq \tau$), and

$$L_i(t) = \frac{p_i c}{\delta - p_i} \left[U(\tau) e{-}p_i (t - \tau) - U(t) \right] + L_i(\tau) e^{-p_i (t-\tau)} \tag{6.6}$$

after label intake ($t > \tau$).
The fraction of labeled DNA in the total T cell population under investigation was subsequently derived from $L(t) = \sum \alpha_i L_i(t)$, and the average turnover rate p was calculated from $p = \sum \alpha_i p_i$. Labeling data were first arc-sin(square-root) transformed, because all enrichment data were expressed as fractions. Best fits to the transformed data were subsequently determined using least square minimization, using the DNLS1 subroutine from the Common Los Alamos

Software Library, which is based on the Levenberg-Marquardt algorithm [83] for solving nonlinear least-squares problems. Ninety-five percent confidence intervals for the inferred parameters were then determined using a bootstrap method [33], where the residuals to the optimal fit were re-sampled 500 times. Half-lives were calculated from the average turnover rates as $\ln 2/p$.

6.5 Supplementary information.

Table. S.6.1: Parameter estimates of the urine enrichment curves of the healthy subjects, where f represents the fraction of ^2H_2O in the drinking water, d is the turnover rate of body water per day, and β represents the baseline urine enrichment attained after the boost of label by the end of day 0.

Individual	f	δ (day$^-$1)	β
A	0.0010	0.0610 0.0086	
B	0.0011	0.0822 0.0071	
C	0.0012	0.0705 0.0082	
D	0.0017	0.1204	0.0073
E	0.0020	0.1338	0.0059

Table. S.6.2: Parameter estimates of the granulocyte enrichment curves of the healthy subjects, where d represents the loss rate of labeled granulocytes, p is the average production rate of granulocytes, and c the amplification factor.

Individual	pc (day$^-$1)	d (day$^-$1)
A	0.4105	0.0938
B	0.4813	0.1016
C	0.3729	0.0751
D	0.3195	0.0853
E	0.4237	0.1052

Table. S.6.3: Parameter estimates of the urine enrichment curves of the HIV-infected subjects, where f represents the fraction of ^2H_2O in the drinking water, d is the turnover rate of body water per day, and β represents the baseline urine enrichment attained after the boost of label by the end of day 0.

Individual	f	δ (day$^-$1)	β
A	0.0007	0.1080	0.0053
B	0.0010	0.0735	0.0087
C	0.0009	0.1221	0.0102
D	0.0012	0.0811	0.0178

Table. S.6.4: Parameter estimates of the granulocyte enrichment curves of the HIV-infected subjects, where d represents the loss rate of labeled granulocytes, p is the average production rate of granulocytes, and c the amplification factor.

Individual	pc (day$^-$1)	d (day$^-$1)
A	0.5265	0.0994
B	0.3391	0.0790
C	0.5390	0.1196
D	0.4174	0.0937

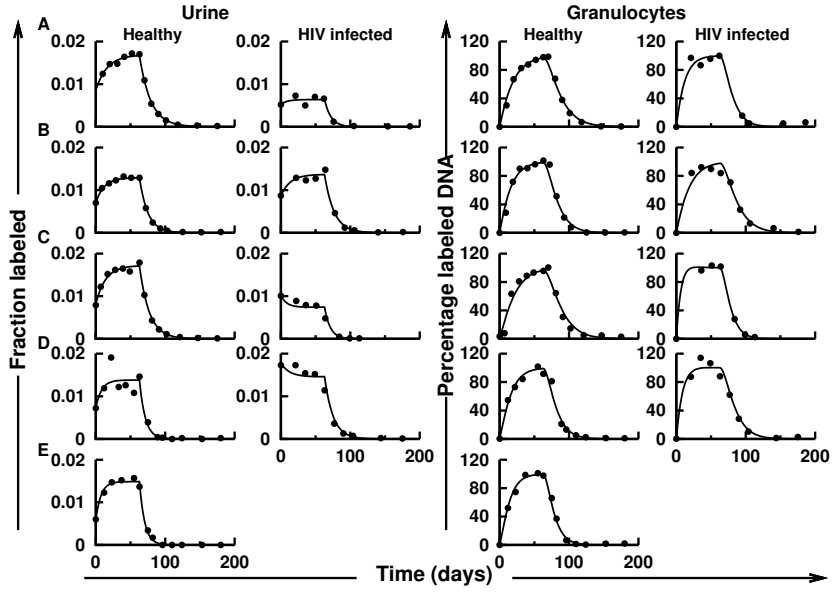

Fig. S.6.2: ^{2}H enrichment of urine and granulocytes of healthy and HIV-infected individuals. Best fits of the fraction of ^2H_2O in urine and of the enrichment curves of granulocytes of 5 healthy volunteers and 4 HIV-infected individuals (see Material and Methods).

7

Biphasic TREC dynamics during HIV-1 infection.

Nienke Vrisekoop[1,*], Tendai Mugwagwa[2,*], Anne Bregje de Boer[1], Sigrid A. Otto[1], Mette D. Hazenberg[1], Kiki Tesselaar[1], Frank Miedema[1], Rob J. de Boer[2], and José A.M. Borghans[1,2].

[1]Department of Immunology, University Medical Center, 3508 AB Utrecht, The Netherlands;
[2]Department of Theoretical Biology, Utrecht University, 3584 CH Utrecht, The Netherlands
* These authors contributed equally to this study

Abstract

HIV-1 infection is frequently associated with a reduction in T cell receptor excision circles (TREC). However, most TREC data come from cross-sectional studies, and little is known about the time course of the changes in TRECs during HIV-disease progression. We have obtained longitudinal data on $CD4^+$ and $CD8^+$ T cell TRECs and T cell counts from human subjects before and after HIV seroconversion. The data demonstrate that $CD4^+$ and $CD8^+$ T cell TREC dynamics during HIV infection are biphasic, with a rapid TREC loss during the first year and a slow loss during the chronic phase of infection. During the first year of HIV infection in our study subjects, the total number of TRECs in the blood at least halved, and the loss of TRECs from the blood exceeded the loss of naive T cells. During later stages of HIV infection, $CD4^+$ T cell TREC contents remained fairly constant because total $CD4^+$ T cell TREC loss paralleled the loss of naive and effector/memory $CD4^+$ T cells, while in the $CD8^+$ T cell pool the loss of TRECs generally exceeded the loss of naive T cells. We interpreted these data using mathematical modeling, which pointed out that massive recruitment of naive T cells into the effector/memory compartment is a likely explanation for the biphasic dynamics of TREC during HIV infection.

7.1 Introduction

HIV-1 infection has repeatedly been associated with reduced absolute T cell receptor excision circle (TREC) numbers per ml blood (TREC total) and reduced TREC levels per peripheral T cell (TREC content) [29, 51, 143]. This observation has widely been interpreted as evidence for impairment of the thymus during HIV infection [29, 143]. However, not only changes in thymic output, but also changes in the naive/memory T cell ratio, T cell division and death rates, and priming rates of naive T cells affect TREC dynamics [29, 51]. Since all of these factors are disturbed in HIV infection, TREC data from HIV-infected subjects cannot be used as evidence for HIV-induced thymic impairment, and the cause of TREC changes during HIV infection seems multifactorial.

During thymic TCR rearrangement, several types of TRECs, including Vβ and Sj TRECs, are formed sequentially. Dion et al. [26] described relatively rapid changes in Sj/Vβ TREC ratios within the first 3 months of HIV infection. These changes were attributed to changes in intrathymic proliferation, because peripheral T cell proliferation dilutes both types of TRECs equally, leaving the Sj/Vβ TREC ratio unaffected. Based on these observations, it was concluded that the changes in Sj TREC in HIV infection are due to the rapid loss of recent thymic emigrants (RTE) containing most of the TRECs. Indeed, the existence of a considerable short-lived RTE pool has been suggested in young mice [117] and chickens [73]. However, our own recent work has indicated that in human

adults recently produced naive T cells are rare and long-lived [136, Chapter 6], which questions the existence of a substantial short-lived RTE pool in human adults. Moreover, the effect of SIV infection on TRECs in sooty mangabeys [89] and rhesus macaques [4] was shown to exceed the effect of thymectomy, which suggests that SIV infection does much more than just remove RTEs [11].

In order to understand the cause of TREC changes during HIV infection, longitudinal TREC analyses over seroconversion and during HIV infection are needed. So far, most TREC data have come from cross-sectional studies, and little is known about the course of the changes in TRECs during HIV-disease progression. Cross-sectional studies are further hampered by the large inter-individual differences in TREC of both healthy and HIV-infected subjects. Indeed, a considerable overlap between TREC content in $CD4^+$ T cells from healthy and HIV-infected individuals has repeatedly been reported [47, 94, 118, 143]. In the absence of longitudinal data, the interpretation of TREC data often remains inconclusive. For example, Nobile et al. [94] reported that HIV-infected individuals with high $CD4^+$ T cell counts had increased $CD4^+$ T cell TREC contents, while HIV-infected individuals with low $CD4^+$ T cell counts had lower $CD4^+$ T cell TREC contents than age-matched controls. Longitudinal interpretation of these cross-sectional data seems to suggest that $CD4^+$ T cell TREC contents increase over HIV seroconversion, and progressively decrease during HIV-disease progression. Alternatively, the observed high TREC contents in HIV-infected individuals with high $CD4^+$ T cell counts may be due to a selection bias, because individuals with high pre-seroconversion $CD4^+$ T cell counts may also have high pre-seroconversion $CD4^+$ TREC contents, e.g. due to high levels of thymic output [94]. Indeed, extrapolation of cross-sectional data to longitudinal interpretation is prone to be erroneous.

The longitudinal studies on TREC dynamics in HIV infection that are available, unfortunately measured TRECs in PBMC [16, 47, 132, 143], and not in the more relevant T cell sub-populations. TREC contents in PBMC may not be representative for the TREC content of $CD4^+$ T cells, since the fraction of $CD4^+$ T cells declines during disease progression, and the TREC content of $CD8^+$ T cells has been found to be lower than the TREC content of $CD4^+$ T cells [94, 118].

To overcome the above problems in elucidating the mechanism behind the dynamics of $CD4^+$ and $CD8^+$ T cell TREC contents during HIV-infection, we performed a longitudinal analysis of T cell counts, naive/memory T cell ratios, and T cell TREC dynamics in the different $CD4^+$ and $CD8^+$ T cell subsets in HIV-1 infected patients. It has recently become clear that even during the acute phase of HIV infection large changes in immune parameters occur. For example, effector $CD4^+$ T cells in the mucosal tissues (e.g. lung and gut) have been shown to be massively depleted during acute HIV and SIV infection [15, 43, 102], and HIV viral load and immune activation levels have

been shown to be much higher during acute compared to chronic HIV infection [111, 118]. Whenever possible our longitudinal analyses therefore included T cell and TREC data over HIV seroconversion and during the acute and chronic phase of infection. The resulting data were interpreted with the help of a mathematical model.

7.2 Results

TREC dynamics in $CD4^+$ and $CD8^+$ T cells over seroconversion and during HIV infection

We performed longitudinal analyses of TREC contents per $CD4^+$ and $CD8^+$ T cell over HIV-seroconversion in 13 individuals, seven of whom we were also able to follow during chronic HIV infection. An additional 5 HIV-infected individuals could only be followed during chronic HIV infection. The median time point at which samples were analyzed before seroconversion was 4.8 years (range 2.8-11.4) and the median times during HIV infection were 1.0 year (range 0.8-1.3) and 5.0 years (range 3.5-5.2) post-seroconversion. We refer to the period between seroconversion and 1 year post-seroconversion (i.e. the acute phase) as phase I, the period between 1 year and 5 years post-seroconversion as phase II. In addition to TRECs, absolute $CD4^+$ and $CD8^+$ T cell counts and fractions of naive and effector/memory $CD4^+$ and $CD8^+$ T cells were determined for all HIV-infected individuals.

Longitudinal analysis of $CD4^+$ T cell TREC contents showed biphasic dynamics during HIV-disease progression, consisting of a rapid decline in $CD4^+$ T cell TREC content over seroconversion ($p=0.01$), and a rather stable TREC content during the chronic phase ($p=0.424$, Fig. 7.1a). Absolute numbers of TRECs per ml blood in the $CD4^+$ T cell population showed a steep decline over seroconversion ($p=0.002$), but continued to decline, albeit to a lesser extent, during chronic infection ($p=0.032$, Fig. 7.1b). The TREC content of $CD8^+$ T cells decreased significantly during phase I ($p=0.001$) and nearly significantly during phase II ($p=0.052$) (Fig. 7.1c). Absolute $CD8^+$ T cell TREC numbers decreased during phase I ($p=0.033$) but - unlike $CD4^+$ T cell TREC numbers - stayed stable during phase II ($p=0.250$) (Fig. 7.1d).

When analysed cross-sectionally, neither the $CD4^+$ T cell TREC content 1 or 5 years after seroconversion in these individuals, nor the $CD4^+$ T cell TREC content of 27 additionally measured chronic HIV-infected individuals differed significantly from 38 healthy age-matched control values. Only HIV-infected individuals who had progressed to AIDS ($n=16$) had significantly lower $CD4^+$ T cell TREC contents compared to healthy individuals when compared cross-sectionally (Fig. 7.1). Similarly, the longitudinally observed decrease in $CD8^+$ T cell TREC contents during HIV infection was neither apparent when $CD8^+$ T cell TREC contents at 1 or 5 years post-seroconversion in these individuals, nor in the additionally studied chronic HIV-infected individuals were compared to

healthy control values (Fig. 7.1a,c), underlining the importance of longitudinal follow-up in TREC analyses.

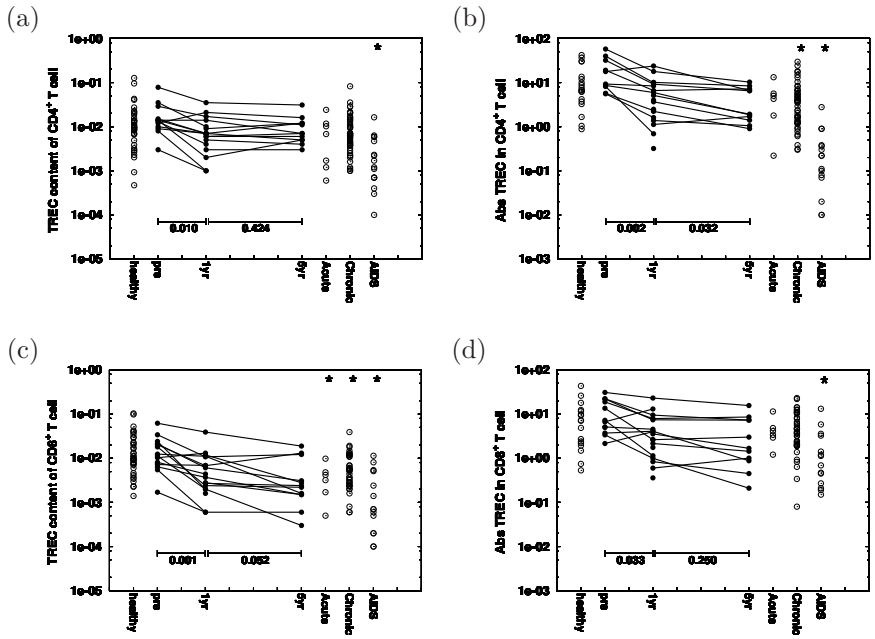

Fig. 7.1: $CD4^+$ and $CD8^+$ T cell TREC dynamics over seroconversion and during HIV infection. $CD4^+$ T cell TREC contents (a), total TREC numbers in $CD4^+$ T cells per ml blood (b), $CD8^+$ T cell TREC contents (c), and total TREC numbers in $CD8^+$ T cells per ml blood (d) measured over seroconversion and during HIV infection. Longitudinal data are connected by straightbp lines, while cross-sectional data are denoted by loose data points. Data were collected during acute and chronic HIV infection as well as during progression to AIDS and were compared to age-matched controls. P-values for phase I and phase II are indicated in the figure, and the P-value for the difference between cross-sectional data from healthy and HIV infected subjects if marked by an asterisk if $p < 0.05$.

We also analysed TREC contents in FACS-sorted naive $CD4^+$ T cells during chronic infection (Phase II) in 7 HIV-infected individuals who were followed longitudinally. The naive $CD4^+$ T cell TREC content did not decrease during follow-up even when HIV-infected individuals progressed to AIDS, or evolved to CXCR4-using virus variants capable of infecting naive $CD4^+$ T cells (p=0.469, comparing first and last time points, Fig. 7.2). Again, no significant difference was found between naive $CD4^+$ T cell TREC contents from HIV-infected individuals and healthy age-matched controls (Fig. 7.2). Unfortunately, we did not have sufficient cells pre-seroconversion to obtain TREC data within the

naive T cell pool during phase I.

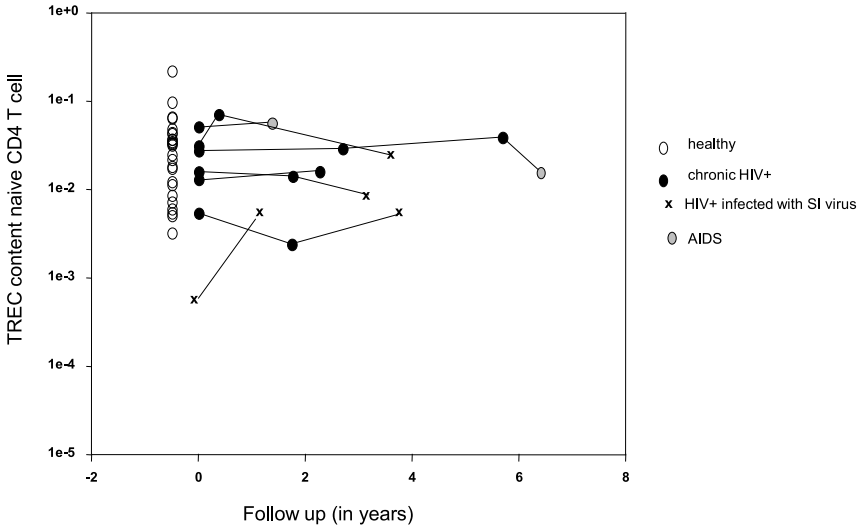

Fig. 7.2: Naive $CD4^+$ T cell TREC-content dynamics during chronic HIV infection. Longitudinal analyses of TREC contents per naive $CD4^+$ T cell in patients during chronic HIV infection (black circles), infection with CXCR4-using/ SI virus variants (x-marked) and progression to AIDS (grey circles) compared to healthy controls (white circles).

To obtain insights into the mechanism behind the early rapid and late slow decay of $CD4^+$ and $CD8^+$ T cell TREC contents, we calculated the fractional changes per year in naive and effector/memory T cell numbers, and in absolute TREC numbers per ml blood during the different phases of infection. During phase I, we found that the fractional loss of TRECs per ml blood in $CD4^+$ and $CD8^+$ T cells tended to be higher than the loss of naive $CD4^+$ and $CD8^+$ T cells, resulting in a decrease in the $CD4^+$ and $CD8^+$ T cell TREC content. In some HIV-infected individuals the number of naive $CD4^+$ or $CD8^+$ T cells even increased over seroconversion despite decreased $CD4^+$ or $CD8^+$ T cell TREC numbers per ml blood (Fig. 7.3a,d), suggesting that naive $CD4^+$ and $CD8^+$ T cells expanded by division during HIV infection. In general, the fractional loss of naive $CD8^+$ T cells during phase I was smaller than the loss of naive $CD4^+$ T cells. Effector/memory $CD4^+$ T cell numbers showed a tendency to decrease during phase I (Fig. 7.3b), while effector/memory $CD8^+$ T cell

numbers increased in all individuals (Fig. 7.3e). As a consequence, the ratio of naive/memory $CD8^+$ T cells tended to decrease during phase I (Fig. 7.3f), while the ratio of naive/memory $CD4^+$ T cells did not show any clear pattern (Fig. 7.3c).

During phase II, the fractional changes of all the variables were much less pronounced than in phase I, but tended to follow the same pattern (Fig. 7.3a,b,d,e). As a consequence, naive/memory $CD4^+$ and $CD8^+$ T cell ratios were mostly stable in this phase (Fig. 7.3c,f), and the proportional loss of TRECs and naive $CD4^+$ and $CD8^+$ T cells was reflected in stable $CD4^+$ and $CD8^+$ TREC contents.

Explaining the biphasic TREC kinetics during HIV-disease progression

Combining the above observations, we sought for a mechanism that could explain the biphasic TREC dynamics during HIV infection. Thanks to the combination of TREC and total cell-number data, several explanations could be ruled out: i) The rapid decline in $CD4^+$ and $CD8^+$ T cell TREC contents during phase I cannot merely be attributed to TREC dilution by peripheral T cell proliferation, because absolute TREC numbers per ml blood also decreased (Fig. 7.1b,d). In half of the individuals $CD4^+$ and $CD8^+$ T cell TREC numbers per ml blood declined more than 50 percent during the first year of HIV infection (Fig. 7.3a,d). ii) The rapid decline in $CD4^+$ T cell TREC contents during phase I cannot be attributed to decreases in naive/memory $CD4^+$ T cell ratios, because both increases and decreases in this ratio were observed during phase I (Fig. 7.3c). Decreased naive/memory $CD8^+$ T cell ratios may, however, explain the rapid decline in $CD8^+$ T cell TREC contents over seroconversion (Fig. 7.3f). iii) We have also ruled out the possibility that the decreases in $CD4^+$ and $CD8^+$ T cell TREC contents in phase I were related to sampling time before seroconversion (data not shown).

To search for an alternative explanation for the biphasic TREC dynamics during HIV infection, we used a previously developed mathematical model [51] for the dynamics of TRECs which we extended to include naive and effector/memory T cells (see Methods). In the model, naive T cells are maintained by thymic output and peripheral renewal, while effector/memory T cells are maintained by activation (and subsequent clonal expansion) of naive T cells and by renewal. HIV infection could influence TREC dynamics of naive and memory T cells in several ways: 1) directly increase the death rates of naive and memory $CD4^+$ T cells, 2) increase the antigen-driven priming of naive $CD4^+$ and $CD8^+$ T cells into the memory compartment, and 3) induce naive and memory $CD4^+$ and $CD8^+$ T cell division as a result of increased activation. We implemented HIV infection in the model by increasing the death rate of memory $CD4^+$ T cells, the activation of naive $CD4^+$ and $CD8^+$ T cells into memory T cells, and the proliferation rate of naive $CD4^+$ and $CD8^+$ T cells.

Simulations of the model showed that such HIV-induced changes in T cell

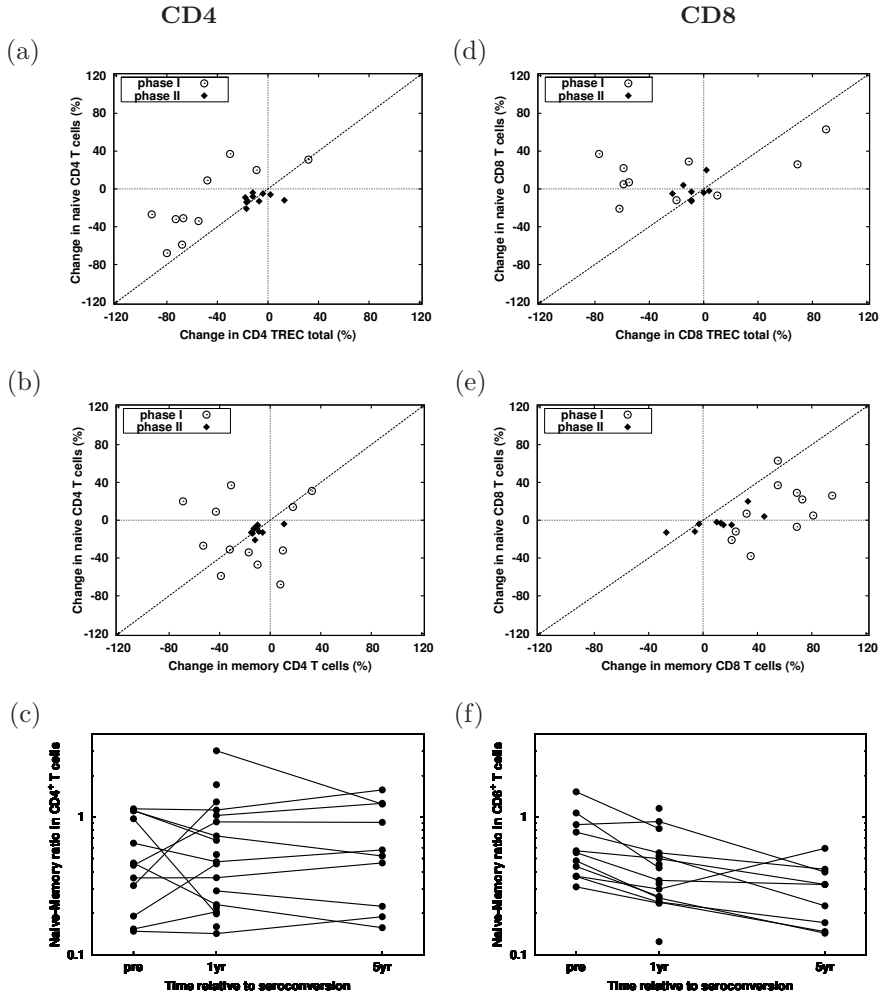

Fig. 7.3: Fractional loss of naive and effector/memory $CD4^+$ and $CD8^+$ T cells and TRECs. The loss of naive T cells during phase I and II as a percentage of the baseline values pre-seroconversion and 1 year after sero-conversion, (a,d) compared to the percentage loss of total TREC numbers per ml blood and (b,e) compared to the percentage loss of effector/memory T cells. Circles represent the percentage lost during the first year of infection (phase I) and diamonds denote the loss during the chronic phase (phase II) of HIV infection. Panel (c,f) depicts longitudinal changes in naive/memory T cell ratios.

dynamics together were sufficient to mimic the experimentally observed biphasic $CD4^+$ and $CD8^+$ (Fig. 7.4) T cell and TREC dynamics. We found that an early loss of naive and memory $CD4^+$ T cells, TREC numbers, and $CD4^+$ T cell TREC contents was achieved if HIV infection leads to the recruitment of a large fraction of naive $CD4^+$ T cells into the effector/memory compartment. Once naive cells and their TRECs have been recruited into the memory pool, they are rapidly lost as a result of the relatively short natural lifespan of effector/memory $CD4^+$ T cells, which might be further shortened by virus-mediated killing of effector/memory $CD4^+$ T cells. Similarly, the early decrease in $CD8^+$ T cell TREC contents can be explained by the recruitment of TREC-bearing naive $CD8^+$ T cells into the $CD8^+$ memory T cell pool, where they are lost by the shorter life span of effector/memory cells. An increase in division of naive $CD8^+$ T cells may compensate for this recruitment, leading to a net increase in naive $CD8^+$ T cell numbers. The increased proliferation and priming of naive $CD8^+$ T cells in the absence of increased death of memory $CD8^+$ T cells during HIV infection could explain the accumulation of cells in the memory $CD8^+$ T cell compartment.

During the chronic stage of HIV infection $CD4^+$ T cell TREC contents remain fairly constant, because total TREC loss remains in pace with the loss of naive and effector/memory $CD4^+$ T cells. The naive $CD4^+$ T cell dynamics predicted by the model displayed a similar biphasic pattern as observed for total $CD4^+$ T cell TREC contents (data not shown).

7.3 Discussion

Our comparison of longitudinal and cross-sectional TREC data demonstrates that evident TREC dynamics can easily be masked by large inter-individual differences in TREC measurements. In line with our own cross-sectional data, Sempowski et al. [118] did not detect differences in $CD4^+$ T cell TREC contents during acute HIV infection in a cross-sectional study, and concluded that TRECs were not affected during acute HIV infection. In similar cross-sectional studies, the TREC content of PBMC was found to decrease over seroconversion in only half of the HIV-infected individuals, while it remained stable in the other half of the patients [143], and decreased $CD4^+$ T cell TREC contents were reported during chronic HIV infection [94].

In contrast, our longitudinal data show that $CD4^+$ and $CD8^+$ T cell TREC dynamics during HIV infection are biphasic, with a rapid decline during the first year and a slow decline during the chronic phase of infection. The sharp decline in $CD4^+$ T cell TREC content in the first year of HIV infection is the result of a more rapid loss of $CD4^+$ T cell TREC numbers per ml blood compared to the loss of naive $CD4^+$ T cells. Remarkably, in the majority of HIV-infected individuals as much as 50% of the number of $CD4^+$ T cell TRECs per ml blood was lost during the first year of infection.

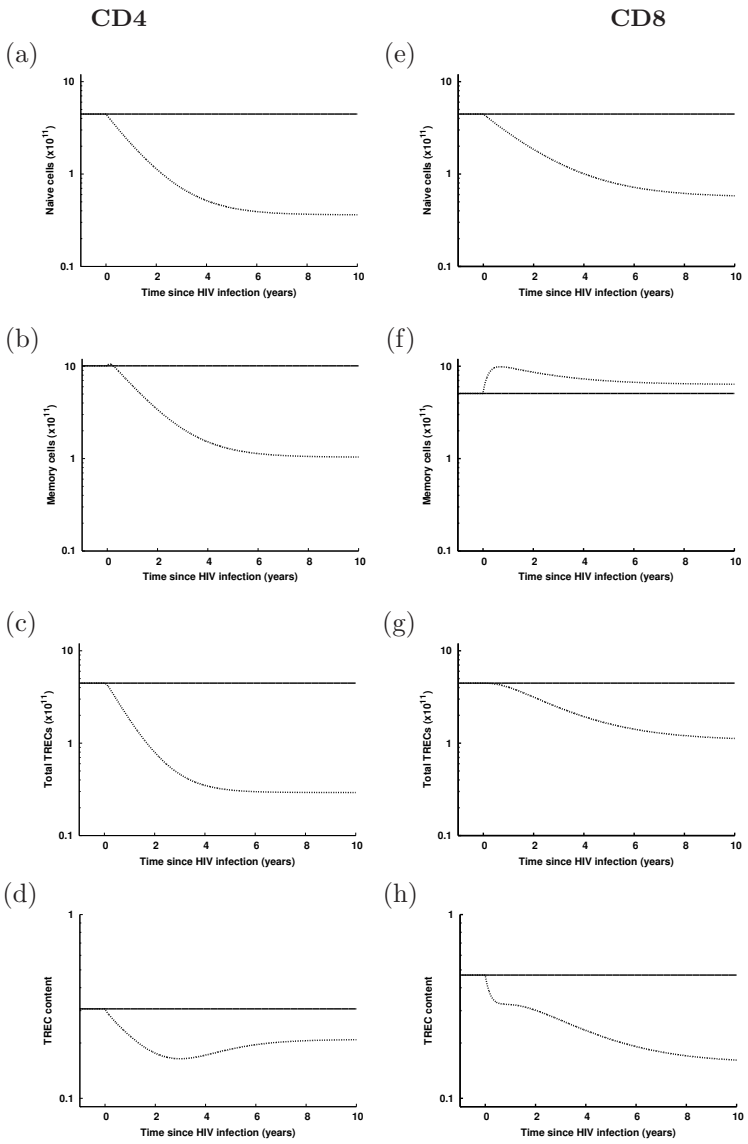

Fig. 7.4: $CD4^+$ and $CD8^+$ T cell and TREC dynamics during HIV infection according to the mathematical model. Simulation results of the model for $CD4^+$ (a-d) and $CD8^+$ (e-h) T cell and TREC dynamics during HIV infection (solid curves) compared to healthy dynamics during the same period (dashed curves). Parameter values for $CD4^+$ T cells of healthy individuals: $\sigma = 8e^8$, $\nu = 0$, $a = 1e^{-6}$, $r_1 = 0$, $d_N = 4e^{-16}$, $q = 64$, $r_2 = 0.004$, $d_M = 3e^{-15}$, $d_\nu = 0.001$, $c = 1$, and upon HIV infection: $a = 3e^{-3}$, $q = 21.3$, $r_1 = 0.0008$, $r_2 = 0.008$, $d_M = 0.03$. Parameter values for $CD8^+$ T cells of healthy individuals: $\sigma = 8e^8$, $\nu = 0$, $a = 1e^{-6}$, $r_1 = 0$, $d_N = 4e^{-16}$, $q = 64$, $r_2 = 0.005$, $d_M = 8e^{-15}$, $d_\nu = 0.001$, $c = 1$, and upon HIV infection :$a = 1.5e^{-3}$, $q = 8$, $r_1 = 0.0001$.

At first glance, the fast decline of TRECs and the smaller loss of naive T cells from the peripheral pool seem in good agreement with the loss of a short-lived TREC-rich RTE pool upon HIV infection, as thymectomy has been shown to cause a similar drop in TREC content in mice [117] and chickens [73]. However, heavy water labeling studies in human adults [136] and thymectomy studies in monkeys [Muthukumar et al][1] have indicated that RTE need not be short-lived (also see chapter 4). We therefore proposed an alternative model, in which a large fraction of naive $CD4^+$ T cells is transferred into the effector/memory T cell compartment during HIV infection. The more rapid loss of cells in the effector/memory compartment is responsible for the loss of TREC-bearing cells. Increased division of naive $CD4^+$ T cells to some extent replaces the cells with non-TREC-bearing cells resulting in a decrease in $CD4^+$ TREC content. This model appeared to be consistent with the longitudinal $CD4^+$ TREC and T cell dynamics that we observed, suggesting that increased activation of naive $CD4^+$ T cells throughout HIV infection is sufficient to explain these biphasic dynamics. Of note, not all naive $CD4^+$ T cells transferred into the effector/memory pool need to be HIV specific. Bystander activation by cytokines, or other pathogens e.g. due to a compromised gastrointestinal mucosal surface, might even play the dominant role in chronic immune activation during HIV infection [14]. The bi-phasic dynamics of $CD8^+$ T cell TREC contents can be explained by the same mechanism, except for the fact that $CD8^+$ T cells seem to compensate better for the loss of cells.

Although our model presents one way to explain the T cell and TREC dynamics without the need for a short-lived RTE pool, we do not exclude that other mechanisms may play a role. For example, increasing naive T cell death rather than increasing naive T cell recruitment to the effector/memory pool upon HIV infection probably explains the data equally well. Furthermore, we did not take redistribution of T cells from the blood to the lymphoid organs into account. Upon HIV infection, the percentage of naive $CD4^+$ T cells was found to be increased in lymphoid tissues and TREC losses were found to be less pronounced in lymphoid tissues than in the periphery. While in PBMC an inverse correlation between TREC and cellular viral load was found, there was a positive relation between TREC and cellular viral load in lymphoid tissue, suggesting that TREC-bearing cells may be selectively trapped in the lymphoid tissue during HIV infection [95].

In conclusion, our study shows that HIV infection has an almost instantaneous and large impact, not only on the memory $CD4^+$ T cell compartment [14], but also on the naive $CD4^+$ and $CD8^+$ T cell pools. The biphasic dynamics of $CD4^+$ and $CD8^+$ T cell TREC contents that we observed are consistent with a model in which both $CD4^+$ and $CD8^+$ naive T cells are massively recruited into the effector/memory compartment due to hyper-immune activation.

[1] Muthukumar A, Wozniakowski A, Matthews C, et al. Impact of thymectomy on SIV infection in macaques. 2004. Presented at: XIV international AIDS conference, Barcelona, Spain.

7.4 Materials and Methods

HIV- infected individuals
Samples from HIV-infected individuals for the longitudinal study and part of the cross-sectional study were derived from the Amsterdam Cohort Studies on HIV infection and AIDS. Cross-sectional data were extended with data obtained from previous studies [137, 138]. None of the HIV-infected individuals had been treated at the time of sampling. Individuals were called acute HIV-infected individuals when sampling took place within 2 months after onset of symptoms of acute HIV infection. Age-matched blood bank donors were used as healthy controls.

Flow cytometry and cell sorting
Peripheral blood mononuclear cells (PBMC) were obtained by Ficoll-Paque density gradient centrifugation from heparinized blood and viably frozen until further processed. Absolute $CD4^+$ and $CD8^+$ T cell counts were determined by dual-platform flow cytometry. Effector/memory ($CD27^+$ $CD45RA^-$, $CD27^-$ $CD45RA^-$ and $CD27^-$ $CD45RA^+$) and naive ($CD27^+$ $CD45RA^+$) $CD4^+$ and $CD8^+$ T cell fractions were assessed by flow cytometry as described previously and analyzed on a FACSCalibur with CellQuest software (Becton Dickinson (BD), San Jose, California) [52]. To measure the TREC content within naive ($CD45RO^-CD27^+$) $CD4^+$ T cells, PBMC were incubated with the monoclonal antibodies $CD45RO^-$FITC (Caltag Laboratories, Burlingame, CA), $CD27^-$PE, $CD4^-$PerCP and $CD8^-$APC (BD) and naive $CD4^+$ T cells were isolated by cell sorting on a MoFlow or a FACSAria (BD). In 14 out of 32 healthy individuals $CD45RA^+$ $CD4^+$ T cells were sorted by magnetic beads. Because $CD45RA^+CD27^-$ effector $CD4^+$ T cells are virtually absent in healthy individuals ($\leq$1.5% in 10 controls in whom we used magnetic beads and were able to measure the effector subset), this fraction represents $CD45RA^+CD27^+$ naive $CD4^+$ T cells. To measure the TREC content within $CD4^+$ and $CD8^+$ T cells, this subset was purified from thawed PBMC by magnetic bead separation, using the MiniMACS multisort kit according to manufacturer's instructions (Miltenyi Biotec Inc, Sunnyvale, California).

TREC analysis
DNA was isolated using the QIAamp Blood Kit according to manufacturer's instructions (Qiagen, Hilden, Germany). Signal joint T cell receptor excision circle (TREC) numbers were quantified using a real-time PCR method as previously described [112].

Mathematical model
To investigate the mechanisms behind the dynamics of $CD4^+$ and $CD8^+$ T cells during the different stages of infection, we extended a previous model [51] to include naive and memory T cells. The dynamics of naive (N) and memory

(M) T cells are given by the following differential equations:

$$\begin{aligned} N' &= \sigma e^{\nu t} + r_1 N - aN - d_N N^2 \\ M' &= qaN + r_2 M - d_M M(1 + \epsilon M) \end{aligned}$$

Naive cells increase due to input from the thymus ($\sigma e^{\nu t}$) and have a constant renewal rate (r_1). Thymic output decreases exponentially with age at rate ν per day. We however assume a constant thymic output for the time period that we model ($\nu = 0$). Naive cells decrease as a result of density-dependent death, and can be recruited into the memory cell pool (a). Memory cells increase by the input from activated naive and clonally expanded cells ($aq, q \gg 1$) and by renewal (r_2) . Memory cells decrease due to density-dependent death ($d_m(1 + \epsilon M)$).

The dynamics of TRECs in naive and memory T cells are given by the following differential equations:

$$\begin{aligned} T'_N &= c\sigma e^{-\nu t} - aT_N - d_N T T_N \\ T'_M &= aT_N - d_M T_M(1 + \epsilon M) \end{aligned}$$

where c is the fraction of naive cells coming from the thymus containing a TREC, and T_N and T_M are the total number of TRECs in the naive and memory T cell pool, respectively.

Statistics

The non-parametric Mann-Whitney U test was performed for group comparisons. Differences between paired data during longitudinal follow-up were tested using the Wilcoxon signed ranks test. Since absolute T cell counts tend to be noisy, we used median T cell counts over a longer period instead of the measured T cell count at a single point in time in Fig. 7.3. As pre-seroconversion values we took the median of all T cell counts that were available pre-seroconversion. Post-seroconversion we took the running median of five consecutive time points around the time point at which TRECs and T cell subsets were measured.

*A*cknowledgments

This research has been funded by AIDS Fonds Netherlands (grants 4024, 4025, 7010), the Netherlands Organization for Scientific Research (NWO, grants 916.36.003 and 016.048.603), the HFSP (grant RGP0010/2004) and the Landsteiner Foundation for Blood Research (grant #0210). The Amsterdam Cohort Studies on HIV infection and AIDS, a collaboration between the Amsterdam Health Service, the Academic Medical Center of the University of Amsterdam, Sanquin Blood Supply Foundation and the University Medical Center Utrecht, part of the Netherlands HIV Monitoring Foundation, which is financially supported by the Netherlands National Institute for Public Health and the Environment.

8

Can TRECs and telomeres be affected differently by naive T cell dynamics?

Tendai Mugwagwa[1], Rachid Ouifki[2], José A.M. Borghans[1,3] and Rob J. de Boer[1].

[1]Department of Theoretical Biology, Utrecht University, 3584 CH Utrecht, The Netherlands
[2]South African Center of Excellence in Epidemiological Modeling and Analysis, Stellenbocsh University, Stellenbosch 7600, South Africa
[3]Department of Immunology, University Medical Center, 3508 AB Utrecht, The Netherlands.

Abstract

Both T-cell receptor excision circles (TRECs) and telomere lengths are widely used to investigate T cell dynamics. TRECs were traditionally proposed as a direct marker for thymic output, while telomeres where proposed as a marker for cell proliferation. In fact both TREC and telomere data are affected by thymic output and proliferation. Here, we develop a mathematical model that takes into account the age of naive $CD4^+$ T cells and allows us to simultaneously compare TREC and telomere length dynamics. With this model we study how changes in thymic output, T cell proliferation and death, including a cell age dependent death rate, affect the average TREC content and telomere dynamics of naive T cells. Typically, such changes in naive T

cell dynamics have a similar effect on TREC dilution and telomere erosion. In one exceptional case TRECs and telomeres are affected differently: if the contribution of the thymus to the peripheral naive T cell pool is small, reducing thymic output results in TREC dilution but no significant telomere erosion. Our model explains the observations on TRECs and telomeres in HIV^+ patients when we allow for increased proliferation, in combination with either increased death rates and/or decreased thymic output.

8.1 Introduction

During V(D)J T cell receptor rearrangement, DNA extra-chromosomal excision products known as T cell receptor excision circles (TRECs) are generated. Because TRECs are not replicated during mitosis, they have been proposed as a marker for thymic output [65, 143]. TREC data is generally expressed as the average number of TRECs per cell (TREC content). However, the interpretation of the average TREC contents is complicated, because TRECs are diluted by peripheral T cell proliferation [51]. The proliferative history of T cells, on the other hand, has been investigated by measuring the average telomere lengths. Telomeres are the ends of chromosomes which shorten with every round of division [109, 140]. The interpretation of telomere length data is also complicated, because changes in thymic output (which is the source of T cells with the longest telomeres), affect the average telomere length of a T cell population in the periphery [22]. Furthermore, the action of telomerase, an enzyme that lengthens telomeres during cell division of activated T cells, may mask the effect of proliferation on the average telomere length of a T cell population. It is therefore a major question how changes in the proliferation rate, thymic output and death rate (including the possibility of cell age dependent death rate) influence the interpretation of TREC and telomere length dynamics.

Because changes in T cell dynamics affect the average TREC content and telomere length dynamics, the two markers have been used to understand the mechanism behind naive $CD4^+$ T cell decline during HIV-1 infection. In naive $CD4^+$ T cells of healthy individuals, the average TREC content declines at a rate of approximately 1% per year [26, 28, 41, 46, 108], and the average telomere length shortens at a rate of 39 bp per year [140]. During HIV infection, the loss of naive $CD4^+$ T cells is accompanied by a relatively rapid 2-10 fold decline in the average TREC content [26, 28, 51, 79, 104, 143, Chapter 7], and a 0.43Kb decrease in the average telomere length of naive $CD4^+$ T cells [141]. This reduction in the average telomere length however failed to breach statistical significance [141]. To explain the observed TREC dilution, some studies suggested that HIV-1 infection interferes with thymic production, which would contribute to the decline of naive $CD4^+$ T cells [9, 28, 113, 125, 143]. However, with the help of mathematical models, it was later shown that the TREC dilution in HIV patients could better be explained by increased proliferation

of naive CD4$^+$ T cells [51]. This explanation was supported by the fact that the fraction of dividing naive CD4$^+$ T cells was significantly higher in HIV$^+$ patients compared to age matched healthy controls [51, 53, 77, 122, Chapter 6]. In principle both increased proliferation rates among naive CD4$^+$ T cells and reduced thymic output should be reflected in accelerated telomere length shortening within naive CD4$^+$ T cells. It is therefore not clear how to reconcile the observation that there is no significant difference between the average telomere length of CD4$^+$ T cells in HIV$^+$ patients and healthy controls [141] with the explanation that the TREC dilution in HIV$^+$ patients is due to increased proliferation of naive CD4$^+$ T cells. [28, 51, 79, 143].

Here, we study how changes in thymic output, T cell proliferation and death (including a cell age dependent death rate) affect average TREC content and telomere dynamics, by developing a mathematical model that takes into account the age structure of naive T cells and allows for a simultaneous comparison of TREC and telomere length dynamics. The model is applied to TREC and telomere data in HIV infection in an attempt to reconcile the observation that naive CD4$^+$ T cell decline after HIV infection is accompanied by TREC dilution and no significant change in the average telomere length.

8.2 Mathematical model

Age structured mathematical model of naive T cells.
r To simultaneously investigate the dynamics of the average telomere length and TREC content of naive T cells, we develop a mathematical model that keeps track of the division history of cells. New undivided T cells (N_0) come from a thymic source ($\sigma(t) = \sigma_0 e^{-\nu t}$) that decreases with the age of the individual (t). Cells die at a rate dependent on their individual age $d(a)$. If the expected lifespan of cells increases with their age we write $d(a) = 2d_0(1 + e^{-\gamma a})$, and if it decreases with age, we write $d(a) = d_0 e^{\gamma a}$. Setting $\gamma = 0$ we study the case in which the cellular death rate is independent of the age of the cells, i.e. $d(a) = d_0$. In the periphery, naive CD4$^+$ T cells divide at a rate $p(N) = r/(1 + N/h)$, which is dependent on the total naive T cell density (N). We group the naive CD4$^+$ T cells into division classes indexed by k such that $N_k(a, t)$ is the number of naive T cells of age a that have undergone k divisions at time t. When cells divide, i.e. move from one division class to the next, they reset their age to zero [48]. Maximally, cells can undergo $\hat{k}$ rounds of division.

8. Can TRECs and telomeres be affected differently by naive T cell dynamics?

The age structured model of naive T cells is formulated as follows:

$$\begin{aligned}
\frac{\partial N_k}{\partial t}(a,t) + \frac{\partial N_k}{\partial a}(a,t) &= -\left(p\left(N\left(t\right)\right) + d\left(a\right)\right) N_k\left(a,t\right) \\
N_0\left(0,t\right) &= \sigma\left(t\right) \\
N_k\left(0,t\right) &= 2\int_0^t p\left(N\right) N_{k-1}\left(a,t\right) da \\
N_k\left(a,0\right) &= 0 \\
N_k\left(a,t\right) &= 0 \text{ if } k > \hat{k}.
\end{aligned} \tag{8.1}$$

where $N\left(t\right)$ is the total number of naive cells at time t given by

$$N\left(t\right) = \sum_{k=0}^{\hat{k}} \int_0^t N_k\left(a,t\right) da.$$

and $N_k\left(t\right)$ is the number of naive cells that have undergone k rounds of division

$$N_k\left(t\right) = \int_0^t N_k\left(a,t\right) da.$$

The average death rate of all cells at time t is given by

$$\bar{d}(t) = \int_0^t \frac{N(a,t)}{N(t)} d(a) da.$$

TRECs are produced by de novo production of naive T cells in the thymus, and are lost when cells die. From the general mathematical model (Equation 8.1) the absolute number of TRECs, T, in the whole naive T cell population can be calculated as follows:

$$T(t) = c \sum_{k=0}^{\hat{k}} \frac{N_k(t)}{2^k}$$

where c is the TREC content of an RTE. The average TREC content, A, of the population is given by $A(t) = T(t)/N(t)$. Note that each time a cell divides and moves into the next division class, the average TREC content of a cell halves.

RTEs enter the periphery with an average telomere length of L_0 bp. With every successive round of division, telomere ends shorten by Δ bp. The average telomere length, L, of the T cell population can be calculated from the difference between the initial telomere length L_0 and the average telomere loss, Δ, as cells move through the division classes.

$$L(t) = L_0 - \Delta \sum_{k=0}^{\hat{k}} \frac{k N_k(t)}{N(t)}$$

8.3 Results

Age structure has no effect on TREC or telomere dynamics. We investigate how the interpretation of both TREC and telomere data is influenced by differences in the death rate of recently produced and older naive T cells. Based on mathematical analysis (A) and computer simulations of equation (8.1) we find that the form of the death rate function $d(a)$ has hardly any effect on the qualitative dynamics of telomere length and TREC content (Fig. 8.1a-c). Initially (in young individuals) the age distribution and the average death rate of cells are skewed towards younger cells. However, the age distribution fairly rapidly approaches a quasi-steady state (QSS), and the average death rate of each sub-population, $\bar{d}$, approaches the same plateau. At this stage the age structured model simplifies into a cascade of ordinary differential equations with a death rate that is equal to the average death rate of the age structured population (A and B). In summary, differences in the way death rates depend on cell age do not influence the interpretation of TREC and telomere dynamics.

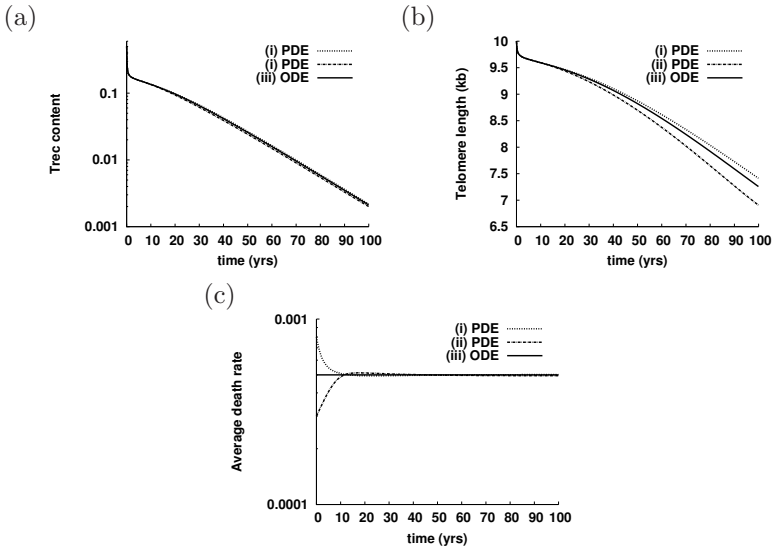

Fig. 8.1: Age dependent cell death rates have little effect on: (a) the average TREC content (TRECs per naive T cell) and (b) the average telomere length (kb). (c) The average death rate ($\bar{d}$) of the three death rate functions (i) PDE $d(a) = d_0(1 + e^{-\gamma a})$, (ii) PDE $d(a) = d_0 e^{\gamma a}$ and (iii) ODE $d(a) = d_0$. The slight deviation in telomere length of the PDE compared to the ODE is an artifact of resetting the age with each division.

TREC content and telomere length dynamics.
Model analysis

8. Can TRECs and telomeres be affected differently by naive T cell dynamics?

Having shown that the cell age structure has hardly any effect on the interpretation of TREC content and telomere length measurements, we take advantage of the fact that our model allows us to simultaneously follow up TREC and telomere length dynamics.

For an in depth analysis of the model behavior, we simulate the cascade ODE model B, in which naive T cells are stratified according to the number of divisions they have undergone (k). In this model, the TREC content and telomere length depend on the frequency of cells in each division class, i.e $A(t) = c\sum_{k=0}^{m} \frac{N_k}{2^k N(t)}$ and $L(t) = L_0 - \Delta \sum_{k=0}^{m} \frac{kN_k}{N(t)}$. We can therefore calculate the contribution of each division class (k) to the average TREC content and average telomere length of the whole population at any age of the individual. For example, in a 40 year old individual, the contribution of each division class k to the average total TREC content is given by $\frac{cN_k(40\times365)}{2^k N(40\times365)}$, and the contribution of division class k to the average telomere length is given by $\frac{(L_0 - k\Delta)N_k(40\times365)}{N(40\times365)}$.

The cascade model (B), can be reduced to 3 differential equations describing the total number of naive T cells (equation 8.5), their average TREC content (equation 8.9), and their average telomere length (equation 8.14). We calculate the QSS expressions for the TREC content to be $\frac{A}{c} = \frac{1}{1+\rho(t)}$ and for the telomere length to be $L = L_0 - 2\rho(t)\Delta$, where $\rho(t) = \frac{p(N(t))N(t)}{\sigma(t)}$ is the ratio of naive T cells produced in the periphery over those produced in the thymus. From these expressions, one can deduce that parameter changes that increase the ratio ρ will result in a hyperbolic decrease in the QSS TREC content and a linear decrease in the QSS telomere length. For example, if recent thymic emigrants (RTEs) have a telomere length of 10kb and loose $\Delta = 100$ bp upon division, a single round of division results in a 1% decrease in telomere length, while in TRECs this would be a 50% drop in TREC content. We therefore plot the average TREC content on a log scale and the average telomere length on a linear scale.

For our analysis, we consider two scenarios: i) the "thymic scenario" in which 10% of newly produced cells come from proliferation and 90% from thymic output ($\rho = 1/9$), and ii) the "renewal scenario" in which 90% of newly produced cells come from proliferation and 10% from thymic output ($\rho = 9$).

In the renewal scenario, the frequency distribution of naive T cells has a peak at cells that have undergone several rounds of division (Fig. 8.2a). In the thymic scenario, the frequency distribution of naive T cells is skewed to the left with a peak at cells in the 0th division class (Fig. 8.2b). The contribution of each division class to the average telomere length tends to follow the frequency distribution of naive T cell numbers (Fig 8.2). This is because the change in telomere length of cells as they move from one division class to the next (Δ bp) is small compared to the change in their frequency. In the renewal scenario, naive T cells that have undergone about 9 rounds of division contribute the most towards the average telomere length (Fig. 8.2a). in the thymic scenario,

in contrast, recent thymic emigrants have the largest contribution towards the average telomere length. For both scenarios, the distribution of the TREC content over the division classes is skewed to the left because cells that have undergone few rounds of division contribute the most towards the average TREC content of the total naive T cell population (Fig. 8.2). This is because of the large decrease in the TREC content (2-fold) with every subsequent round of division compared to the change in the frequency of cells. With these reference distributions in mind, we investigate how changing different parameters affects the average TREC content and the average telomere length of the naive T cell population.

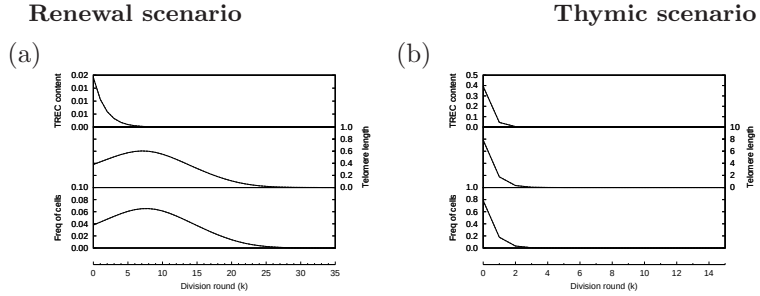

Fig. 8.2: The contribution of each division class to: the average TREC content (TRECs per naive T cell) (upper graph), the average naive T cell telomere length (Kb) (middle graph), and the frequency distribution of naive T cells (lower graph). The distributions are plotted for a 40 year old healthy individual in (a) the renewal scenario and (b) the thymic scenario.

Effect of reduced thymic output.
Reducing thymic output ($\sigma(t)$) to 10% of the original value at 30 years of age results in a rapid drop in the average TREC content compared to the normal age associated TREC dilution (Fig. 8.3a,e). This is true for both scenarios. In contrast, the changes in the average telomere length depend on the scenario. In the renewal scenario, the average telomere length remains relatively unchanged compared to age matched healthy controls. In this case, telomeres behave differently compared to TRECs. However, in the thymic scenario, the same reduction in thymic output results in a decrease in the average telomere length in line with what is observed in the TREC content (see Table 8.1 and compare Fig. 8.3b to Fig. 8.3f).

The reasons for TREC dilution after reducing thymic output are different in the 2 scenarios. In the renewal scenario, thymic output is already small in a 30 year old individual, and further reducing thymic output has hardly any impact on naive T cell numbers (Fig. 8.3c), and thus hardly any compensatory homeostatic proliferation is induced. However, if thymic output were set to zero, TREC^+ naive T cells would be lost at a rate d, while the total number

of naive T cells would be lost at a rate $p - d$. Since the proliferation rate is almost equal to the death rate ($p \approx d$), the dynamics of TREC$^+$ naive T cells are slow, but much faster than the dynamics of the total number of naive T cells, and this difference in kinetics results in a long transient TREC dilution. On the other hand, in the thymic scenario, reducing the significant thymic output triggers homeostatic proliferation to compensate for reduced naive T cell numbers. This proliferation results in TREC dilution, and a lower average telomere length as proliferation shifts the peak of the frequency distribution to higher division classes where cells have shorter telomeres (Fig. 8.3h).

Effect of increased death rate.
In the absence of homeostatic proliferation, an increased naive T cell death rate, d, results in a decrease in naive T cell numbers, an increase of the average naive T cell TREC content, and an increase of the average naive T cell telomere length (Fig 8.4a-c,e-g). This is because an increased death rate of naive T cells, shifts the frequency distribution to the left, such that the T cell population becomes dominated by RTEs. Since RTEs bear the highest TREC content and longest telomeres, their increased relative frequency results in an increase in the average TREC content and the average telomere length (Fig. 8.4).

In the presence of homeostatic proliferation, increased death rates result in a smaller decrease in naive T cell numbers, and a relatively unchanged average TREC content, for both the renewal and thymic scenarios (Fig. 8.5a,b,e,f). However the impact of an increased death rate on the average telomere length depends on the relative contribution of the thymus. In the renewal scenario, a significant decrease in the average telomere length is observed (Fig. 8.5a-c), while in the thymic scenario, there is hardly any telomere erosion (Fig. 8.5c-g). In both cases, the reduced naive T cell numbers trigger cells to undergo more rounds of division. This shifts the frequency distribution of cells to the right towards cells that have shorter telomeres (Fig. 8.5d,h). Since, in the thymic scenario, RTEs dominate the naive T cells (Fig. 8.5h), homeostatic proliferation hardly changes the frequency distribution of cells (Fig. 8.5h), and increasing death rate therefore has hardly any impact on the average telomere length

In summary, in the thymic scenario, increasing the death rate in the presence of homeostatic proliferation has little effect on TRECs and telomeres because thymic output remains the dominant source of naive T cells. However,in the renewal scenario, increasing the death rate in the presence of homeostatic proliferation leads to both TREC dilution and telomere erosion because of compensatory proliferation.

Effect of increased proliferation rate.
Increasing the proliferation rate (r), results in a marked decrease in both the average TREC content and the average telomere length (Fig. 8.6a,b and e,f) accompanied by an increase in total cell numbers (Fig 8.6c). As the proliferation rate increases, in both scenarios the frequency of cells in the higher division

classes increases (Fig. 8.6d,h). These cells contribute low TREC contents and short telomere lengths (Fig. 8.6a-d with Fig. 8.6e-h).

Summarizing, when expressed as accelerated aging (Table 8.1), one can see that TRECs are affected similarly in the thymic scenario and the renewal scenario by the different parameter changes (the second and forth column), whereas telomeres are affected differently in the two scenarios (first and third column).

Effect of HIV infection on average TREC and average telomere dynamics.
The decrease in naive $CD4^+$ T cell TREC contents that accompanies the loss of naive $CD4^+$ T cells in HIV infection was previously explained by increased proliferation together with increased cell death rates [51]. It remains unclear why despite increased division rates, no significant telomere length shortening was observed in naive $CD4^+$ T cells of HIV-1 infected individuals compared to healthy individuals [141]. ^2H_2O labeling studies have shown that naive $CD4^+$ T cells from HIV^+ patients have a 3.3 fold higher death (turnover) rate than naive $CD4^+$ T cells from healthy individuals (Chapter 6). Above we showed that increasing the naive $CD4^+$ T cell death rate alone cannot explain the TREC dilution observed in HIV infection (Fig. 8.5a,e). Therefore, we investigated whether simultaneous changes in parameter combinations can explain the observed dynamics during HIV infection. We ran simulations using parameter values for healthy controls until the age of 30 years, after which we increased the death rate (d) to previous estimates (Chapter 6), and either increased the proliferation rate (r) 2-fold or reduced thymic output (σ) to 10% of its normal value.

Effect of increased death and proliferation rates.
If HIV-1 infection increases both the death rate (3.3-fold) and the proliferation rate (2-fold), we find a reduction of naive $CD4^+$ T cell numbers accompanied by a decrease in naive $CD4^+$ T cell TREC contents and shorter telomere lengths. For the current parameter values, in the renewal scenario, a 40 year old HIV^+ patient would have a naive $CD4^+$ T cell TREC content of a 58 year old HIV^- individual (Fig. 8.7a, Table 8.1) and a telomere length of a 61 year old HIV^- individual (Fig. 8.7b, Table 8.1). Similarly, in the thymic scenario, a 40 year old HIV^+ patient would have a naive $CD4^+$ T cell TREC content of a 58 year old HIV^- individual (Fig. 8.7e, Table 8.1) and a telomere length of a 59 year old HIV^- individual (Fig. 8.7f, Table 8.1). Earlier we showed that increasing the death rate enriches the T cell pool with RTEs while homeostatic proliferation in response to lower T cell numbers has the opposite effect by shifting the frequency distribution of cells to higher division classes (Fig. 8.5d,h). The combined effect of increasing the death rate and the proliferation rate is that the naive $CD4^+$ T cell pool becomes enriched with cells in higher division classes at the expense of cells in the lower division classes (Fig. 8.7). This results in a lower average TREC content and shorter average telomere length.

Effect of increased death rate and reduced thymic output.
If HIV-1 infection were to increase the death rate of naive $CD4^+$ T cells, and to reduce thymic output, we also find a decrease in naive $CD4^+$ T cell numbers accompanied by TREC dilution and shorter telomere lengths because of homeostatic proliferation. For the current parameter values, in the renewal scenario, a 40 year old HIV^+ patient would have the TREC content of an 86 year old HIV^- individual (Fig. 8.8a, Table 8.1) and a telomere length of a 63 year old HIV^- individual (Fig. 8.8b, Table 8.1). In the thymic scenario, a 40 year old HIV^+ patient would have a naive $CD4^+$ T cell TREC content of an 85 year old HIV^- individual (Fig. 8.8e, Table 8.1) and a telomere length of an 86 year old HIV^- individual (Fig. 8.8f, Table 8.1). We already showed that a

Table. 8.1: Summary of the effect of changing different model parameters on the average TREC content and the average telomere length of naive $CD4^+$ T cells. We consider a 40 year old individual with a specified parameter changed at age 30. We report the age of a control individual with the same average TREC content or average telomere length as the case study individual at age 40. For example 42.58 in the average TREC content column means that the 40 year old case study individual has an average TREC content of a 42.58 year old healthy individual.

	Renewal scenario		**Thymic scenario**	
	Telomere length	TREC content	Telomere length	TREC content
$\downarrow \sigma$	43	60	59	61
$\uparrow d$	51	44	45	44
$\uparrow p$	46	52	52	52
$\uparrow d, \downarrow \sigma$	63	86	85	86
$\uparrow d, \uparrow p$	61	58	59	58

decrease in thymic output reduces the frequency of cells in the lower division classes which bear the highest TREC content (Fig. 8.3d,h). When a reduction in thymic output is accompanied by an increased naive $CD4^+$ T cell death rate, the increase in homeostatic proliferation shifts the frequency of cells to higher division classes, k. Thus the decline in naive $CD4^+$ T cell numbers is accompanied by a decrease in both the average TREC content and the average telomere length of naive $CD4^+$ T cells (Fig. 8.7 a-c and e-g).

To summarize, increasing the naive $CD4^+$ T cell death rate to the observed value in HIV infection (Chapter 6), combined with either an increased proliferation rate or reduced thymic output, results in similar dynamics, with a decrease in naive $CD4^+$ T cells that is accompanied by lower average TREC content and shorter telomere length (compare Fig 8.7a-c with Fig. 8.8a-c and Fig. 8.7e-g with Fig 8.8 e-g)). In both cases, increased proliferation plays a major role in the dilution of TRECs and shortening of telomeres.

8.4 Discussion

In this study, we have shown that cell age dependent death rates have hardly any effect on the qualitative dynamics of telomere lengths and TREC contents (Fig. 8.1). This finding implies that a simpler mathematical model without age structure is sufficient to investigate the effects of different parameter changes of average TREC content and average telomere length dynamics. Although TRECs were originally proposed as a marker for thymic output [65, 143] and telomeres were proposed as a marker for the proliferative history of cells [109, 140], our model simulation results suggest that the two markers typically measure both proliferation and thymic output. We showed that in general, both TRECs and telomeres, are similarly affected by changes in thymic output, death rates and proliferation rates. We identify one exception (were small thymic output is already small), in which reducing thymic output resulted in TREC dilution, and no change in the average naive T cell telomere length. In this exceptional case, were the contribution of the thymus to naive T cell maintenance is negligible, we can achieve a TREC content decline without invoking an increase in the proliferation rate. This case is a counter example to Hazenberg et al. [51]'s findings that a change in the proliferation rate is required for TREC dilution.

Telomere length and TREC content data have been used to explain the mechanisms underlying naive $CD4^+$ T cell decline during HIV-1 infection. During HIV-1 infection, a loss of naive $CD4^+$ T cells is accompanied by a relatively rapid 2-10 fold decline in the average naive $CD4^+$ T cell TREC content [26, 28, 51, 79, 104, 143, Chapter 7], and a non-significant decrease in the average telomere length of naive $CD4^+$ T cells of 0.43Kb after HIV-1 infection [141]. TREC content declines have previously been interpreted as evidence for HIV-1 driven thymic impairment [28, 109]. However, Hazenberg et al. [51] showed that increased naive $CD4^+$ T cell division could better explain TREC dilution in HIV infection. Indeed, naive $CD4^+$ T cell turnover rates were found to be several fold increased [77, 88, 143, Chapter 6]. The TREC dilution and telomere shortening in HIV^+ patients provides additional evidence for increased division rates of naive $CD4^+$ T cells during HIV infection.

Contrary to the significant TREC dilution after HIV infection, the change in the average naive $CD4^+$ T cell telomere length failed to breach statistical significance [141]. Our model simulations that were compatible with decreased naive $CD4^+$ T cell numbers and TREC dilution always predicted shortened naive $CD4^+$ T cell telomere lengths. Only in one case did we observe TREC dilution and no significant decrease in the average naive T cell telomere length (Fig. 8.3a-b). However, because in this case thymic output is already small, the reduction in thymic output hardly affected the naive T cell numbers, and this special case is not compatible with HIV infection data.

Since the study by Wolthers et al. [141] was based on cross sectional data,

variations between individuals may mask a true longitudinal shortening of telomeres and thus should be treated with caution when extrapolating to longitudinal dynamics (Chapter 7). The observed decline of 0.43Kb is in fact entirely compatible with our simulation results. For the mean duration of HIV-1 infection in the cross-sectional study which ranged from 1 to 12 years, our model (for example, with large ρ and assuming an increase in the proliferation rate and death rate), would predict between 0.02Kb and 0.67Kb drop in telomere length for the same duration of HIV infection (Fig 8.7). The estimated 0.43Kb change that was observed falls within this range [141]. Our simulations therefore suggest that in a longitudinal study one should be able to see a significant decrease in average naive $CD4^+$ T cell telomere length during HIV infection.

In conclusion, TREC dilution and telomere shortening after HIV infection, can only be explained if there is increased naive $CD4^+$ T cell division. The concomitant reduction in naive $CD4^+$ T cell numbers is explained by we can call the observed increased death rates (Chapter 6), and possibly reduced thymic output.

Table. 8.2: Summary of the parameter values used in the model simulations. Changes to parameters in specific simulations are given in the respective figure captions.

Parameter	**Description**	**value**	**units**
σ_0	Initial thymic output[1]	$2e^{10}$	cells/d^{-1}
σ_0	Initial thymic output[2]	$2.5e^{8}$	cells/d^{-1}
μ	Thymic involution rate	$1.4e^{-4}$	d^{-1}
r	Maximum proliferation rate	0.05	d^{-1}
h	Saturation constant	$1e^{10}$	cells
Δ	Telomere length loss per division	100	bp
c	RTE TREC content	0.5	$cells^{-1}$
L_0	RTE telomere length	10	Kb
(i) PDE			
d_0	Death rate of new born cells	$3e^{-4}$	d^{-1}
γ	constant	$5e^{-4}$	scalar
(ii) PDE			
d_0	Death rate of new born cells	$4e^{-4}$	d^{-1}
γ	constant	$2.8e^{-3}$	scalar
(iii) ODE			
d_0	Death rate of new born cells	$5e^{-4}$	d^{-1}
γ	constant	0	scalar

[1] Thymic scenario
[2] Renewal scenario

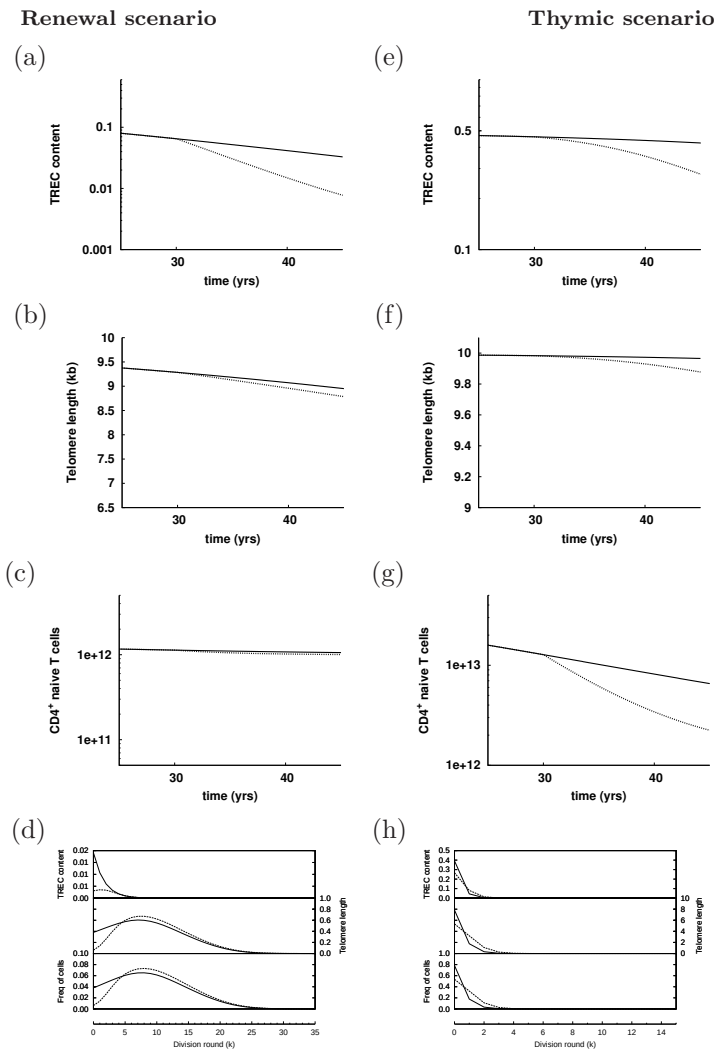

Fig. 8.3: Impact of reducing thymic output in a 30 year old individual to 10% of a healthy age-matched individuals on: (a and e) the average TREC content (TRECs per naive $CD4^+$ T cell), (b and f) the average naive $CD4^+$ T cell telomere length (Kb), (c and g) the number of $CD4^+$ naive T cells, and (d and h) the contribution of each division class to the TREC content (upper graph), and to the average naive $CD4^+$ T cell telomere length (middle graph) and the frequency distribution of naive $CD4^+$ T cells (lower graph). Dynamics in healthy individual (continuous line) are compared to dynamics of an age matched case study individual (dotted line). Parameter values given in Table 8.2 with 10% of $\sigma(t)$ from 30 years onwards. For (a-d), $\rho = 9$ and (e-h), $\rho = 1/9$.

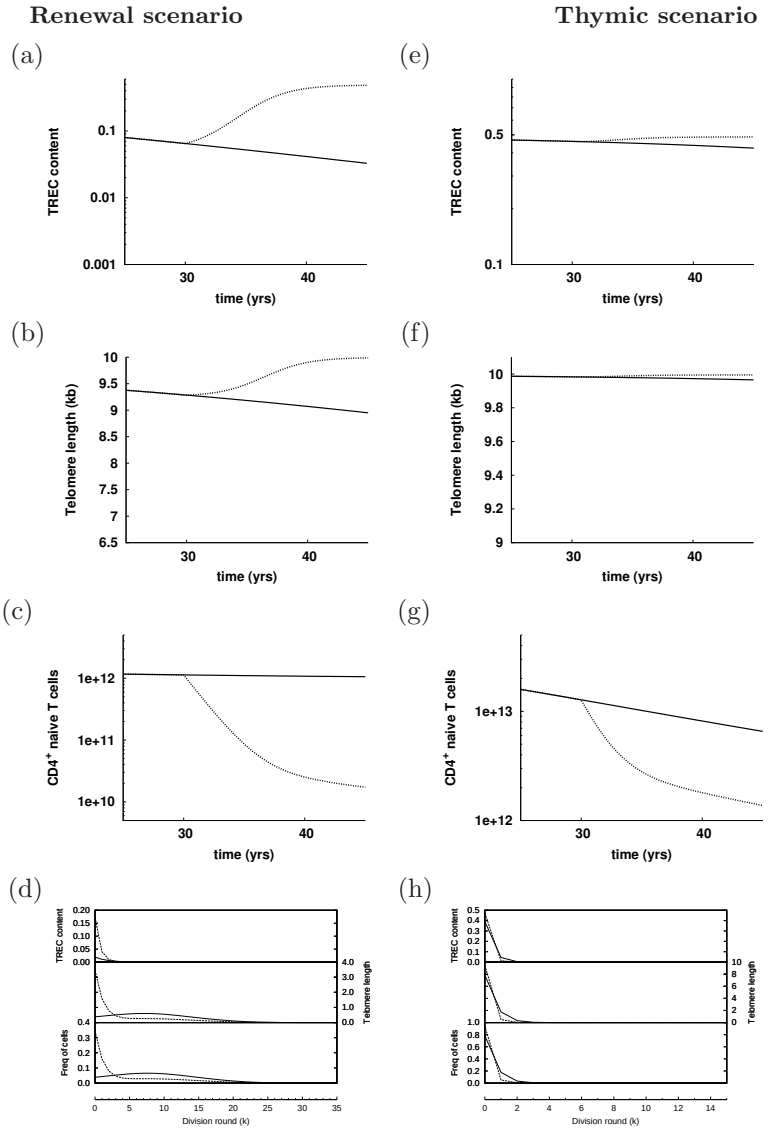

Fig. 8.4: Impact of a 3.3 fold increase in the death rate ($d = 0.0016$) in a 30 year old individual in the absence of homeostatic proliferation (i.e proliferation if fixed to the value at age 30). See legend of Fig. 8.3

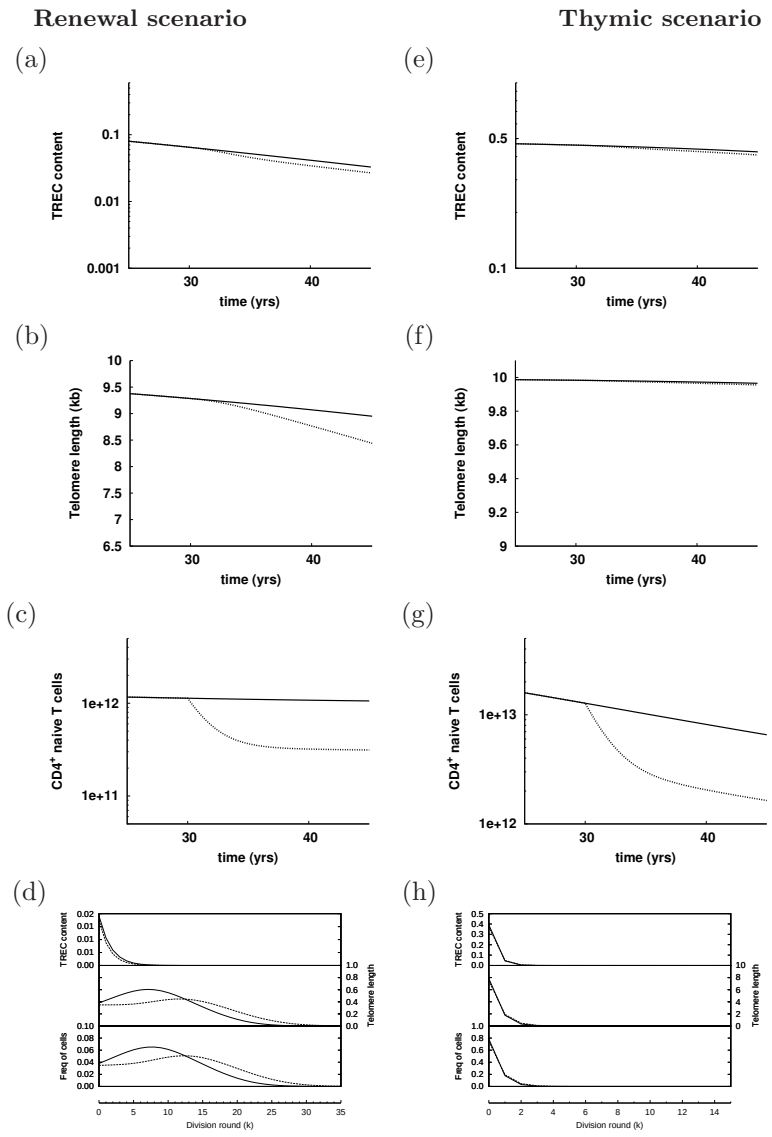

Fig. 8.5: Impact of a 3.3 fold increase in the death rate ($d = 0.0016$) in a 30 year old individual in the presence of homeostatic proliferation. See legend of Fig. 8.3

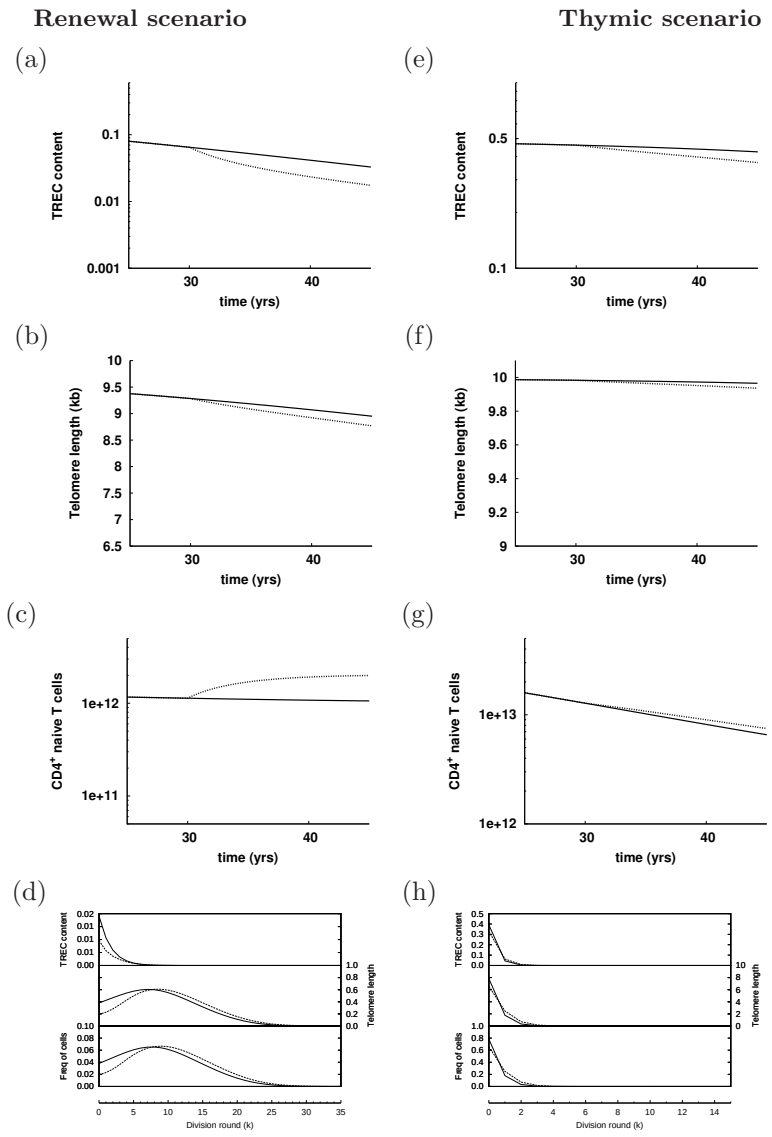

Fig. 8.6: Impact of a 2 fold increase in the proliferation rate ($r = 0.01$) in a 30 year old individual. See legend of Fig. 8.3

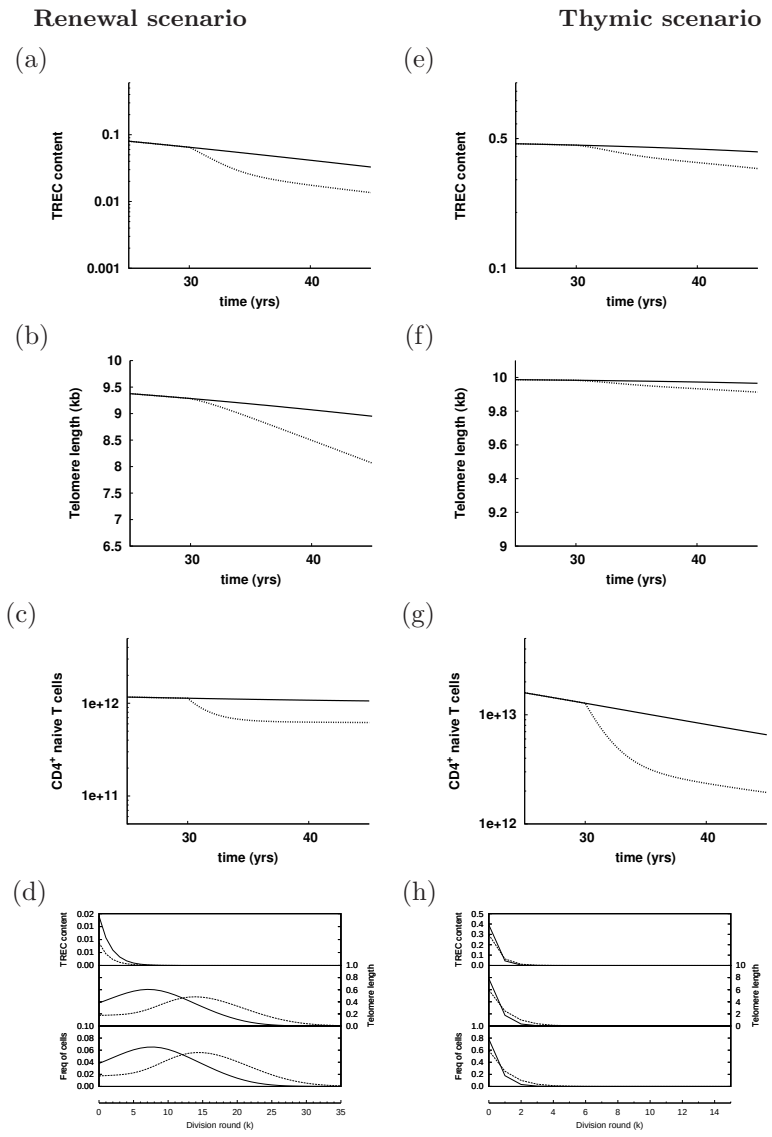

Fig. 8.7: Impact of increasing the death rate ($d = 0.0016$) and proliferation rate ($r = 0.01$) in a 30 year old individual. See legend of Fig. 8.3

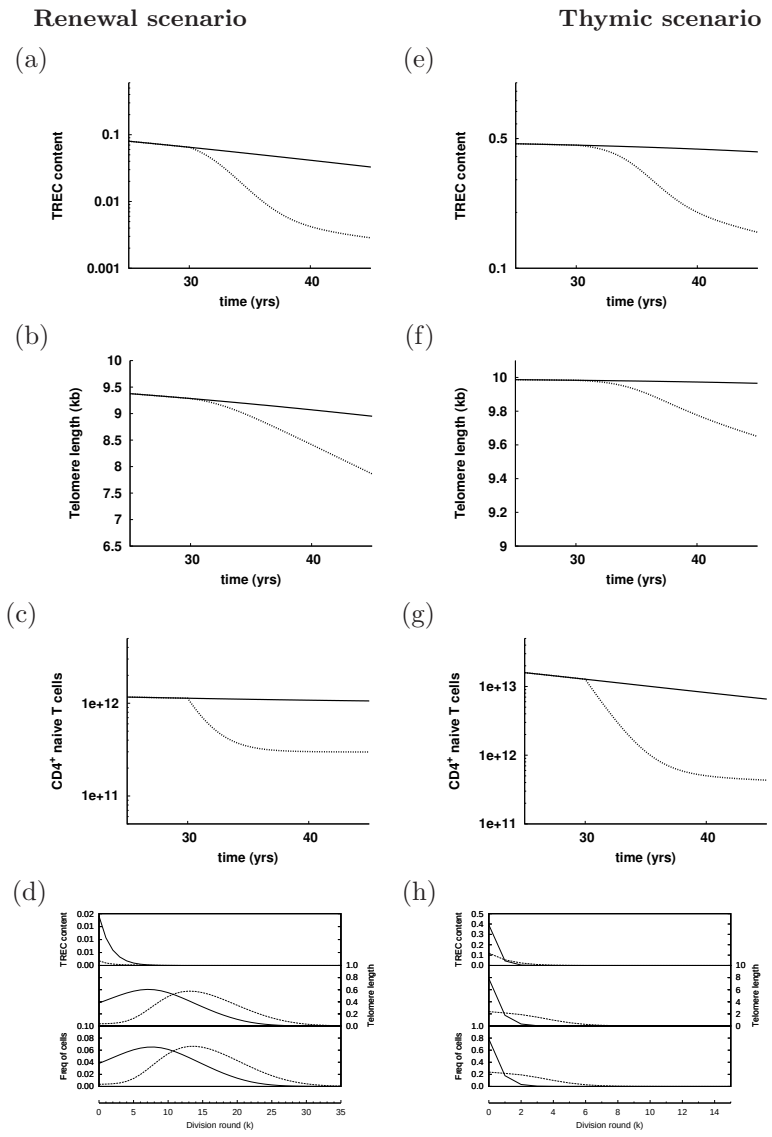

Fig. 8.8: The impact of increasing the death rate ($d = 0.0016$) and reducing thymic output σ to 10% in a 30 year old individual. See legend of Fig. 8.3

A Appendix: The age structured model.

In this section we present a mathematical analysis to show that the age structured partial differential equation (PDE) model can be reduced to an age independent ordinary differential equation (ODE) model with a death rate $\bar{d}$.

Let $N_k(a,t)$ denote the number of naive cells with age a at time t that result from k divisions and $N(t)$ the total number of cells at time t. We have the following system:

$$\begin{aligned}
\frac{\partial N_k}{\partial t}(a,t) + \frac{\partial N_k}{\partial a}(a,t) &= -\left(p\left(N\left(t\right)\right) + d\left(a\right)\right) N_k(a,t) \\
N_0(0,t) &= \sigma(t) \\
N_k(0,t) &= 2\int_0^t p\left(N(t)\right) N_{k-1}(a,t)\, da \\
N_k(a,0) &= 0 \\
N_k(a,t) &= 0 \text{ if } k > \hat{k}
\end{aligned} \tag{8.2}$$

From equation 8.2, the dynamics of naive T cells in the different division classes are given by the following differential equations:

$$\frac{\partial N_0}{\partial t}(t) = \sigma(t) - \int_0^t \left(p\left(N(t)\right) + d\left(a\right)\right) N_0(a,t)\, da \tag{8.3}$$

$$\frac{\partial N_k}{\partial t}(t) = 2\int_0^t p\left(N(t)\right) N_{k-1}(a,t)\, da - \int_0^t \left(p\left(N(t)\right) + d\left(a\right)\right) N_k(a,t)\, da$$

where $N_0(0) = \sigma(0)$ and $N_0(0) = 0$ for $k = 1, 2, \cdots, \hat{k}$. Let $N(a,t)$ be the number of naive T cells of age a at time t such that $N(a,t) = \sum_{k=0}^{\hat{k}} N_k(a,t)$. The total number of naive cells $N(t)$ at time t is therefore given by $N(t) = \int_0^t N(a,t)\, da = \sum_{k=0}^{\hat{k}} N_k(t)$ $N(a,t)$ satisfies the following system:

$$\begin{aligned}
\frac{\partial N}{\partial t}(a,t) + \frac{\partial N}{\partial a}(a,t) &= -\left(p\left(N(t)\right) + d\left(a\right)\right) N(a,t) \\
N(0,t) &= \sigma(t) + 2\int_0^t p\left(N(t)\right) N(a,t)\, da \\
N(a,0) &= 0
\end{aligned} \tag{8.4}$$

We can rewrite the PDE (equation 8.4) as an ordinary differential equation (ODE)

$$N'(t) = \sigma(t) + p\left(N(t)\right) N(t) - \bar{d} N(t). \tag{8.5}$$

where the average death rate of all naive T cells is given by

$$\bar{d}(t) = \int_0^t \frac{N(a,t)}{N(t)} d(a) da.$$

The model behavior of the age structured PDE (equation 8.4) is therefore similar to that of the ODE (equation 8.5).

TREC content

If a fraction, c, of RTEs are TREC$^+$, from equation 8.4 we can describe the dynamics of the total number of TREC$^+$ cells of age a at time t as follows:

$$\begin{aligned} \frac{\partial T}{\partial t}(a,t) + \frac{\partial T}{\partial a}(a,t) &= -\left(p\left(N(t)\right) + d\left(a\right)\right) T\left(a,t\right) \\ T\left(0,t\right) &= c\sigma + \int_0^t p\left(N(t)\right) T\left(a,t\right) da \\ T\left(a,0\right) &= 0 \end{aligned} \tag{8.6}$$

Similar to equation 8.4, we rewrite this PDE as an ODE with the same model behavior. The ODE if given by:

$$T' = c\sigma\left(t\right) - \bar{d}T \tag{8.7}$$

By definition the TREC content, $A = \frac{T}{N}$ is given by the frequency of TREC$^+$ T cells within the total naive T cell population. Using equation(8.4) and (8.6) we define the dynamics of the TREC content, A by;

$$A' = \frac{\sigma}{N}\left(c - A\right) - Ap\left(N\right) + A\left[\frac{\int_0^t d\left(a\right) N\left(a,t\right) da}{N\left(t\right)} - \frac{\int_0^t d\left(a\right) T\left(a,t\right) da}{T\left(t\right)}\right] \tag{8.8}$$

Note that the average death rate of all cells at time t, $\int_0^t d(a)\frac{N(a,t)}{N(t)}da$, is the same as the average death rate of TREC positive cells at time t, $\int_0^t d(a)\frac{T(a,t)}{T(t)}da$. Therefore equation (8.8) simplifies to

$$A' = \frac{\sigma}{N}\left(c - A\right) - p\left(N\right)A \tag{8.9}$$

or (8.10)

$$T' = \frac{c\sigma\left(t\right)}{N(t)} - \bar{d}A$$

Assuming a quasi-steady state of equation (8.9) yields,

$$\frac{A(t)}{c} = \frac{1}{1 + \frac{p\left(N(t)\right)N(t)}{\sigma(t)}} = \frac{\sigma(t)}{\bar{d}N(t)} \tag{8.11}$$

Average telomere length

Given that cells coming out of the thymus have a telomere length L_0 bp and with every division cells shorten their telomeres by Δ bp, we can calculate the telomere length of a cell that has undergone k rounds of division by, $L_0 - \Delta k$.

If we know the frequency of naive T cells in each division class ($\frac{N_k}{N(t)}$) we can calculate the average telomere length of the naive T cell population as follows:

$$\begin{aligned} L(a,t) &= \frac{\sum_{k=0}^{\hat{k}} (L_0 - k\Delta) N_k(a,t)}{N(a,t)} \\ &= L_0 - \Delta \frac{\sum_{k=0}^{\hat{k}} k N_k(a,t)}{N(a,t)} \end{aligned}$$

This implies that

$$\frac{\partial L}{\partial t}(a,t) + \frac{\partial L}{\partial a}(a,t) = 0 \tag{8.12}$$

We can therefore calculate

$$\begin{aligned} L(t) &= \frac{\int_0^t \sum_{k=0}^{\hat{k}} (L_0 - k\Delta) N_k(a,t)\, da}{\int_0^t N(a,t)\, da} \\ &= L_0 - \Delta \frac{\sum_{k=0}^{\hat{k}} k N_k(t)}{N(t)} \\ &= \frac{1}{N(t)} \int_0^t N(a,t) L(a,t)\, da \end{aligned} \tag{8.13}$$

Using equation (8.13) we calculated the dynamics of the average telomere length as follows:

$$\begin{aligned} L'(t) &= \frac{\sigma(t)}{N}(L_0 - L(t)) - 2\Delta p(N) + p(N) \int_0^t \frac{N(a,t)}{N(t)} L(a,t) da \\ &- p(N) L(t) \int_0^t \frac{N(a,t)}{N(t)} da - \int_0^t \frac{N(a,t)}{N(t)} L(a,t) d(a) da \\ &- L(t) \int_0^t \frac{N(a,t)}{N(t)} d(a) da \end{aligned}$$

Since $\int_0^t \frac{N(a,t)}{N(t)} da = 1$, and because the average telomere length lost due to death at time t can be given by $\int_0^t \frac{N(a,t)}{N(t)} L(a,t) d(a) da$ or $L(t) \int_0^t \frac{N(a,t)}{N(t)} d(a) da$, equation(8.14) simplifies to:

$$L' = \frac{\sigma(t)}{N(t)}(L_0 - L(t)) - 2\Delta p(N(t)) \tag{8.14}$$

Assuming quasi-steady state of equation (8.14) we have,

$$L(t) = L_0 - \frac{2p(N(t))N(t)}{\sigma(t)}\Delta \tag{8.15}$$

B Appendix: The cascade model.

In order to model telomere length dynamics, we need to keep a history of the number of divisions that a cell has undergone. To achieve this we rewrite equation 8.5 as a cascade model. If the total number of cells is $N(t) = \sum_{k=1}^{\hat{k}} N_k(t)$ where $N_k(t)$ is the number of cells that result from k rounds of divisions, then

$$\begin{aligned} N_0' = &\quad \sigma(t) - (p(N) + d) N_0 \\ N_k' = &\quad 2pN_{k-1} - (p(N) + d) N_i \\ &\text{for } k = 1...\hat{k} \end{aligned} \tag{8.16}$$

From equation (8.16) we can directly calculate the TREC content $A(t)$ and the average telomere length $L(t)$ as follows:

$$A(t) = \frac{c}{N(t)} \sum_{k=0}^{\hat{k}} \frac{N_k(t)}{2^k} \tag{8.17}$$

$$\begin{aligned} L(t) &= \frac{\sum_{k=0}^{\hat{k}} (L_0 - k\Delta) N_k(t)}{N(t)} \\ &= L_0 - \frac{\Delta}{N(t)} \sum_{k=0}^{\hat{k}} k N_k(t) \end{aligned} \tag{8.18}$$

9

General Discussion.

This thesis focuses on understanding the dynamics of different T cell subsets in healthy situations as well as disturbed situations. By combining mathematical modeling with experimental data we have not only quantified these T cell dynamics but also gained a deeper understanding of the different mechanisms of T cell maintenance.

9.1 T cell dynamics in healthy mice and humans.

Estimates of T cell lifespans have been marred by irregularities due to a number of factors including differences in the experimental protocols. For example, different studies have used the non-radioactive stable isotopes $^2H_2$-glucose and ^2H_2O to quantify leukocyte production rates and death rates. The average life spans of naive, memory and total $CD4^+$ and $CD8^+$ T cells that have been estimated using these two compounds, however, differ considerably between different laboratories [10]. The origin of these differences has so far not been explained but one suggestion is that the current single compartment models [5] that are used to interpret this data tend to underestimate the expected lifespan especially when longer labeling periods are used.

Here we used the in vivo non-invasive ^2H_2O labeling technique and developed a multi-compartment mathematical model that can be used to estimate the average T cell lifespans independent of the length of the labeling period. In young adult mice, we estimated that naive $CD4^+$and $CD8^+$ T cells have expected lifespans of 48 and 91 days, respectively and that $CD4^+$and CD8 memory T cells have expected lifespans of 12 and 17 days, respectively (Chapter 2). This implies that 1-2% of naive T cells and 6-9% of memory T cells are replenished daily in the periphery (Chapter 2). ^2H_2O labeling cannot distin-

guish between the relative contribution of the thymus and peripheral proliferation to the maintenance of naive T cells. We used thymectomy to quantify the contribution of peripheral proliferation and thymic output. We showed that in mice throughout life, naive T cell production almost exclusively occurs in the thymus (Chapter 3). This conclusion was confirmed by the observation that TREC frequencies of naive T cells hardly dilute with the age of the mice, or even after thymectomy (chapter 3). The limited role for peripheral T-cell proliferation in the maintenance of the naive T-cell pool in mice that we report here is fully compatible with results from a classical study by Tough and Sprent [131], who reported that a small fraction (10%) of naive T cells is $BrdU^+$ after five weeks of BrdU-labeling in thymectomized C57Bl/6 mice. Our own previous findings in thymectomized C57Bl/6 mice after nine weeks of deuterium labeling [136] suggested that maximally 0.3% of all naive T cells in mice undergo peripheral proliferation while maintaining their naive phenotype. These results imply that in the event of lymphopenia in mice, thymic output is central to successful immune reconstitution.

In contrast to our findings in mice, human studies have suggested that proliferation plays a role in naive T cell maintenance during adult life [32, 51]. Naive T-cell TREC contents in humans decline about 10-100 fold from early adulthood to old age [46, 65, 69]. This gradual TREC dilution has been shown to be evidence for peripheral T-cell proliferation within the naive lymphocyte pool of humans [32, 51]. Thus there is an important qualitative difference in T cell dynamics between mice and humans (Chapter 3). Extrapolation of experimental results from mice to humans should therefore be done with caution.

Although proliferation may play a role in maintaining naive T cell numbers, it does not result in new T cell receptor (TCR) specificities. In the absence of thymic output, proliferation may therefore be responsible for the decline in the naive T cell repertoire size around the seventh decade in humans [92, 101]. Studies [92] have suggested that in humans, the ability of the thymus to rebuild a diverse repertoire ceases in the fifth decade of life. If this is the case, it seems surprising that the naive T cell repertoire only collapses two decades on in the seventh decade. A possible answer is provided in chapter 6, where we estimated that naive $CD4^+$ and $CD8^+$ T cells are relatively long lived, with expected lifespans of 5.59 and 8.84 years, respectively. Considering that thymic output is so limited in adult humans, this long lifespan of naive T cells could be a way of ensuring a substantial amount of naive T cells to combat novel pathogens over a prolonged length of time. This simple way of maintaining naive T cells may also explain why 20 years after thymectomy in humans (either for myasthenia gravis or in the context of thoracic surgeries), no signs of immune deficiency, or of a shrinking T cell repertoire are visible [49, 115]. In chapter 3, we showed that thymectomy prolongs the lifespan of naive T cells as a homeostatic response (Table 9.1).

Table 9.1: A summary of estimated lifespans of naive and memory $CD4^+$ and $CD8^+$ T cells in mice and humans.

	Mice		**Humans**[a]	
	control[b]	Thymectomized[c]	HIV^-	HIV^+
$CD4^+$ naive	48 days	62 days	5.59 years	1.69 years
$CD8^+$ naive	91 days	113 days	8.84 years	0.74 years
$CD4^+$ memory	12 days	12 days	164 days	53 days
$CD8^+$ memory	17 days	17 days	120 days	43 days

[a] Chapter 6
[b] Chapter 2
[c] Chapter 3

If thymic output is the main mechanism for maintaining a broad T cell repertoire, our finding that thymic output is substantial in old mice (up to 65 weeks), suggests that old mice should have a normal repertoire diversity. However, studies have shown that also in mice, T cell repertoire diversity declines with age leading to "holes in the repertoire" [1, 142]. This discrepancy suggests that at old age other factors, in addition to the effects of reduced thymic output, affect the T cell repertoire [142].

9.2 RTEs: a separate sub-population?

It has been suggested that RTEs cannot mount efficient immune responses [82]. In mice, when activated with a noninflammatory stimulus or a bacterial or viral pathogen, $CD8^+$ RTEs generated a lower proportion of cytokine producing effector cells and long-lived memory precursors compared with their mature counterparts [82]. Furthermore, there is current consensus that RTEs form a separate short-lived sub-population of naive T cells [7, 8, 73, 117]. The concept of a short lived RTE pool has influenced the interpretation of T cell dynamics in HIV infection. For example, TREC dilution in acute HIV infection was attributed to reduced thymic output causing rapid loss of RTEs, which bear the highest TREC content [26, 41]. However, recent work using deuterium labeling from our group indicated that in human adults naive T cells are kinetically homogeneous and long-lived [136], which questions the existence of a substantial short-lived RTE pool in human adults. In several studies described in this thesis (Chapters 2-4), we never find any evidence that RTEs form a separate sub-population with different dynamics from resident naive T cells. In chapter 2, the best fit to the naive T cell ^2H_2O labeling data was with a single compartment model suggesting a kinetically homogeneous naive T cell pool. Likewise, in chapter 3, we were able to describe the naive T cell population dynamics of control and thymectomized mice assuming that the naive T cell pool is kinetically homogeneous, but has a density dependent death rate. The strongest evidence that RTEs form a kinetically separate sub-population within the naive T cell pool comes from a series of thymus transplantation

experiments [7, 8]. Berzins et al. [8] showed that the absolute increase in T cell numbers after grafting extra neonatal thymic lobes into 6 week old mice, correlated with 3 weeks worth of cumulative thymic output. In chapter 4, we revisit these thymus implantation experiments and show that both data from thymectomy studies and thymus transplantation data are in fact fully compatible with a mathematical model in which there is no kinetic distinction between RTE and resident naive T cells. Collectively, these analyses take away the evidence, both in humans and mice, that RTE form a kinetically distinct sub-population within the naive T cell pool.

9.3 T cell dynamics during HIV infection.

HIV infection has an almost instantaneous and large impact on the size of naive $CD4^+$ and $CD8^+$ T-cell pools (Chapter 7). In contrast to thymectomy in mice, HIV infection also affects the memory $CD4^+$ T-cell compartment [14]. During HIV infection, the typical decline in T cell numbers is accompanied by a shift in the kinetics of both naive and memory $CD4^+$ and CD8 T cells to faster turnover rates compared to healthy controls (Chapter 6). In HIV^+ patients, we estimated that naive $CD4^+$ and $CD8^+$ T cells have a 3.3-12 fold shorter expected lifespan, and that $CD4^+$ and $CD8^+$ memory T cells have a 2.8-3.1 fold shorter expected lifespan compared to healthy controls (Table 9.1). The increased loss rates in HIV infection are accompanied by higher per capita production rates for both naive and memory T cells. If the expected lifespan of a T cell is dependent on the availability of survival signals, such as MHC-peptide ligands or cytokines like IL-7, T lymphocytes will experience less competition for survival signals at low T cell numbers, and as a consequence are expected to obtain a longer life expectancy [37]. In chapter 3, we showed that reduced naive T cell densities in thymectomized mice resulted in about 1.5 fold increased average lifespans of both naive $CD4^+$ and $CD8^+$ T cells compared to control mice (chapter 2-3). The result that after HIV infection (i.e. at low naive T cell densities), T cells have *shorter* expected lifespans implies that, increased cell death imposed by the virus is overriding a possible homeostatic response.

Although our findings in chapter 6 show faster T cell dynamics post HIV infection, the mechanism behind the $CD4^+$ T cell decline during HIV infection remains unclear. Several studies have suggested that chronic immune activation is responsible for the loss of T cells [42, 53, 77, 122] while other studies have pointed at reduced thymic output [9, 29, 113, 125, 143]. The majority of the latter studies are based on TREC data from cross-sectional studies. Until recently, we knew little about the longitudinal course of the changes in TRECs during HIV-disease progression. In chapter 7, we demonstrate how extrapolation of cross-sectional data to longitudinal dynamics is prone to erroneous interpretations. The inter-individual differences in TRECs of both healthy and HIV-infected subjects may lead to a considerable overlap between TREC con-

tent in $CD4^+$ T cells from healthy and HIV-infected individuals [94, 118, 143]. In the absence of longitudinal data, the interpretation of TREC data often remains inconclusive. In a longitudinal study (Chapter 7), we show that the decrease in TREC content during the acute phase of HIV infection is biphasic. Without any need for a short-lived RTE pool, this data can be explained by the recruitment of a large fraction of naive $CD4^+$ T cells into the effector/memory $CD4^+$ T cell pool, where they are quickly lost.

Keeping in mind that thymic output may also play a role in the observed T cell and TREC content dynamics in HIV infection, we investigated the role of thymic output in a model were $CD4^+$ T cell decline is driven by immune activation, via the over-expression of CD70 in CD70-Tg mice (Chapter 4). By comparing T cell dynamics in these CD70-Tg mice to wild-type mice, we showed that chronic immune activation is sufficient to cause severe naive T cell depletion and is aggravated by decreased thymic output. This result suggests that therapeutic strategies for HIV infection that are aimed at boosting thymic function may fail to reconstitute the $CD4^+$ T cell numbers if immune activation is not simultaneously kept under control.

While our results in chapter 7 imply that the TREC content decline after HIV infection is due to increased immune activation, we cannot rule out possible effects of thymic output on the observed T cell decline. TREC content data were initially used as a marker for thymic output [65, 143], but it was later shown that the interpretation of TREC data is complicated by dilution by peripheral T cell proliferation [51]. Reversely, telomeres were initially used as a measure for the proliferative history of T cells [109, 140], but they were later shown to be also influenced by thymic output [22]. In chapter 8, we reviewed the use of these two markers in analyses of naive T cell dynamics by developing a new mathematical model that simultaneously describes both TREC and telomere dynamics, and applied our analysis to HIV infection. We showed that changes in thymic output, death and proliferation tend to affect TREC contents and the average telomere lengths similarly. There is one exception where reducing thymic output results in TREC dilution and hardly any telomere shortening. Acknowledging the increased turnover rates of naive T cells during HIV infection (Chapter 6), the observed TREC dilution can only be explained by increased proliferation, and a reduced thymic output could help to explain the observed decline of naive T cells. These results illustrate how complicated the interpretation of TREC and telomere data is if multiple parameters are changed in the T cell dynamic system. It will be interesting to investigate how the recently introduced RTE marker, PTK-7 [44], will help in pin-pointing the mechanism of T cell decline during HIV infection.

In summary, in this thesis we have demonstrated how mathematical modeling can be used to interpret immunological data. Not only were we able to quantify the kinetics of T cells in mice and men, but we also resolved some of the discrepancies in previous estimates. Our results revealed the dangers of

extrapolating mouse T cell dynamics to humans by highlighting the qualitative differences in the two systems. The mathematical models also showed how the interpretation of different immunological data can be complicated by different immunological processes and in some cases lead to the wrong description of the underlying mechanism or kinetics of different T cell sub-populations.

Bibliography

[1] Ahmed, M., Lanzer, K. G., Yager, E. J., Adams, P. S., Johnson, L. L., and Blackman, M. A. (2009). Clonal expansions and loss of receptor diversity in the naive CD8 T cell repertoire of aged mice. *J. Immunol.*, 182(2):784–792.

[2] Arens, R., Baars, P. A., Jak, M., Tesselaar, K., Van der Valk, M., Van Oers, M. H., and Van Lier, R. A. (2005). Cutting edge: CD95 maintains effector T cell homeostasis in chronic immune activation. *J. Immunol.*, 174(10):5915–5920.

[3] Arens, R., Tesselaar, K., Baars, P. A., Van Schijndel, G. M., Hendriks, J., Pals, S. T., Krimpenfort, P., Borst, J., Van Oers, M. H., and Van Lier, R. A. (2001). Constitutive CD27/CD70 interaction induces expansion of effector-type T cells and results in IFNgamma-mediated B cell depletion. *Immunity*, 15(5):801–812.

[4] Arron, S. T., Ribeiro, R. M., Gettie, A., Bohm, R., Blanchard, J., Yu, J., Perelson, A. S., Ho, D. D., and Zhang, L. (2005). Impact of thymectomy on the peripheral T cell pool in rhesus macaques before and after infection with simian immunodeficiency virus. *Eur. J. Immunol.*, 35(1):46–55.

[5] Asquith, B., Debacq, C., Macallan, D. C., Willems, L., and Bangham, C. R. (2002). Lymphocyte kinetics: the interpretation of labelling data. *Trends Immunol.*, 23(12):596–601.

[6] Bennett, F., Luxenberg, D., Ling, V., Wang, I. M., Marquette, K., Lowe, D., Khan, N., Veldman, G., Jacobs, K. A., Valge-Archer, V. E., Collins, M., and Carreno, B. M. (2003). Program death-1 engagement upon TCR activation has distinct effects on costimulation and cytokine-driven proliferation: attenuation of ICOS, IL-4, and IL-21, but not CD28, IL-7, and IL-15 responses. *J. Immunol.*, 170(2):711–718.

[7] Berzins, S. P., Boyd, R. L., and Miller, J. F. (1998). The role of the thymus and recent thymic migrants in the maintenance of the adult peripheral lymphocyte pool. *J. Exp. Med.*, 187(11):1839–1848.

[8] Berzins, S. P., Godfrey, D. I., Miller, J. F., and Boyd, R. L. (1999). A central role for thymic emigrants in peripheral T cell homeostasis. *Proc. Natl. Acad. Sci. U.S.A.*, 96(17):9787–9791.

[9] Bonyhadi, M. L., Rabin, L., Salimi, S., Brown, D. A., Kosek, J., McCune, J. M., and Kaneshima, H. (1993). HIV induces thymus depletion in vivo. *Nature*, 363(6431):728–732.

[10] Borghans, J. A. and De Boer, R. J. (2007). Quantification of T-cell dynamics: from telomeres to DNA labeling. *Immunol. Rev.*, 216:35–47.

[11] Borghans, J. A., Hazenberg, M. D., and Miedema, F. (2005). Limited role for the thymus in SIV pathogenesis. *Eur. J. Immunol.*, 35(1):42–45.

[12] Borghans, J. A., Noest, A. J., and De Boer, R. J. (1999). How specific should immunological memory be? *J. Immunol.*, 163(2):569–575.

[13] Boursalian, T. E., Golob, J., Soper, D. M., Cooper, C. J., and Fink, P. J. (2004). Continued maturation of thymic emigrants in the periphery. *Nat. Immunol.*, 5(4):418–425.

[14] Brenchley, J. M., Price, D. A., Schacker, T. W., Asher, T. E., Silvestri, G., Rao, S., Kazzaz, Z., Bornstein, E., Lambotte, O., Altmann, D., Blazar, B. R., Rodriguez, B., Teixeira-Johnson, L., Landay, A., Martin, J. N., Hecht, F. M., Picker, L. J., Lederman, M. M., Deeks, S. G., and Douek, D. C. (2006). Microbial translocation is a cause of systemic immune activation in chronic HIV infection. *Nat. Med.*, 12(12):1365–1371.

[15] Brenchley, J. M., Schacker, T. W., Ruff, L. E., Price, D. A., Taylor, J. H., Beilman, G. J., Nguyen, P. L., Khoruts, A., Larson, M., Haase, A. T., and Douek, D. C. (2004). $CD4^+$ T cell depletion during all stages of HIV disease occurs predominantly in the gastrointestinal tract. *J. Exp. Med.*, 200(6):749–759.

[16] Chattopadhyay, P. K., Douek, D. C., Gange, S. J., Chadwick, K. R., Hellerstein, M., and Margolick, J. B. (2006). Longitudinal assessment of de novo T cell production in relation to HIV-associated T cell homeostasis failure. *AIDS Res. Hum. Retroviruses.*, 22(6):501–507.

[17] Choudhary, S. K., Vrisekoop, N., Jansen, C. A., Otto, S. A., Schuitemaker, H., Miedema, F., and Camerini, D. (2007). Low immune activation despite high levels of pathogenic human immunodeficiency virus type 1 results in long-term asymptomatic disease. *J. Virol.*, 81(16):8838–8842.

[18] Combadere, B., Blanc, C., Li, T., Carcelain, G., Delaugerre, C., Calvez, V., Tubiana, R., Debre, P., Katlama, C., and Autran, B. (2000). $CD4^+Ki67^+$ lymphocytes in HIV-infected patients are effector T cells accumulated in the G1 phase of the cell cycle. *Eur. J. Immunol.*, 30(12):3598–3603.

[19] Dardenne, M. and Tubiana, N. (1979). Neonatal thymus grafts. II. Cellular events. *Immunology.*, 36(2):215–220.

[20] Day, C. L., Kaufmann, D. E., Kiepiela, P., Brown, J. A., Moodley, E. S., Reddy, S., Mackey, E. W., Miller, J. D., Leslie, A. J., DePierres, C., Mncube, Z., Duraiswamy, J., Zhu, B., Eichbaum, Q., Altfeld, M., Wherry, E. J., Coovadia, H. M., Goulder, P. J., Klenerman, P., Ahmed, R., Freeman, G. J., and Walker, B. D. (2006). PD-1 expression on HIV-specific T cells is associated with T-cell exhaustion and disease progression. *Nature*, 443(7109):350–354.

[21] De Boer, R. J. (2007). Understanding the failure of $CD8^+$ T-cell vaccination against simian/human immunodeficiency virus. *J. Virol.*, 81(6):2838–2848.

[22] De Boer, R. J. and Noest, A. J. (1998). T cell renewal rates, telomerase, and telomere length shortening. *J. Immunol.*, 160(12):5832–5837.

[23] De Boer, R. J. and Perelson, A. S. (1993). How diverse should the immune system be? *Proc. Biol. Sci.*, 252(1335):171–175.

[24] Deeks, S. G., Kitchen, C. M., Liu, L., Guo, H., Gascon, R., Narvaez, A. B., Hunt, P., Martin, J. N., Kahn, J. O., Levy, J., McGrath, M. S., and Hecht, F. M. (2004). Immune activation set point during early HIV infection predicts subsequent $CD4^+$ T-cell changes independent of viral load. *Blood*, 104(4):942–947.

[25] Di Rosa, F., Ramaswamy, S., Ridge, J. P., and Matzinger, P. (1999). On the lifespan of virgin T lymphocytes. *J. Immunol.*, 163(3):1253–1257.

[26] Dion, M. L., Poulin, J. F., Bordi, R., Sylvestre, M., Corsini, R., Kettaf, N., Dalloul, A., Boulassel, M. R., Debre, P., Routy, J. P., Grossman, Z., Sekaly, R. P., and Cheynier, R. (2004). HIV infection rapidly induces and maintains a substantial suppression of thymocyte proliferation. *Immunity*, 21(6):757–768.

[27] Dominguez-Gerpe, L. and Rey-Mendez, M. (2003). Evolution of the thymus size in response to physiological and random events throughout life. *Microsc. Res. Tech.*, 62(6):464–476.

[28] Douek, D. C., Betts, M. R., Hill, B. J., Little, S. J., Lempicki, R., Metcalf, J. A., Casazza, J., Yoder, C., Adelsberger, J. W., Stevens, R. A., Baseler, M. W., Keiser, P., Richman, D. D., Davey, R. T., and Koup, R. A. (2001). Evidence for increased T cell turnover and decreased thymic output in HIV infection. *J. Immunol.*, 167(11):6663–6668.

[29] Douek, D. C., McFarland, R. D., Keiser, P. H., Gage, E. A., Massey, J. M., Haynes, B. F., Polis, M. A., Haase, A. T., Feinberg, M. B., Sullivan, J. L., Jamieson, B. D., Zack, J. A., Picker, L. J., and Koup, R. A. (1998). Changes

in thymic function with age and during the treatment of HIV infection. *Nature*, 396(6712):690–695.

[30] Douek, D. C., Roederer, M., and Koup, R. A. (2009). Emerging concepts in the immunopathogenesis of AIDS. *Annu. Rev. Med.*, 60:471–484.

[31] Dufour, C., Corcione, A., Svahn, J., Haupt, R., Poggi, V., Beka'ssy, A. N., Scime, R., Pistorio, A., and Pistoia, V. (2003). TNF-alpha and IFN-gamma are overexpressed in the bone marrow of Fanconi anemia patients and TNF-alpha suppresses erythropoiesis in vitro. *Blood*, 102(6):2053–2059.

[32] Dutilh, B. E. and De Boer, R. J. (2003). Decline in excision circles requires homeostatic renewal or homeostatic death of naive T cells. *J. theor. Biol.*, 224(3):351–358.

[33] Efron, B. and Tibshirani, R. (1986). Bootstrap methods for standard errors, confidence intervals, and other measures of statistical accuracy. *Statistical Science*, 1(1):54–75.

[34] Fagnoni, F. F., Vescovini, R., Passeri, G., Bologna, G., Pedrazzoni, M., Lavagetto, G., Casti, A., Franceschi, C., Passeri, M., and Sansoni, P. (2000). Shortage of circulating naive CD8($^+$) T cells provides new insights on immunodeficiency in aging. *Blood*, 95(9):2860–2868.

[35] Felli, N., Pedini, F., Zeuner, A., Petrucci, E., Testa, U., Conticello, C., Biffoni, M., Di Cataldo, A., Winkles, J. A., Peschle, C., and De Maria, R. (2005). Multiple members of the TNF superfamily contribute to IFN-gamma-mediated inhibition of erythropoiesis. *J. Immunol.*, 175(3):1464–1472.

[36] Ferguson, N. M., DeWolf, F., Ghani, A. C., Fraser, C., Donnelly, C. A., Reiss, P., Lange, J. M., Danner, S. A., Garnett, G. P., Goudsmit, J., and Anderson, R. M. (1999). Antigen-driven CD4$^+$ T cell and HIV-1 dynamics: residual viral replication under highly active antiretroviral therapy. *Proc. Natl. Acad. Sci. U.S.A.*, 96(26):15167–15172.

[37] Freitas, A. A. and Rocha, B. (2000). Population biology of lymphocytes: the flight for survival. *Annu. Rev. Immunol.*, 18:83–111.

[38] Ganusov, V., Borghans, J. A. M., and De Boer, R. J. (In Press). Explicit kinetic heterogeneity: mathematical models for interpretation of deuterium labeling of heterogeneous cell populations. *PloS Pathogens*.

[39] Giorgi, J. V., Hultin, L. E., McKeating, J. A., Johnson, T. D., Owens, B., Jacobson, L. P., Shih, R., Lewis, J., Wiley, D. J., Phair, J. P., Wolinsky, S. M., and Detels, R. (1999). Shorter survival in advanced human immunodeficiency virus type 1 infection is more closely associated with T lymphocyte activation than with plasma virus burden or virus chemokine coreceptor usage. *J. Infect. Dis.*, 179(4):859–870.

[40] Goronzy, J. J. and Weyand, C. M. (2005). T cell development and receptor diversity during aging. *Curr. Opin. Immunol.*, 17(5):468–475.

[41] Grossman, Z. (2005). Immune reconstitution in HIV infection: how to measure thymic function? *Clin. Immunol.*, 115(2):115–117.

[42] Grossman, Z. and Paul, W. E. (2000). The impact of HIV on naive T-cell homeostasis. *Nat. Med.*, 6(9):976–977.

[43] Guadalupe, M., Reay, E., Sankaran, S., Prindiville, T., Flamm, J., McNeil, A., and Dandekar, S. (2003). Severe $CD4^+$ T-cell depletion in gut lymphoid tissue during primary human immunodeficiency virus type 1 infection and substantial delay in restoration following highly active antiretroviral therapy. *J. Virol.*, 77(21):11708–11717.

[44] Haines, C. J., Giffon, T. D., Lu, L. S., Lu, X., Tessier-Lavigne, M., Ross, D. T., and Lewis, D. B. (2009). Human $CD4^+$ T cell recent thymic emigrants are identified by protein tyrosine kinase 7 and have reduced immune function. *J. Exp. Med.*, 206(2):275–285.

[45] Hale, J. S., Boursalian, T. E., Turk, G. L., and Fink, P. J. (2006). Thymic output in aged mice. *Proc. Natl. Acad. Sci. U.S.A.*, 103(22):8447–8452.

[46] Harris, J. M., Hazenberg, M. D., Poulin, J. F., Higuera-Alhino, D., Schmidt, D., Gotway, M., and McCune, J. M. (2005). Multiparameter evaluation of human thymic function: interpretations and caveats. *Clin. Immunol.*, 115(2):138–146.

[47] Hatzakis, A., Touloumi, G., Karanicolas, R., Karafoulidou, A., Mandalaki, T., Anastassopoulou, C., Zhang, L., Goedert, J. J., Ho, D. D., and Kostrikis, L. G. (2000). Effect of recent thymic emigrants on progression of HIV-1 disease. *Lancet*, 355(9204):599–604.

[48] Hawkins, E. D., Turner, M. L., Dowling, M. R., Van Gend, C., and Hodgkin, P. D. (2007). A model of immune regulation as a consequence of randomized lymphocyte division and death times. *Proc. Natl. Acad. Sci. U.S.A.*, 104(12):5032–5037.

[49] Haynes, B. F., Markert, M. L., Sempowski, G. D., Patel, D. D., and Hale, L. P. (2000). The role of the thymus in immune reconstitution in aging, bone marrow transplantation, and HIV-1 infection. *Annu. Rev. Immunol.*, 18:529–560.

[50] Hazenberg, M. D., Hamann, D., Schuitemaker, H., and Miedema, F. (2000a). T cell depletion in HIV-1 infection: how $CD4^+$ T cells go out of stock. *Nat. Immunol.*, 1(4):285–289.

[51] Hazenberg, M. D., Otto, S. A., Cohen Stuart, J. W., Verschuren, M. C., Borleffs, J. C., Boucher, C. A., Coutinho, R. A., Lange, J. M., Rinke de

Wit, T. F., Tsegaye, A., Van Dongen, J. J., Hamann, D., De Boer, R. J., and Miedema, F. (2000b). Increased cell division but not thymic dysfunction rapidly affects the T-cell receptor excision circle content of the naive T cell population in HIV-1 infection. *Nat. Med.*, 6(9):1036–1042.

[52] Hazenberg, M. D., Otto, S. A., Van Benthem, B. H., Roos, M. T., Coutinho, R. A., Lange, J. M., Hamann, D., Prins, M., and Miedema, F. (2003). Persistent immune activation in HIV-1 infection is associated with progression to AIDS. *AIDS*, 17(13):1881–1888.

[53] Hazenberg, M. D., Otto, S. A., Van Rossum, A. M., Scherpbier, H. J., De Groot, R., Kuijpers, T. W., Lange, J. M., Hamann, D., De Boer, R. J., Borghans, J. A., and Miedema, F. (2004). Establishment of the $CD4^+$ T-cell pool in healthy children and untreated children infected with HIV-1. *Blood*, 104(12):3513–3519.

[54] Hazenberg, M. D., Stuart, J. W., Otto, S. A., Borleffs, J. C., Boucher, C. A., De Boer, R. J., Miedema, F., and Hamann, D. (2000c). T-cell division in human immunodeficiency virus (HIV)-1 infection is mainly due to immune activation: a longitudinal analysis in patients before and during highly active antiretroviral therapy (HAART). *Blood*, 95(1):249–255.

[55] Hellerstein, M., Hanley, M. B., Cesar, D., Siler, S., Papageorgopoulos, C., Wieder, E., Schmidt, D., Hoh, R., Neese, R., Macallan, D., Deeks, S., and McCune, J. M. (1999). Directly measured kinetics of circulating T lymphocytes in normal and HIV-1-infected humans. *Nat. Med.*, 5(1):83–89.

[56] Hellerstein, M. K. (1999). Measurement of T-cell kinetics: recent methodologic advances. *Immunol. Today*, 20(10):438–441.

[57] Hellerstein, M. K., Hoh, R. A., Hanley, M. B., Cesar, D., Lee, D., Neese, R. A., and McCune, J. M. (2003). Subpopulations of long-lived and short-lived T cells in advanced HIV-1 infection. *J. Clin. Invest.*, 112(6):956–966.

[58] Hellerstein, M. K. and Neese, R. A. (1992). Mass isotopomer distribution analysis: a technique for measuring biosynthesis and turnover of polymers. *Am. J. Physiol.*, 263(5 Pt 1):E988–E1001.

[59] Hellerstein, M. K. and Neese, R. A. (1999). Mass isotopomer distribution analysis at eight years: theoretical, analytic, and experimental considerations. *Am. J. Physiol.*, 276(6 Pt 1):E1146–E1170.

[60] Henderson, A. R. (2005). The bootstrap: a technique for data-driven statistics. Using computer-intensive analyses to explore experimental data. *Clin. Chim. Acta*, 359(1-2):1–26.

[61] Hinsull, S. M. and Bellamy, D. (1974). Development and involution of thymus grafts in rats with reference to age and sex. *Differentiation*, 2(5):299–305.

[62] Ho, D. D., Neumann, A. U., Perelson, A. S., Chen, W., Leonard, J. M., and Markowitz, M. (1995). Rapid turnover of plasma virions and CD4 lymphocytes in HIV-1 infection. *Nature*, 373(6510):123–126.

[63] Ho Tsong Fang, R., Colantonio, A. D., and Uittenbogaart, C. H. (2008). The role of the thymus in HIV infection: a 10 year perspective. *AIDS*, 22(2):171–184.

[64] Hosseinzadeh, H. and Goldschneider, I. (1993). Recent thymic emigrants in the rat express a unique antigenic phenotype and undergo post-thymic maturation in peripheral lymphoid tissues. *J. Immunol.*, 150(5):1670–1679.

[65] Jamieson, B. D., Douek, D. C., Killian, S., Hultin, L. E., Scripture-Adams, D. D., Giorgi, J. V., Marelli, D., Koup, R. A., and Zack, J. A. (1999). Generation of functional thymocytes in the human adult. *Immunity*, 10(5):569–575.

[66] Jones, R. B., Ndhlovu, L. C., Barbour, J. D., Sheth, P. M., Jha, A. R., Long, B. R., Wong, J. C., Satkunarajah, M., Schweneker, M., Chapman, J. M., Gyenes, G., Vali, B., Hyrcza, M. D., Yue, F. Y., Kovacs, C., Sassi, A., Loutfy, M., Halpenny, R., Persad, D., Spotts, G., Hecht, F. M., Chun, T. W., McCune, J. M., Kaul, R., Rini, J. M., Nixon, D. F., and Ostrowski, M. A. (2008a). Tim-3 expression defines a novel population of dysfunctional T cells with highly elevated frequencies in progressive HIV-1 infection. *J. Exp. Med.*, 205(12):2763–2779.

[67] Jones, S. C., Clise-Dwyer, K., Huston, G., Dibble, J., Eaton, S., Haynes, L., and Swain, S. L. (2008b). Impact of post-thymic cellular longevity on the development of age-associated $CD4^+$ T cell defects. *J. Immunol.*, 180(7):4465–4475.

[68] Kaufmann, D. E., Kavanagh, D. G., Pereyra, F., Zaunders, J. J., Mackey, E. W., Miura, T., Palmer, S., Brockman, M., Rathod, A., Piechocka-Trocha, A., Baker, B., Zhu, B., Le Gall, S., Waring, M. T., Ahern, R., Moss, K., Kelleher, A. D., Coffin, J. M., Freeman, G. J., Rosenberg, E. S., and Walker, B. D. (2007). Upregulation of CTLA-4 by HIV-specific $CD4^+$ T cells correlates with disease progression and defines a reversible immune dysfunction. *Nat. Immunol.*, 8(11):1246–1254.

[69] Kilpatrick, R. D., Rickabaugh, T., Hultin, L. E., Hultin, P., Hausner, M. A., Detels, R., Phair, J., and Jamieson, B. D. (2008). Homeostasis of the naive $CD4^+$ T cell compartment during aging. *J. Immunol.*, 180(3):1499–1507.

[70] Kimmig, S., Przybylski, G. K., Schmidt, C. A., Laurisch, K., Mowes, B., Radbruch, A., and Thiel, A. (2002). Two subsets of naive T helper cells with distinct T cell receptor excision circle content in human adult peripheral blood. *J. Exp. Med.*, 195(6):789–794.

[71] Koenen, P. G., Hofhuis, F. M., Oosterwegel, M. A., and Tesselaar, K. (2007). T cell activation and proliferation characteristic for HIV-Nef transgenic mice is lymphopenia induced. *J. Immunol.*, 178(9):5762–5768.

[72] Kong, F., Chen, C. H., and Cooper, M. D. (1998). Thymic function can be accurately monitored by the level of recent T cell emigrants in the circulation. *Immunity*, 8(1):97–104.

[73] Kong, F. K., Chen, C. L., Six, A., Hockett, R. D., and Cooper, M. D. (1999). T cell receptor gene deletion circles identify recent thymic emigrants in the peripheral T cell pool. *Proc. Natl. Acad. Sci. U.S.A.*, 96(4):1536–1540.

[74] Kovacs, J. A., Baseler, M., Dewar, R. J., Vogel, S., Davey, Jr, R. T., Falloon, J., Polis, M. A., Walker, R. E., Stevens, R., Salzman, N. P., et al. (1995). Increases in CD4 T lymphocytes with intermittent courses of interleukin-2 in patients with human immunodeficiency virus infection. A preliminary study. *N. Engl. J. Med.*, 332(9):567–575.

[75] Kovacs, J. A., Lempicki, R. A., Sidorov, I. A., Adelsberger, J. W., Herpin, B., Metcalf, J. A., Sereti, I., Polis, M. A., Davey, R. T., Tavel, J., Falloon, J., Stevens, R., Lambert, L., Dewar, R., Schwartzentruber, D. J., Anver, M. R., Baseler, M. W., Masur, H., Dimitrov, D. S., and Lane, H. C. (2001a). Identification of dynamically distinct subpopulations of T lymphocytes that are differentially affected by HIV. *J. Exp. Med.*, 194(12):1731–1741.

[76] Kovacs, J. A., Vogel, S., Metcalf, J. A., Baseler, M., Stevens, R., Adelsberger, J., Lempicki, R., Hengel, R. L., Sereti, I., Lambert, L., Dewar, R. L., Davey, Jr, R. T., Walker, R. E., Falloon, J., Polis, M. A., Masur, H., and Lane, H. C. (2001b). Interleukin-2 induced immune effects in human immunodeficiency virus-infected patients receiving intermittent interleukin-2 immunotherapy. *Eur. J. Immunol.*, 31(5):1351–1360.

[77] Lempicki, R. A., Kovacs, J. A., Baseler, M. W., Adelsberger, J. W., Dewar, R. L., Natarajan, V., Bosche, M. C., Metcalf, J. A., Stevens, R. A., Lambert, L. A., Alvord, W. G., Polis, M. A., Davey, R. T., Dimitrov, D. S., and Lane, H. C. (2000). Impact of HIV-1 infection and highly active antiretroviral therapy on the kinetics of $CD4^+$ and $CD8^+$ T cell turnover in HIV-infected patients. *Proc. Natl. Acad. Sci. U.S.A.*, 97(25):13778–13783.

[78] Lerner, A., Yamada, T., and Miller, R. A. (1989). Pgp-1hi T lymphocytes accumulate with age in mice and respond poorly to concanavalin A. *Eur. J. Immunol.*, 19(6):977–982.

[79] Lewin, S. R., Ribeiro, R. M., Kaufmann, G. R., Smith, D., Zaunders, J., Law, M., Solomon, A., Cameron, P. U., Cooper, D., and Perelson, A. S. (2002). Dynamics of T cells and TCR excision circles differ after treatment of acute and chronic HIV infection. *J. Immunol.*, 169(8):4657–4666.

[80] Macallan, D. C., Asquith, B., Irvine, A. J., Wallace, D. L., Worth, A., Ghattas, H., Zhang, Y., Griffin, G. E., Tough, D. F., and Beverley, P. C. (2003). Measurement and modeling of human T cell kinetics. *Eur. J. Immunol.*, 33(8):2316–2326.

[81] Macallan, D. C., Wallace, D., Zhang, Y., De Lara, C., Worth, A. T., Ghattas, H., Griffin, G. E., Beverley, P. C., and Tough, D. F. (2004). Rapid turnover of effector-memory CD4(+) T cells in healthy humans. *J. Exp. Med.*, 200(2):255–260.

[82] Makaroff, L. E., Hendricks, D. W., Niec, R. E., and Fink, P. J. (2009). Postthymic maturation influences the CD8 T cell response to antigen. *Proc. Natl. Acad. Sci. U.S.A.*, 106(12):4799–4804.

[83] Marquardt, D. W. (1963). An Algorithm for Least-Squares Estimation of Nonlinear Parameters. *SIAM J. Appl. Math.*, 11(2):431–441.

[84] Marusic-Galesic, S. and Pavelic, K. (1990). Dynamics of positive and negative selection in the thymus: review and hypothesis. *Immunol. Lett.*, 24(3):149–154.

[85] McCaughtry, T. M., Wilken, M. S., and Hogquist, K. A. (2007). Thymic emigration revisited. *J. Exp. Med.*, 204(11):2513–2520.

[86] McCune, J. M., Hanley, M. B., Cesar, D., Halvorsen, R., Hoh, R., Schmidt, D., Wieder, E., Deeks, S., Siler, S., Neese, R., and Hellerstein, M. (2000). Factors influencing T-cell turnover in HIV-1-seropositive patients. *J. Clin. Invest.*, 105(5):R1–R8.

[87] Metcalf, D. (1963). The autonomous behaviour of normal thymus grafts. *Aust. J. Exp. Biol. Med. Sci.*, 41:SUPPL437–SUPPL447.

[88] Mohri, H., Perelson, A. S., Tung, K., Ribeiro, R. M., Ramratnam, B., Markowitz, M., Kost, R., Hurley, A., Weinberger, L., Cesar, D., Hellerstein, M. K., and Ho, D. D. (2001). Increased turnover of T lymphocytes in HIV-1 infection and its reduction by antiretroviral therapy. *J. Exp. Med.*, 194(9):1277–1287.

[89] Muthukumar, A., Zhou, D., Paiardini, M., Barry, A. P., Cole, K. S., McClure, H. M., Staprans, S. I., Silvestri, G., and Sodora, D. L. (2005). Timely triggering of homeostatic mechanisms involved in the regulation of T-cell levels in SIVsm-infected sooty mangabeys. *Blood*, 106(12):3839–3845.

[90] Napolitano, L. A., Grant, R. M., Deeks, S. G., Schmidt, D., De Rosa, S. C., Herzenberg, L. A., Herndier, B. G., Andersson, J., and McCune, J. M. (2001). Increased production of IL-7 accompanies HIV-1-mediated T-cell depletion: implications for T-cell homeostasis. *Nat. Med.*, 7(1):73–79.

[91] Napolitano, L. A., Schmidt, D., Gotway, M. B., Ameli, N., Filbert, E. L., Ng, M. M., Clor, J. L., Epling, L., Sinclair, E., Baum, P. D., Li, K., Killian, M. L., Bacchetti, P., and McCune, J. M. (2008). Growth hormone enhances thymic function in HIV-1-infected adults. *J. Clin. Invest.*, 118(3):1085–1098.

[92] Naylor, K., Li, G., Vallejo, A. N., Lee, W. W., Koetz, K., Bryl, E., Witkowski, J., Fulbright, J., Weyand, C. M., and Goronzy, J. J. (2005). The influence of age on T cell generation and TCR diversity. *J. Immunol.*, 174(11):7446–7452.

[93] Neese, R. A., Misell, L. M., Turner, S., Chu, A., Kim, J., Cesar, D., Hoh, R., Antelo, F., Strawford, A., McCune, J. M., Christiansen, M., and Hellerstein, M. K. (2002). Measurement in vivo of proliferation rates of slow turnover cells by 2H2O labeling of the deoxyribose moiety of DNA. *Proc. Natl. Acad. Sci. U.S.A.*, 99(24):15345–15350.

[94] Nobile, M., Correa, R., Borghans, J. A., D'Agostino, C., Schneider, P., De Boer, R. J., and Pantaleo, G. (2004). De novo T-cell generation in patients at different ages and stages of HIV-1 disease. *Blood*, 104(2):470–477.

[95] Nokta, M. A., Li, X. D., Al-Harthi, L., Nichols, J., Pou, A., Asmuth, D., Landay, A., and Pollard, R. B. (2002). Entrapment of recent thymic emigrants in lymphoid tissues from HIV-infected patients: association with HIV cellular viral load. *AIDS*, 16(16):2119–2127.

[96] Nottet, H. S., Van Dijk, S. J., Fanoy, E. B., Goedegebuure, I. W., De Jong, D., Vrisekoop, N., Van Baarle, D., Boltz, V., Palmer, S., Borleffs, J. C., and Boucher, C. A. (2009). HIV-1 can persist in aged memory $CD4^+$ T lymphocytes with minimal signs of evolution after 8.3 years of effective highly active antiretroviral therapy. *J. Acquir. Immune Defic. Syndr.*, 50(4):345–353.

[97] Paiardini, M., Frank, I., Pandrea, I., Apetrei, C., and Silvestri, G. (2008). Mucosal immune dysfunction in AIDS pathogenesis. *AIDS Rev.*, 10(1):36–46.

[98] Pandrea, I., Sodora, D. L., Silvestri, G., and Apetrei, C. (2008). Into the wild: simian immunodeficiency virus (SIV) infection in natural hosts. *Trends Immunol.*, 29(9):419–428.

[99] Parretta, E., Cassese, G., Santoni, A., Guardiola, J., Vecchio, A., and Di Rosa, F. (2008). Kinetics of in vivo proliferation and death of memory and naive CD8 T cells: parameter estimation based on 5-bromo-2'-deoxyuridine incorporation in spleen, lymph nodes, and bone marrow. *J. Immunol.*, 180(11):7230–7239.

[100] Perelson, A. S., Essunger, P., and Ho, D. D. (1997). Dynamics of HIV-1 and $CD4^+$ lymphocytes in vivo. *AIDS*, 11:S17–S24.

[101] Pfister, G., Weiskopf, D., Lazuardi, L., Kovaiou, R. D., Cioca, D. P., Keller, M., Lorbeg, B., Parson, W., and Grubeck-Loebenstein, B. (2006). Naive T cells in the elderly: are they still there? *Ann. N. Y. Acad. Sci.*, 1067:152–157.

[102] Picker, L. J., Hagen, S. I., Lum, R., Reed-Inderbitzin, E. F., Daly, L. M., Sylwester, A. W., Walker, J. M., Siess, D. C., Piatak, Jr, M., Wang, C., Allison, D. B., Maino, V. C., Lifson, J. D., Kodama, T., and Axthelm, M. K. (2004). Insufficient production and tissue delivery of $CD4^+$ memory T cells in rapidly progressive simian immunodeficiency virus infection. *J. Exp. Med.*, 200(10):1299–1314.

[103] Pido-Lopez, J., Imami, N., Andrew, D., and Aspinall, R. (2002). Molecular quantitation of thymic output in mice and the effect of IL-7. *Eur. J. Immunol.*, 32(10):2827–2836.

[104] Poulin, J. F., Viswanathan, M. N., Harris, J. M., Komanduri, K. V., Wieder, E., Ringuette, N., Jenkins, M., McCune, J. M., and Sekaly, R. P. (1999). Direct evidence for thymic function in adult humans. *J. Exp. Med.*, 190(4):479–486.

[105] Prelog, M., Keller, M., Geiger, R., Brandstatter, A., Wurzner, R., Schweigmann, U., Zlamy, M., Zimmerhackl, L. B., and Grubeck-Loebenstein, B. (2009). Thymectomy in early childhood: significant alterations of the $CD4(^+)CD45RA(^+)CD62L(^+)$ T cell compartment in later life. *Clin. Immunol.*, 130(2):123–132.

[106] Previs, S. F., Hazey, J. W., Diraison, F., Beylot, M., David, F., and Brunengraber, H. (1996). Assay of the deuterium enrichment of water via acetylene. *J. Mass. Spectrom.*, 31(6):639–642.

[107] Ribeiro, R. M. and De Boer, R. J. (2008). The contribution of the thymus to the recovery of peripheral naive T-cell numbers during antiretroviral treatment for HIV infection. *J. Acquir. Immune Defic. Syndr.*, 49(1):1–8.

[108] Ribeiro, R. M., Mohri, H., Ho, D. D., and Perelson, A. S. (2002). In vivo dynamics of T cell activation, proliferation, and death in HIV-1 infection: why are $CD4^+$ but not $CD8^+$ T cells depleted? *Proc. Natl. Acad. Sci. U.S.A.*, 99(24):15572–15577.

[109] Richardson, M. W., Sverstiuk, A., Hendel, H., Cheung, T. W., Zagury, J. F., and Rappaport, J. (2000). Analysis of telomere length and thymic output in fast and slow/non-progressors with HIV infection. *Biomed. Pharmacother.*, 54(1):21–31.

[110] Roederer, M., Dubs, J. G., Anderson, M. T., Raju, P. A., Herzenberg, L. A., and Herzenberg, L. A. (1995). CD8 naive T cell counts decrease progressively in HIV-infected adults. *J. Clin. Invest.*, 95(5):2061–2066.

[111] Roos, M. T., De Leeuw, N. A., Claessen, F. A., Huisman, H. G., Kootstra, N. A., Meyaard, L., Schellekens, P. T., Schuitemaker, H., and Miedema, F. (1994). Viro-immunological studies in acute HIV-1 infection. *AIDS*, 8(11):1533–1538.

[112] Roos, M. T., Prins, M., Koot, M., De Wolf, F., Bakker, M., Coutinho, R. A., Miedema, F., and Schellekens, P. T. (1998). Low T-cell responses to CD3 plus CD28 monoclonal antibodies are predictive of development of AIDS. *AIDS*, 12(14):1745–1751.

[113] Rosenzweig, M., Bunting, E. M., and Gaulton, G. N. (1994). Neonatal HIV-1 thymic infection. *Leukemia.*, 8:S163–S165.

[114] Sallusto, F., Geginat, J., and Lanzavecchia, A. (2004). Central memory and effector memory T cell subsets: function, generation, and maintenance. *Annu. Rev. Immunol.*, 22:745–763.

[115] Sauce, D., Larsen, M., Fastenackels, S., Duperrier, A., Keller, M., Grubeck-Loebenstein, B., Ferrand, C., Debre, P., Sidi, D., and Appay, V. (2009). Evidence of premature immune aging in patients thymectomized during early childhood. *J. Clin. Invest.*, 119(10):3070–3078.

[116] Scollay, R. G., Butcher, E. C., and Weissman, I. L. (1980). Thymus cell migration. Quantitative aspects of cellular traffic from the thymus to the periphery in mice. *Eur. J. Immunol.*, 10(3):210–218.

[117] Sempowski, G. D., Gooding, M. E., Liao, H. X., Le, P. T., and Haynes, B. F. (2002). T cell receptor excision circle assessment of thymopoiesis in aging mice. *Mol. Immunol.*, 38(11):841–848.

[118] Sempowski, G. D., Hicks, C. B., Eron, J. J., Bartlett, J. A., Hale, L. P., Ferrari, G., Edwards, L. J., Fiscus, S., and Haynes, B. F. (2005). Naive T cells are maintained in the periphery during the first 3 months of acute HIV-1 infection: implications for analysis of thymus function. *J. Clin. Immunol.*, 25(5):462–472.

[119] Silvestri, G., Sodora, D. L., Koup, R. A., Paiardini, M., O'Neil, S. P., McClure, H. M., Staprans, S. I., and Feinberg, M. B. (2003). Nonpathogenic SIV infection of sooty mangabeys is characterized by limited bystander immunopathology despite chronic high-level viremia. *Immunity*, 18(3):441–452.

[120] Soares, M. V., Borthwick, N. J., Maini, M. K., Janossy, G., Salmon, M., and Akbar, A. N. (1998). IL-7-dependent extrathymic expansion of $CD45RA^+$ T cells enables preservation of a naive repertoire. *J. Immunol.*, 161(11):5909–5917.

[121] Sportes, C., Hakim, F. T., Memon, S. A., Zhang, H., Chua, K. S., Brown, M. R., Fleisher, T. A., Krumlauf, M. C., Babb, R. R., Chow, C. K., Fry, T. J., Engels, J., Buffet, R., Morre, M., Amato, R. J., Venzon, D. J., Korngold,

R., Pecora, A., Gress, R. E., and Mackall, C. L. (2008). Administration of rhIL-7 in humans increases in vivo TCR repertoire diversity by preferential expansion of naive T cell subsets. *J. Exp. Med.*, 205(7):1701–1714.

[122] Starr, S. E., Sarr, M., Campbell, D. E., Wilson, C. M., and Douglas, S. D. (2002). Increased proliferation within T lymphocyte subsets of HIV-infected adolescents. *AIDS Res. Hum. Retroviruses.*, 18(17):1301–1310.

[123] Steffens, C. M., Managlia, E. Z., Landay, A., and Al-Harthi, L. (2002). Interleukin-7-treated naive T cells can be productively infected by T-cell-adapted and primary isolates of human immunodeficiency virus 1. *Blood*, 99(9):3310–3318.

[124] Steinmann, G. G., Klaus, B., and Muller-Hermelink, H. K. (1985). The involution of the ageing human thymic epithelium is independent of puberty. A morphometric study. *Scand. J. Immunol.*, 22(5):563–575.

[125] Su, L., Kaneshima, H., Bonyhadi, M., Salimi, S., Kraft, D., Rabin, L., and McCune, J. M. (1995). HIV-1-induced thymocyte depletion is associated with indirect cytopathogenicity and infection of progenitor cells in vivo. *Immunity*, 2(1):25–36.

[126] Surh, C. D. and Sprent, J. (2008). Homeostasis of naive and memory T cells. *Immunity*, 29(6):848–862.

[127] Tanchot, C. and Rocha, B. (1997). Peripheral selection of T cell repertoires: the role of continuous thymus output. *J. Exp. Med.*, 186(7):1099–1106.

[128] Tesselaar, K., Arens, R., Van Schijndel, G. M., Baars, P. A., Van der Valk, M. A., Borst, J., Van Oers, M. H., and Van Lier, R. A. (2003). Lethal T cell immunodeficiency induced by chronic costimulation via CD27-CD70 interactions. *Nat. Immunol.*, 4(1):49–54.

[129] Tokoyoda, K., Zehentmeier, S., Hegazy, A. N., Albrecht, I., Grun, J. R., Lohning, M., and Radbruch, A. (2009). Professional memory $CD4^+$ T lymphocytes preferentially reside and rest in the bone marrow. *Immunity*, 30(5):721–730.

[130] Tough, D. F. and Sprent, J. (1994). Turnover of naive- and memory-phenotype T cells. *J. Exp. Med.*, 179(4):1127–1135.

[131] Tough, D. F. and Sprent, J. (1998). Lifespan of gamma/delta T cells. *J. Exp. Med.*, 187(3):357–365.

[132] Touloumi, G., Pantazis, N., Karafoulidou, A., Mandalaki, T., Goedert, J. J., Kostrikis, L. G., and Hatzakis, A. (2004). Changes in T cell receptor excision DNA circle (TREC) levels in HIV type 1-infected subjects pre- and post-highly active antiretroviral therapy. *AIDS Res. Hum. Retroviruses.*, 20(1):47–54.

[133] Trautmann, L., Janbazian, L., Chomont, N., Said, E. A., Gimmig, S., Bessette, B., Boulassel, M. R., Delwart, E., Sepulveda, H., Balderas, R. S., Routy, J. P., Haddad, E. K., and Sekaly, R. P. (2006). Upregulation of PD-1 expression on HIV-specific $CD8^+$ T cells leads to reversible immune dysfunction. *Nat. Med.*, 12(10):1198–1202.

[134] Velu, V., Titanji, K., Zhu, B., Husain, S., Pladevega, A., Lai, L., Vanderford, T. H., Chennareddi, L., Silvestri, G., Freeman, G. J., Ahmed, R., and Amara, R. R. (2009). Enhancing SIV-specific immunity in vivo by PD-1 blockade. *Nature*, 458(7235):206–210.

[135] Von Boehmer, H. and Hafen, K. (1993). The life span of naive alpha/beta T cells in secondary lymphoid organs. *J. Exp. Med.*, 177(4):891–896.

[136] Vrisekoop, N., Den Braber, I., De Boer, A. B., Ruiter, A. F., Ackermans, M. T., Van der Crabben, S. N., Schrijver, E. H., Spierenburg, G., Sauerwein, H. P., Hazenberg, M. D., De Boer, R. J., Miedema, F., Borghans, J. A., and Tesselaar, K. (2008a). Sparse production but preferential incorporation of recently produced naive T cells in the human peripheral pool. *Proc. Natl. Acad. Sci. U.S.A.*, 105(16):6115–6120.

[137] Vrisekoop, N., Sankatsing, S. U., Jansen, C. A., Roos, M. T., Otto, S. A., Schuitemaker, H., Lange, J. M., Prins, J. M., and Miedema, F. (2005). Short communication: No detrimental immunological effects of mycophenolate mofetil and HAART in treatment-naive acute and chronic HIV-1-infected patients. *AIDS Res. Hum. Retroviruses.*, 21(12):991–996.

[138] Vrisekoop, N., Van Gent, R., De Boer, A. B., Otto, S. A., Borleffs, J. C., Steingrover, R., Prins, J. M., Kuijpers, T. W., Wolfs, T. F., Geelen, S. P., Vulto, I., Lansdorp, P., Tesselaar, K., Borghans, J. A., and Miedema, F. (2008b). Restoration of the CD4 T cell compartment after long-term highly active antiretroviral therapy without phenotypical signs of accelerated immunological aging. *J. Immunol.*, 181(2):1573–1581.

[139] Wallace, D. L., Zhang, Y., Ghattas, H., Worth, A., Irvine, A., Bennett, A. R., Griffin, G. E., Beverley, P. C., Tough, D. F., and Macallan, D. C. (2004). Direct measurement of T cell subset kinetics in vivo in elderly men and women. *J. Immunol.*, 173(3):1787–1794.

[140] Weng, N. P., Levine, B. L., June, C. H., and Hodes, R. J. (1995). Human naive and memory T lymphocytes differ in telomeric length and replicative potential. *Proc. Natl. Acad. Sci. U.S.A.*, 92(24):11091–11094.

[141] Wolthers, K. C., Noest, A. J., Otto, S. A., Miedema, F., and De Boer, R. J. (1999). Normal telomere lengths in naive and memory $CD4^+$ T cells in HIV type 1 infection: a mathematical interpretation. *AIDS Res. Hum. Retroviruses.*, 15(12):1053–1062.

[142] Yager, E. J., Ahmed, M., Lanzer, K., Randall, T. D., Woodland, D. L., and Blackman, M. A. (2008). Age-associated decline in T cell repertoire diversity leads to holes in the repertoire and impaired immunity to influenza virus. *J. Exp. Med.*, 205(3):711–723.

[143] Zhang, L., Lewin, S. R., Markowitz, M., Lin, H. H., Skulsky, E., Karanicolas, R., He, Y., Jin, X., Tuttleton, S., Vesanen, M., Spiegel, H., Kost, R., Van Lunzen, J., Stellbrink, H. J., Wolinsky, S., Borkowsky, W., Palumbo, P., Kostrikis, L. G., and Ho, D. D. (1999). Measuring recent thymic emigrants in blood of normal and HIV-1-infected individuals before and after effective therapy. *J. Exp. Med.*, 190(5):725–732.

Summary

An essential branch of the adaptive immune system is formed by T cells which are produced in the thymus. The absence of T cells can be detrimental to the host as is the case in acquired immuno-deficiency syndrome (AIDS). The goal of this thesis is to gain insights into the dynamics of different T cell subsets in healthy as well as disturbed situations. This information is important not only in understanding how the immune system is regulated normally, but also in guiding therapeutic strategies when the immune system gets disturbed. By combining mathematical modeling with experimental data, this thesis demonstrates how the two can complement each other in quantifying the kinetics of T cells, and in resolving some of the discrepancies in previous kinetic estimates and in the mechanisms of T cell maintenance in mice and men.

In young adult mice, we estimate that naive $CD4^+$ and $CD8^+$ T cells have expected life spans of 48 and 91 days, while $CD4^+$ and $CD8^+$ memory T cells have expected life spans of 12 and 17 days, respectively. Our analyses show that throughout life, naive T cell production in mice almost exclusively occurs in the thymus, which implies that in the event of lymphopenia in mice, thymic output is central to successful immune reconstitution. In contrast, studies based on T cell receptor excision circles (TRECs) have suggested that in humans T cell proliferation plays a key role in naive T cell maintenance during adult life. Our results therefore highlight an important qualitative difference in T cell dynamics between mice and humans. Extrapolation of experimental results from mice to humans should hence be done with caution. Recent work using deuterium labeling from our group indicated that in human adults naive T cells are kinetically homogeneous and very long-lived. This is in contrast to the current consensus that recent thymic emigrants (RTEs) form a separate short-lived sub-population of naive T cells. In several studies described in this thesis, we find no evidence that RTEs in either mice or men form a kinetically separate sub-population of naive T cells.

The typical decline in $CD4^+$ T cell numbers that is observed during HIV infection is accompanied by a shift in the kinetics of both naive and memory $CD4^+$ and $CD8^+$ T cells to faster turnover rates compared to healthy controls. Our analyses show that in HIV-infected individuals, naive $CD4^+$ and $CD8^+$ T

cells have a 3.3-12 fold shorter expected lifespan, and $CD4^+$ and $CD8^+$ memory T cells a 2.8-3.1 fold shorter expected lifespan compared to healthy controls. The increased T cell loss rates in HIV infection are accompanied by higher per capita production rates of both naive and memory T cells. We show that these increased rates of T cell turnover are fully compatible with our observation that longitudinal TREC dynamics after infection are biphasic. By mathematical modeling, we show that the large and rapid loss of naive T cells during the first year of infection can be explained by a massive recruitment of naive T cells into the effector/memory compartment where they are quickly lost. We also predict shortening of naive T cell telomeres after HIV infection contrary to previous findings that telomeres are normal in HIV patients. This discrepancy can be attributed to the effect of individual variations when extrapolating cross-sectional data to longitudinal dynamics.

We show that changes in thymic output, and T cell death and proliferation rates tend to affect average TREC contents and telomere lengths similarly. Especially when naive T cell life spans are affected, as is the case in HIV infection, the observed TREC dilution can only be explained by increased proliferation rates. Reduced thymic output could however add to the observed decline of naive T cells. Indeed, our mouse model of HIV-independent chronic immune activation shows that chronic immune activation is sufficient to cause severe naive T cell depletion, while decreased thymic output aggravates the naive T cell loss. This suggests that therapeutic strategies for HIV infection that are aimed at boosting thymic function may fail to reconstitute the $CD4^+$ T cell pool if immune activation is not simultaneously kept under control.

Samenvatting

Een belangrijke tak van het adaptieve immuunsysteem wordt gevormd door T-cellen, witte bloedcellen die in de thymus worden geproduceerd. Het ontbreken van T-cellen kan desastreuze gevolgen hebben, zoals o.a. het geval is in AIDS-patiënten. Het doel van dit proefschrift is inzicht te verkrijgen in de dynamica van verschillende T-cel-populaties in gezonde en verstoorde omstandigheden. Deze informatie is niet alleen van belang om inzicht te verkrijgen in de normale regulatie van het immuunsysteem, maar ook in de ontwikkeling van therapeutische strategieën voor situaties waarin het immuunsysteem verstoord is geraakt. Dit proefschrift laat zien hoe de combinatie van wiskundige modellering en experimentele technieken kan leiden tot kwantificering van T-cel-dynamica, discrepanties kan helpen oplossen in bestaande kinetische schattingen, en inzicht kan geven in de mechanismes verantwoordelijk voor het behoud van T-cellen in muis en mens.

Onze analyses laten zien dat naïeve $CD4^+$ en $CD8^+$ T-cellen in jongvolwassen muizen respectievelijk gemiddeld 48 en 91 dagen leven, terwijl $CD4^+$ en $CD8^+$ geheugen T-cellen gemiddeld 12 en 17 dagen leven. Ons onderzoek laat ook zien dat gedurende het hele leven van de muis, naïeve T-cel-productie bijna exclusief plaatsvindt in de thymus, hetgeen impliceert dat productie van nieuwe T-cellen in de thymus een centrale rol speelt tijdens het herstel van de T-cel-populatie in lymfopene muizen. In tegenstelling tot onze bevindingen in de muis, laten studies gebaseerd op TRECs (DNA-cirkels geproduceerd tijdens de vorming van de T-cel-receptor) zien dat in mensen juist de productie van T-cellen in de periferie een essentiële rol speelt in het behoud van de naïeve T-cel-populatie. Onze resultaten geven daarmee een belangrijk kwalitatief verschil aan in de T-cel-dynamica tussen muis en mens. Dit laat zien dat experimentele resultaten op het gebied van T-cel-dynamica niet klakkeloos geëxtrapoleerd kunnen worden van de muis naar de mens en vice versa. Recent werk gebaseerd op deuterium-labeling uit onze groep heeft laten zien dat naïeve T-cellen in gezonde volwassenen kinetisch homogeen en heel langlevend zijn. Deze bevinding staat in scherp contrast met het heersende idee dat T-cellen die recentelijk uit de thymus zijn gekomen (RTEs) een aparte, kortlevende populatie vormen binnen het naïeve T-cel-compartiment. In diverse studies in

dit proefschrift vinden we geen enkel bewijs dat RTEs in mens of muis een kinetisch aparte sub-populatie van naïeve T-cellen zouden vormen.

Het karakteristieke verlies van $CD4^+$ T-cellen tijdens HIV-infectie gaat gepaard met een snellere dynamica van zowel naïeve als geheugen $CD4^+$ en $CD8^+$ T-cellen vergeleken met gezonde controles. Onze analyses laten zien dat naïeve $CD4^+$ en $CD8^+$ T-cellen in HIV-geïnfecteerde individuen 3.3-12 maal korter leven, en $CD4^+$ en $CD8^+$ geheugen T-cellen 2.8-3.1 maal korter dan in gezonde controles. Deze verkorte levensduur van T-cellen in HIV-infectie gaat gepaard met hogere productiesnelheden van zowel naïeve als geheugen T-cellen. We laten zien dat deze verhoogde productiesnelheden compatibel zijn met een bi-fasisch longitudinaal verloop van TRECs tijdens HIV-infectie. Uit onze modellen blijkt bovendien dat het grote en snelle verlies van naïeve T-cellen tijdens het eerste jaar van infectie verklaard kan worden door een massale overgang van T-cellen van het naïeve fenotype naar het geheugen fenotype, waarna deze cellen snel verloren gaan. Onze modellen voorspellen dat de gemiddelde telomeerlengte van naïeve T-cellen tijdens HIV-infectie zou moeten afnemen, hoewel zulke veranderingen nooit significant zijn waargenomen. Deze discrepantie is waarschijnlijk te wijten aan individuele variaties die de extrapolatie van cross-sectionele data naar longitudinale interpretatie bemoeilijken.

We laten zien dat de gemiddelde hoeveelheid TRECs en de gemiddelde telomeerlengte van T-cellen op vergelijkbare manier beïnvloed worden door veranderingen in de hoeveelheid cellen die door de thymus worden geproduceerd, en door veranderingen in sterfte- en delingssnelheden van T-cellen. In het bijzonder wanneer de levensverwachting van naïeve T-cellen verkort is, zoals het geval is tijdens HIV-infectie, moet de gevonden verdunning van TRECs het gevolg zijn van verhoogde delingssnelheden van T-cellen. Een verminderde productie van T-cellen in de thymus kan echter bijdragen aan het verlies van naïeve T-cellen tijdens HIV-infectie. Inderdaad laten we in een muizenmodel zien dat chronische immuunactivatie (onafhankelijk van HIV) voldoende is om een ernstig verlies van T-cellen te bewerkstelligen, terwijl verminderde uitvoer van cellen uit de thymus het verlies van naïeve T-cellen nog kan verergeren. Dit suggereert dat therapeutische interventies die erop gericht zijn de functie van de thymus ter vergroten tijdens HIV-infectie, waarschijnlijk niet in staat zullen zijn de $CD4^+$ T-cel-populatie te herstellen, als het niveau van immuunactivatie niet tegelijkertijd wordt verlaagd.

Curriculum Vitæ

The author of this thesis, Tendai Mugwagwa, was born on November 2nd, 1979 in Gokwe, Zimbabwe. From 1991 until 1997 she attended Pakame high school in Zimbabwe specializing in mathematics, biology and chemistry. In 1998 she moved to Bindura University of science education where she majored in mathematics, biology and education. She graduated in 2002 earning her bachelor of science degree and the qualifying of a high school teacher. Although Tendai had a full time teaching job in Bulawayo, Zimbabwe, her passion for research persisted. In 2003, she came across an exciting opportunity to study mathematical sciences at the African institute of mathematical sciences (AIMS), in Cape town, South Africa. At AIMS, Tendai took a variety of applied mathematics courses, but she found epidemiology most intriguing. The fact that she could combine her knowledge in mathematics and biology to solve exciting problems in health, was simply irresistible. Furthermore, while searching for a topic for her final AIMS project, Tendai met Dr Gareth Witten who introduced her to the field of theoretical immunology. She went on to do a master's in applied mathematical biology, modeling in vivo HIV and immune response dynamics at the University of Cape town with Dr Gareth Witten.

Towards the end of her masters studies in 2005, Dr Gareth Witten introduced Tendai to Prof Rob. J. de Boer to discuss a possibility of doing a PhD in the theoretical biology group at Utrecht University. After a visit to Utrecht for an interview during a heat wave, Tendai was convinced that Utrecht would be home for the four years that followed. Tendai thereafter started her PhD studies in 2005, supervised by Prof. Rob J. de Boer and Dr José A. M. Borghans, which resulted in this thesis. Currently, Tendai will remain in the field of theoretical immunology, moving to the department of biostatistics and computational biology at Rochester University, New York, USA.

Publications

T Mugwagwa and G Witten. Coreceptor switching in HIV-1 subtype B and subtype C. *Bulletin of Mathematical Biology, 2007 Jan;69(1):55-75.*

Ineke den Braber, **Tendai Mugwagwa,** Liset Westera, Elise H.R. Schrijver, Gerrit Spierenburg, Koos Gaiser, An F.C. Ruiter, Mariette T. Ackermans, Frank Miedema, José A.M. Borghans, Rob J. de Boer, Kiki Tesselaar. Lack of peripheral division in naive T cell maintenance: a mouse-man divide. *submitted*

Nienke Vrisekoop, Rogier van Gent, **Tendai Mugwagwa,** Anne Bregje de Boer, Sigrid A. Otto, An F.C. Ruiter, Mariëtte T. Ackermans, Joost N. Vermeulen, Hidde H. Huidekoper, Koos Gaiser, Hans P. Sauerwein, Jan M. Prins, Frank Miedema, Rob J. de Boer, Kiki Tesselaar and José A.M. Borghans. Qualitative changes in T cell turnover during HIV-1 infection. *submitted*

Tendai Mugwagwa, Ineke den Braber, Lydia Kwast, Elise H.R. Schrijver, Gerrit Spierenburg, Koos Gaiser, An F.C. Ruiter, Mariette T. Ackermans, Rob J. de Boer, Kiki Tesselaar, José A.M. Borghans. Naive and memory T cell turnover in mice. *in preparation*

Tendai Mugwagwa, Ineke den Braber, Kiki Tesselaar, José A.M Borghans and Rob J. de Boer. No evidence for separate dynamics of recent thymic emigrants: thymus grafting experiments revisited. *in preparation*

Ineke den Braber, **Tendai Mugwagwa,** Elise H.R. Schrijver, Erik Mul, Floris van Alphen, Rob J. de Boer, José A.M Borghans, Kiki Tesselaar, T cell exhaustion and depletion in mice with chronic immune activation via CD7/CD70 costimulation. *in preparation*

Nienke Vrisekoop, **Tendai Mugwagwa**, Anne Bregje de Boer, Sigrid A. Otto,

Mette D. Hazenberg, Kiki Tesselaar, Frank Miedema, Rob J. de Boer and José A.M. Borghans. Biphasic TREC dynamics during HIV-1 infection. *in preparation*

Tendai Mugwagwa, Rachid Ouifki, José A.M. Borghans, and Rob J. de Boer. Can TRECs and telomeres be affected differently by naive T cell dynamics? *in preparation*

Acknowledgments

As we the people from southern African would put it, “ubuntu”, meaning we are people through other people and as Archbishop Desmond Tutu explained it, we cannot be fully human alone. I therefore dedicated this section to all those who helped me through my journey each one in their own unique way.

When I first visited Utrecht in August 2005, I was a nervous rack ahead on my interview. However, after getting a warm reception from Rob and José and an impressive overview of their research work, I was soon moving to the Netherlands to start work on my PhD. Over the four years that followed, Rob and José taught me a lot about mathematical modeling and immunology. Even though I did not have much experience in research, they constantly guided and molded me into the research scientist that I am today. Their support continued outside of work as they always looked out for my well being. I could not have asked for better supervisors. For all this and much more, Rob and José, I am deeply grateful, thank you very much.

This thesis would not be here were it not for the great contribution from my collaborators at the Wilhelmina children’s hospital (WKZ) immunology department. Kiki Tesselaar, Frank Miedema, Ineke den Braber, Nienke Vrisekoop, Liset Westera, and Vera van Hoeven, thank you for sharing your data with me, for all the informative discussions. You were always patient when I could not follow the technical details of experiments, and gave me helpful feedback on the mathematical models. I would also like to thank Rogier van Gent for also sharing his data with me. In South Africa at the center for epidemiological modeling and analysis, I would like to thank Dr Rachid Ouifki for the great collaboration and taking great care of me during my visit on the staff exchange project. I would also like to thank Dr Gareth Witten who did not only introduce me to the field of theoretical immunology but also introduced me to Rob and Rachid. You were a great supervisor to me. A special thank you to Becca Asquith for all the great scientific discussions and feedback on my work. To Alan Perelson, Ruy Ribeiro and Rustom Antia, thank you for hosting me when I came to visit the Los alamos labs and Emory university respectively in 2009.

Next, I would also like to thank the members of the reading committee who spent their valuable time evaluating this thesis: Frank Miedema, Derek

C. Macallan, Luc Willems, Robin Callard, and Jorge Carneiro.

To the members of the theoretical biology and bio-informatics group at Utrecht university, thank you all for the scientific talks, discussions and all the good times we had together. Special mention to Vitaly who was always patient when I came nagging with a new idea in my head. Thank you Vitaly and Elena for taking care of us when we visited Santa Fe as well as for the lovely cakes you used to bring to the coffee room. To Can, Pauline, Ben, Ludo, Joost, and Klaartje, thank you for always looking out for my well being during my stay in Utrecht. Boris Schimd, Rao Xiangyu, Jorg Calis, Henk-Jan van den Ham, Christian Althaus, Tjibbe Donker, Hanneke van Deutekom, and Ilka Hoof thank you for sharing the office with me and tolerating me when I stressed out about my dear friend 'FUI'. To Nobuto, thanks for putting up with my random visits to your office to talk about random things.

The great thing about studying abroad is that you get to meet different people and make new friends. To my wonderful friends in Utrecht, Chiseche, Jecinta, Pearlmira, Haika and Anne, thank you ladies for being there for me through both happy and difficult moments. I will miss the "ladies' day" outings we used to have together. Debby, Marc, and Tamar ("my puddings"), you always brought me joy. A very special thank you to all the members of Holy Trinity Church Utrecht who took care of my spiritual and emotional well being. I will miss the Sunday lunches, the diners and flower and music festivals. Pam and John you constantly helped, advised me and encouraged me to grow spiritually. Steffani, Jouke, Rosemarie, Marijn and Ina you are such wonderful friends. Mamolepa, M'nono and Kim thank you for all the lovely African diners we organized together. I was always rejuvenated at the start of each week by your hospitality and friendship. You gave me a sense of belonging in Utrecht. May the good Lord bless you all abundantly.

Although we lived in different countries, Nneoma and Rejoice you were always there to discuss the stresses of doing a PhD and share my vacations. You are amazing friends. Dr Michael Pickles, thank you for the continued support. To my family and friends in the UK, you supported me tirelessly and made sure I had a home away from home. Robert, Johannes, Tafadzwa, Ms Z Ndhlela, Tapiwa, Simba, and the Chibwana family, *ndinokutendai mose nerudo rwenyu rwukuru.* Buddhika, Nilmini and Vimukthi Hewakandamby, thank you for your hospitality. To Marazanye family in Sweden, and the Takaidza Family in South Africa, we surely had some great times together. Ms K Ndhlela, I am looking forward to being closer to you in the US. *Mwari wavakukomborerei mose hama neshamwari dzangu nokusingaperi.*

I would not be where I am today were it not for my family who love me unconditionally. To my mother, thank you for all the sacrifices you made to educate me and allow me to follow my dreams. To my father, thank you for always being curious and wanting to hear more about my work. To my sisters, Dollen, Naume, Milker, Patience, Grace, Faith, Dorcus and Noster, thank you

is not a big enough word to express my gratitude. I will always treasure your love, support, patience, and all the dinners we had over the phone. I can not ask for a better family. Thank you also to my nephews, nieces and brother-in-laws for all the support.

Finaly, I would like to thank Laurent for all his patience, support, encouragement and all the wonderful times we had together as we criss-crossed the world. Grandma and Grandpa Dudot, merci beaucoup!

"Two are better than one, because they have a good return for their work: If one falls down, his friend can help him up. But pity the man who falls and has no one to help him up! " **Ecclesiastes 4:9-10**